Chemistry–A European Journal
Review
doi.org/10.1002/chem.202104191
Chemistry Europe
European Chemical Societies Publishing
www.chemeurj.org

From Light to Structure: Photo Initiators for Radical Two-Photon Polymerization

Thomas Wloka,[a, b] Michael Gottschaldt,[a, b] and Ulrich S. Schubert*[a, b]

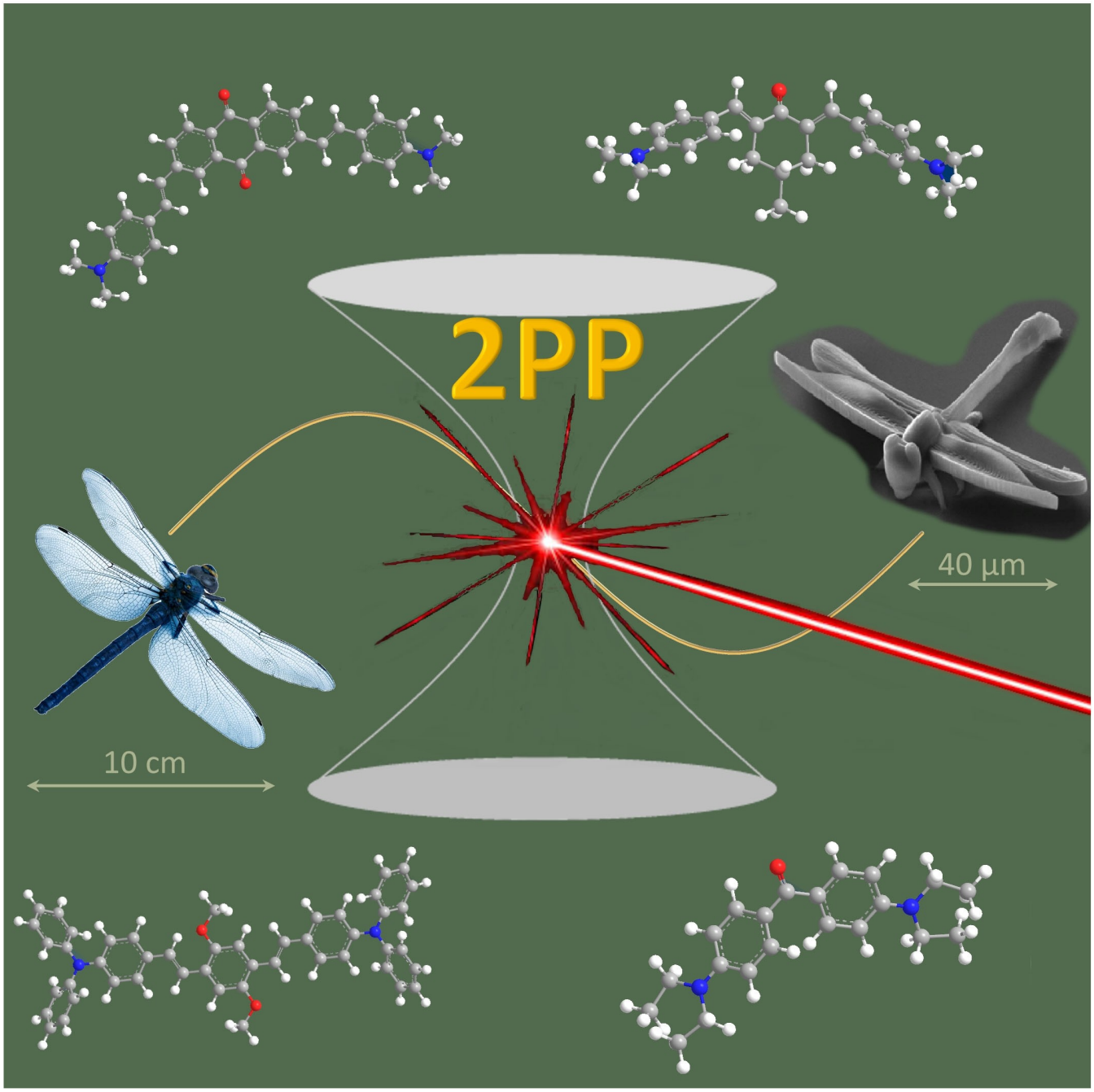

Abstract: Two-photon polymerization (2PP) represents a powerful technique for the fabrication of precise three-dimensional structures on a micro- and nanometer scale for various applications. While many review articles are focusing on the used polymeric materials and their application in 2PP, in this review the class of two-photon photo initiators (2PI) used for radical polymerization is discussed in detail. Because the demand for highly efficient 2PI has increased in the last decades, different approaches in designing new efficient 2PIs occurred. This review summarizes the 2PIs known in literature and discusses their absorption behavior under one- and two-photon absorption (2PA) conditions, their two-photon cross sections (σ_{TPA}) as well as their efficiency under 2PP conditions. Here, the photo initiators are grouped depending on their chromophore system (D-π-A-π-D, D-π-D, etc.). Their polymerization efficiencies are evaluated by fabrication windows (FW) depending on different laser intensities and writing speeds.

1. Introduction

1.1. Two-photon polymerization and photo initiators

In 1931, Maria Göppert-Mayer postulated the theoretical possibility of the two-photon absorption (2PA) by one molecule in her doctoral thesis.[1] In this process, the energies of two photons add up during simultaneous absorption and stimulate the molecule into its excited state. However, this process requires a very precise temporal and spatial resolution, which was not possible during that time because of the lack of the required technical equipment. With the help of a laser, two-photon absorption was demonstrated by Kaiser et al. in 1962.[2] Since then, and due to rapid technical developments, two-photon absorption has been intensively studied. Maruo et al. were one of the first to report a fabricated 3D spiral microstructure using the 2PA effect to initiate polymerization.[3] Since then, the technique of two-photon polymerization (2PP) has found its way into various application areas such as direct laser writing (DLW),[4–5] functional micro devices,[6] biomaterials,[7–8] 3D data storage[9–10] and tissue engineering.[11–13] The principle of 2PP is based on the fact that a photo initiator in a monomer solution is excited within the focal point of the laser and, thus, initiates polymerization locally within the focal point. While there have been many reviews reporting on the materials produced via 2PP and their applications,[14–23] to the best of our knowledge no review has been published yet that addresses the design and efficiencies of the photo initiators. In this review, we will focus on the structural properties, the resulting values, and efficiencies of type I and type II photo initiators for radical 2PP. Type I photo initiators are compounds which generate radicals by cleavage of a bond under excitation. Type II photo initiators initiate polymerization by undergoing an H-abstraction reaction when irradiated. In literature it is also known that cationic polymerization under 2PA condition is possible. A brief summary on photo acid generators (PAGs) which initiate cationic polymerization under 2PA condition was reported elsewhere recently.[24]

[a] T. Wloka, Prof. Dr. M. Gottschaldt, Prof. Dr. U. S. Schubert
Laboratory of Organic and Macromolecular Chemistry (IOMC)
Friedrich Schiller Universität Jena
Humboldtstraße 10, 07743 Jena (Germany)
E-mail: ulrich.schubert@uni-jena.de

[b] T. Wloka, Prof. Dr. M. Gottschaldt, Prof. Dr. U. S. Schubert
Jena Center for Soft Matter (JCSM)
Friedrich Schiller Universität Jena
Philosophenweg 7, 07743 Jena (Germany)

1.2. Commonly used values for 2PIs and their measurement

A repeatedly discussed unit with which two-photon initiators (2PI) are characterized, is the Göppert-Mayer value (GM). The Göppert-Mayer value is the unit of the two-photon cross-section (σ_{TPA}) and states that at a photon flow of one photon per second and cm^2 in a material of density of one molecule per cm^3 over a distance of 1 cm one of 10^{50} photons is absorbed. Two main methods are used to determine the two-photon cross-section: The Z-scan and the two-photon excited fluorescence.

1.2.1. The Z-scan technique

During the Z-scan measurement the light intensity of a focused laser beam is measured while the sample is moved along the z-axis.[25] Two different setups can be used. The "closed-aperture" method uses a narrow aperture at the detector. This results in a sensitive output, which depends on intensity changes in the refractive index, thus leading to defocusing or self-focusing of the laser beam. In contrast, the "open-aperture" measurement uses a wide aperture and collects all light from the sample, reflecting only the intensity dependent transmission.[26] However, two major effects can influence the 2PA cross-section measurement with this technique: 1) Due to the nonlinear scattering or the loss of light due to self-defocusing (due to the wrong adjustment of the detector) an extra contribution to the apparent nonlinear absorption is added. 2) The non-linear transmission can be influenced by excited-state absorption (ESA). The influence can be reduced by using wavelengths where the 1PA (one photon absorption) is negligible, short laser pulses (<1 ps), as well as low repetition rates.[25,27]

1.2.2. Two-photon excited fluorescence (TPEF)

First developed by Xu and Webb the TPEF-method provides direct information on the efficiency of 2PA.[28] The σ_{TPA}-value is received by comparing the one- and two-fluorescence spectrum of the sample with the spectra of a reference compound. By double-referencing the obtained data a large number of variables, like the parameters of the excitation light or the wavelength dependence of the detector, are automatically quitted. This technique depents on exact measurements, since a uncertainty in the one-photon absorption leads directly to an uncertainty in σ_{TPA} value.[26] In addition, the TPEF technique has two limitations, since it cannot be applied on regions with one-photon absorption and the measured sample must bear a photoluminescence.[26] While, the first restriction is general to all σ_{TPA} measurement techniques, by quantifying a secondary photochemical process, like the luminescence of single oxygen, the second restriction can be overcome. However, chromophores designed to act as a photo initiator in 2PP have a low fluorescence. Therefore, measurement applying TPEF often requires intensive measuring time. Since the establishment of this technique, it was further optimized and a wide range of accurate reference 2PA spectra of commercially available dyes have been reported.[29] In general, σ_{TPA}-values obtained from Z-scan measurements tend to be exaggerated compared to TPEF values.[30–31]

1.2.3. Fabrication properties

Besides the determination of the two-photon cross-section, there are several other parameters discussed related to the practical fabrication of 2PP-produced microstructures. For many years, it was assumed that compounds with a high σ_{TPA} result in efficient 2PI for 2PP. But besides the σ_{TPA}, factors like the fluorescence quantum yield (Φ_{fl}), intersystem crossing efficiency, and solubility play also crucial roles in fabricating structures. To estimate the 2PIs potential, fabrication tests with different laser intensities and writing speeds are required. With such arrays, the energy threshold E_{th} and the burning threshold (also described as E_{damage}) can be determined. The energy threshold is defined as the minimal laser power which is needed to ensure that fabricated structures survive the development stage. Some groups use the term of the polymerization threshold (P_{th}), which is defined as the average power before the lens, below which the polymer line cannot be fabricated. The burning threshold E_{damage} describes the level of laser power at which good quality fabrication can no longer be achieved due to the micro explosions from optical damage that can occur during the fabrication process.[32] The fabrication window (FW) is the power range between the polymerization/energy threshold and the burning threshold (Table 1).[33] Since a standard for the evaluation of 2PIs has not been established yet, many research groups deviate from the mentioned parameters and use other measurands, which are explained thoroughly for each case.

For the evaluation of a 2PI, the parameters listed in Table 1 cannot be considered individually, but have to be discussed as

Thomas Wloka was born in Ravensburg (Germany) in 1989. He studied Chemistry at the Ludwig Maximilians University (LMU) in Munich (Germany). Since 2017 he has been a PhD student in the group of Prof. Schubert at the Friedrich Schiller University Jena. His research interests cover the development of water-soluble photo initiators for two-photon polymerization and the synthesis of macromonomers based on poly(2-oxazoline)s.

Michael Gottschaldt was born in Jena (Germany) in 1973. After studying Chemistry in Jena (Germany) and Virginia Tech University (USA), he completed his dissertation in Jena in 2002. After a postdoctoral stay as a Marie Currie Fellow in Nara (Japan) with Prof. S. Yano he returned to Jena and obtained his habilitation in 2010. Since 2018 he is adjunct professor at the Friedrich Schiller University Jena.

Ulrich S. Schubert was born in Tübingen (Germany) in 1969. He studied chemistry in Frankfurt and Bayreuth (both Germany) and at Virginia Commonwealth University, Richmond (USA). His PhD studies were performed at the Universities of Bayreuth and South Florida. After a post-doctoral training with J.-M. Lehn at the University of Strasbourg (France), he moved to the TU Munich (Germany) and obtained his Habilitation in 1999. During 1999 to 2000 he was Professor at the University of Munich and during 2000–20007 Full-Professor at the TU Eindhoven (the Netherlands). Since 2007, he has been Full-Professor at the Friedrich Schiller University Jena, Germany.

Table 1. Summary of the essential photophysical and process parameters by which 2PIs are characterized.

Abbreviations	Definition
E_{th}	Energy threshold: The minimal laser power which is required to ensure that fabricated structures survive the development stage
P_{th}	Polymerization threshold: The average laser power before the lens, below which the polymer line cannot be fabricated
E_{Damage}	Burning threshold: The level of laser power at which good quality fabrication can no longer be achieved
R_p	Polymerization rates
FW	Fabrication window: Power range between the polymerization/energy threshold and the burning threshold
σ_{TPA}	Two-photon cross-section: Probability to undergo 2PA
Φ_{fl}	Fluorescence quantum yield

an interaction of all of them. In addition, parameters like solubility, viscosity and the applied monomer mixtures influences the efficiency of a 2PI. In the following review, the 2PI known to literature will be described by means of their chemical structure, respectively grouped by their chromophore systems. With the development of 2PP fabricated hydrogels for tissue engineering the demand for water-soluble photo initiators had increased in the last two decades. Therefore, the respective water-soluble photo initiators are discussed in this review in separate paragraphs for each chromophore system.

2. D-π-A-π-D Chromophores

2.1. Benzophenones

One of the most prominent representatives of two-photon initiators (2PI) of the D-π-A-π-D chromophores is bis(diethylamino)benzophenone (**BDAB**) known as Michlers' ethyl ketone (Figure 1). It was used as a common UV initiator in photopolymerizations before Haq et al. discovered its potential to act as a 2PI. They successfully applied **BDAB** for the 2PP of the monomer EBPADMA (ethoxylated bisphenol A dimethacrylate).[34]

BDAB exhibits a linear absorption at around 400 nm in ethanol and EBPADMA, while in ethyl acetate a maximum at 350 nm was detected. The influence of the solvent was also observed in the measurement of the extinction coefficient ε. While in ethanol ε exhibits 11,366 M^{-1} cm^{-1}, it decreases with decreasing polarity. In EBPADMA ε was 4450 M^{-1} cm^{-1} and in ethyl acetate 65.4 mM^{-1} cm^{-1}.

The σ_{TPA} values for **BDAB** were determined by using a modified version of the TPEF technique by Song et al.[35] with a concentration of 3×10^{-3} M. With a σ_{TPA} of 14 GM **BADB** exhibits the largest cross-section in ethanol but only 1 GM when dissolved in the monomer EBPDMA.

In addition to the photophysical properties of **BDAB**, the parameters for polymerization were determined by using EBPADMA with 1 % **BDAB**. The parameters like line widths, were investigated as a function of laser power, writing speed, exposure time, and numerical aperture.[36] Figure 2A displays the width of structured lines with different laser powers (0.4, 1.0, and 1.3 mW) *versus* the writing speed. It should be noted that the line width becomes significantly narrower as the writing speed increases. The opposite effect is observed with the laser power *versus* the line width (Figure 2B). With increasing laser power, a significant increase in line width can be noticed and the lowest laser power determined for the fabrication of solid lines at a writing speed of 10 mm/min was 80 μW. This determined value was set as the limit value for EBPADMA. It could also be shown that the exposure time is a significant parameter influencing the line width. Even a slight increase of the exposure time leads to an enlargement of the voxel and, thus, to a broadening of the line, as shown in Figure 2C. To achieve high resolutions it is important to adjust the exposure time, as well as the intensity carefully.[36]

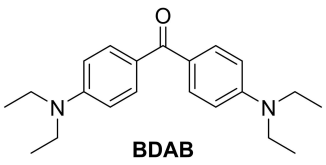

Figure 1. Schematic representation of the structure of bis(diethylamino)benzophenone (BDAB).

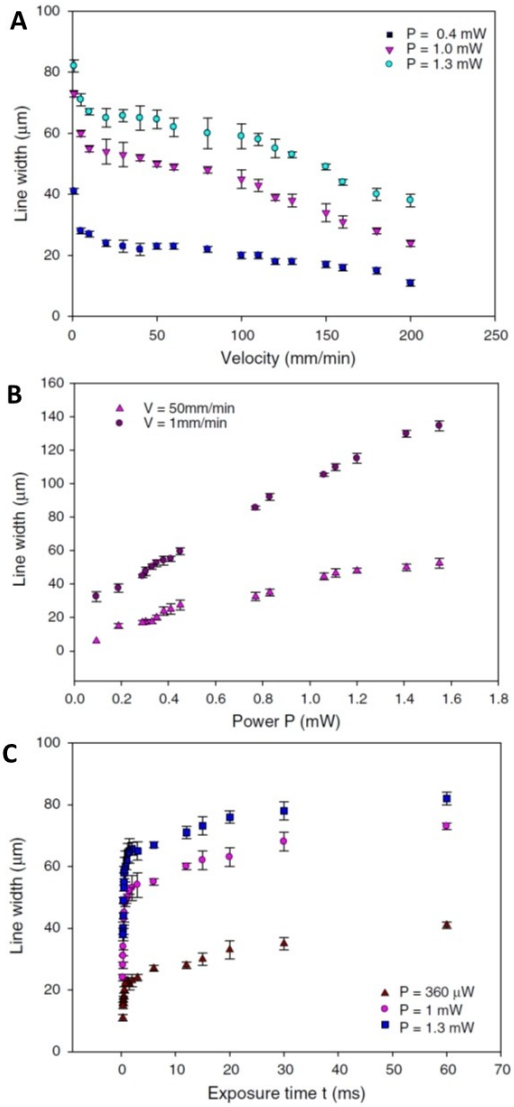

Figure 2. Line width investigations of **BDAB** in EBPADMA depending on (A) writing speed/velocity, (B) laser power and (C) laser exposure time.[36] Adapted with permission from Ref. [36] © The Optical Society.

3D-microstructures manufactured for tissue engineering are facing high requirements like stability and degradability. In addition, biocompatibility and cytotoxicity play decisive roles in the development of such scaffolds. Apart from the polymer used, it is also essential that the photo initiator has similar or even identical compatibilities since a considerable proportion remains in the structure. Ovsianikov et al. performed biological

tests on PEG-based structures to investigate the influence of **BDAB** on cell viability.[37] Structures were prepared with a **BDAB** concentration of 2 wt.% (Figure 3) and the viability of L929 fibroblasts grown on the obtained scaffolds was determined. It was shown that aging the samples in distilled water for six days led to a reduction of the water soluble toxic compounds to a level where no further cytotoxicity was determined.

Besides polymerization of PEG and PEG copolymers,[38] **BDAB** has often been used for organic-inorganic hybrid materials. These hybrid materials, some of which are commercially available, are based on methacryloxypropyl trimethoxysilanes (MAPTMS) and zirconium propoxide (ZPO).[13,39–41] In addition to the application of microstructures for tissue engineering, Xin et al. dealt with the fabrication of specially designed micro helices based on these hybrid materials produced with **BDAB** as 2PI (Figure 4) for effective drug delivery in the human body.[42]

Although **BDAB** is such a frequently used 2PI, no fabrication window (FW) is reported yet.

One structural variant of **BDAB** is the initiator **B3BP** produced by Liska et al. (Figure 5), which has an extended π-system via bridging triple bonds.[43]

B3BP exhibits a linear absorption at 405 nm (DCM) and has a fluorescence quantum yield of 0.16 (with fluorescein and coumarin 515 as references). Compared to **BDAB**, **B3BP** shows an enormously increased two-photon cross-section of 336 GM (Z-scan at 800 nm). Structuring tests with a 1:1 mixture of trimethylolpropane triacrylate (TTA) and ethoxylated (20/3)-trimethylolpropane triacrylate (ETA) revealed a fabrication window (FW) of around 2.5 to 7 mW.

A series of photo initiators based on the benzophenone core structure were reported by Zhang et al.[44] Similar to **B3BP** the initiators have expanded π-systems via a triple bond bridge to different heterocycles and aryl-substituents (Figure 6).

All photo initiators show absorption maxima between 370 and 400 nm in dichloromethane, which slightly shift in solvents with altered polarity. The measured fluorescence quantum yields of the 2PIs were between 40% and 50%, except **BT–PTAA–C$_6$** which exhibits a quantum yield below 1%. While **BT–CAA–C$_6$**, **BT–CAA–Bn** and **BT–TPAA** exhibit σ_{TPA} values in a range of 370 to 500 GM, **BT–PTAA–C$_6$** reveals a large σ_{TPA} value of 1907 GM (Table 2). Unfortunately, the authors do not

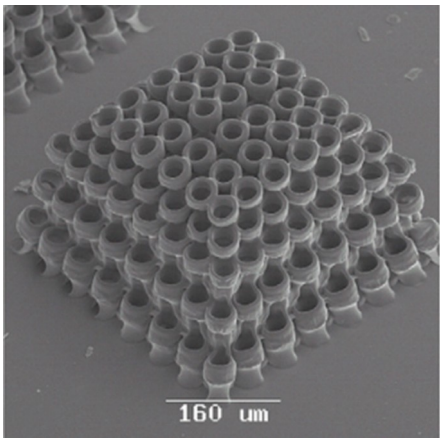

Figure 3. SEM image of fabricated PEG structure with 2 wt% **BDAB**.[37] Reproduced with the permission of Ref. [37]. Copyright 2011, Elsevier.

Figure 4. SEM images of microhelices fabricated with a zirconium–silicon hybrid sol-gel material and 1 wt% BDAB.[42] Adapted with the permission of Ref. [42]. Copyright 2019, John Wiley and Sons.

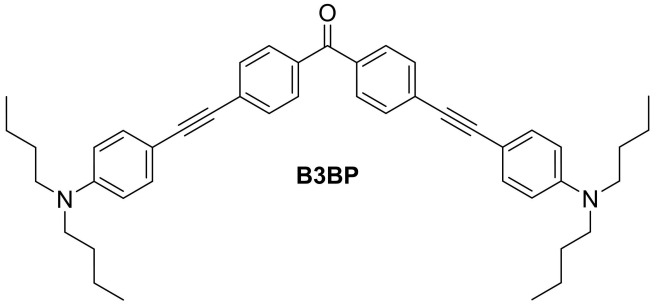

Figure 5. Schematic representation of the structure of B3BP.

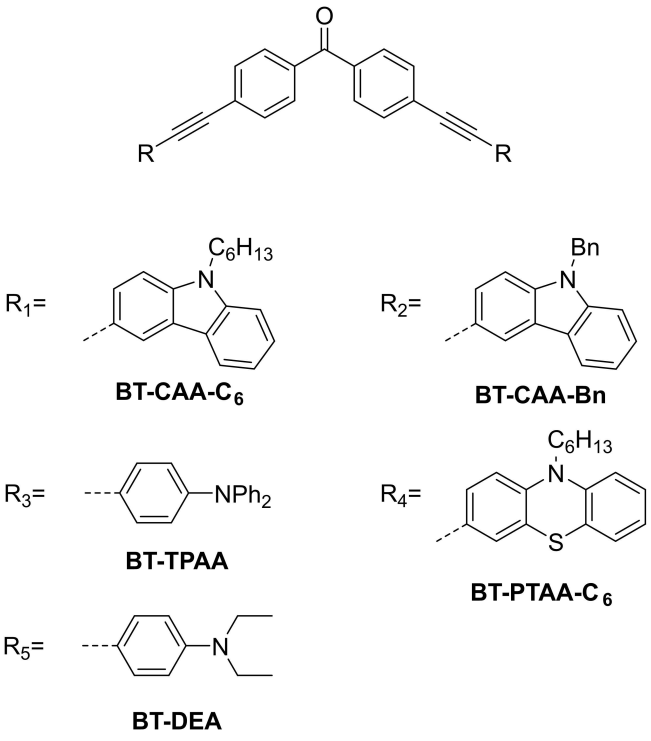

Figure 6. Schematic representation of the structures of the benzophenone derivatives.

Table 2. Photophysical and polymerization data of the benzophenone based photo initiators **BT**–**CAA**–**C_6** to **BT**–**DEA**.

Compound	λ_{max} [nm][a]	Φ_{fl}[%]	σ_{TPA} [GM][b]	FW [mW][c]
BT–**CAA**–**C_6**	375	51.70	446	30 to 50
BT–**CAA**–**Bn**	370	38.52	501	–
BT–**TPAA**	393	40.29	372	30 to 50
BT–**PTAA**–**C_6**	392	0.97	1907	30 to 50
BT–**DEA**				40–50

[a] Measured in dichloromethane. [b] Two-photon cross-section were calculated using up-conversion fluorimetry at 780 nm. [c] Fabrication windows at a writing speed of 100,000 μm/s with TTA as monomer.

report in which solvent the fluorescence quantum yields or the two-photon cross-sections were determined, and, for **BT**–**DEA** no photophysical data was reported. Polymerization tests were performed using TTA as monomer adding 10 μmol 2PI per gram of monomer. A laser power range of 5 to 50 mW was applied and writing speeds between 100 to 100,000 μm/s were tested. All photo initiators except **BT**–**CAA**–**Bn** revealed good initiation properties even at the highest writing speed. The fabrication windows at 100,000 μm/s for all 2PIs were nearly the same with exception of **BT**–**DEA**. **BT**–**TPAA** revealed the best overall initiation properties and further polymerization test in different monomers like PETA and bisphenol A epoxyacrylate (BAEA) were performed. These tests showed that by changing the monomer the fabrication window is greatly affected. Thus, in the case of PETA (FW = 15 to 50 mW) and BAEA (FW = 20 to 50 mW), the fabrication window could be slightly broadened, which shows that the type of monomer used influences the fabrication window.

2.2. Benzylidenacetones/-cycloalkanes

The interest in benzylidene derivatives in the development of novel 2PIs for 2PP has grown steadily. One of the main reasons is that the desired D-π-A-π-D structure can be build up quite effectively by classical aldol condensation. No expensive catalysts are required, because the reaction already proceeds with the help of strong bases or acids. In the case of the benzylidene derivatives mentioned here, the reactions also proceed quickly, in high yields, and are chemoselective, as various references report. Scheme 1 shows the aldol condensation starting from *N*,*N*-dimethylaminobenzaldehyde and acetone to yield **BA-1**.[45]

BA-1 reveals a linear absorption maximum at 441 nm in chloroform (ε of 47000 $M^{-1} \times cm^{-1}$). Two-photon cross-section

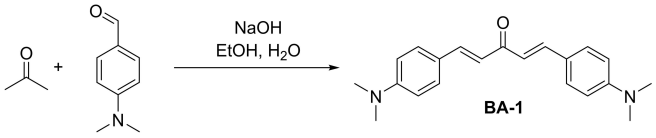

Scheme 1. Schematic representation of the aldol condensation of acetone and N,N-dimethylaminobenzaldehyde with NaOH as base.

Z-scan measurements in MeOH and THF show different values. While in MeOH the σ_{TPA} is 349 GM, in the less polar THF 269 GM were determined. Structures were written at a 2PI concentration of 6.3×10^{-6} mol/g of polymer in a 1:1 monomer mixture of trimethylolpropane triacrylate and ethoxylated (20/3) trimethylolpropane triacrylat (writing speed was 50 μm/s). Stable structures without major defects could only be obtained within a range of laser intensity of about 8 to 11 mW.[45] The small FW of **BA-1** can be explained by possible cis-trans isomerization, which is not blocked by additional substituents.

Lemercier et al. synthesized benzylidene acetones with π-systems of different lengths (**BA-2** to **BA-5**) and stilbene moieties (**BA-6** to **BA-8**, Figure 7) and investigated the effects on the two-photon absorption behavior.[46]

Figure 8 displays the linear UV/Vis absorption spectra of **BA-2** to **BA-5**. By increasing the length of the π-system the linear absorption maxima were shifted bathochromically (Table 3). In the case of **BA-4**, the data obtained are consistent with other

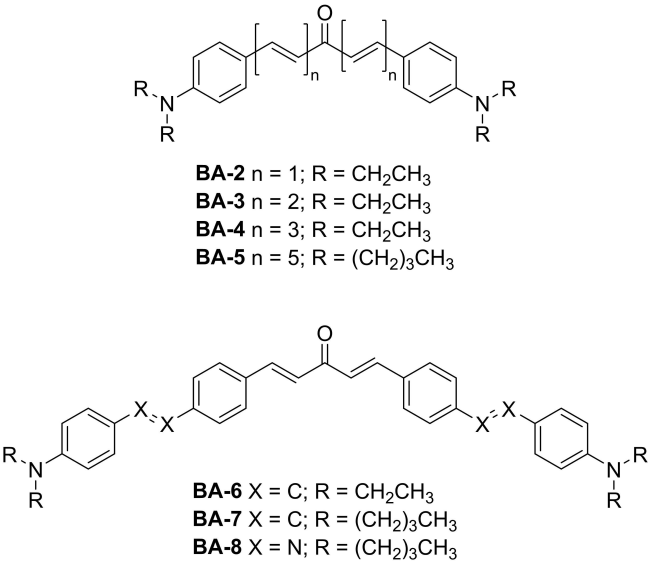

Figure 7. Schematic representation of the structure of benzylidene acetone derivatives with extended π-systems.

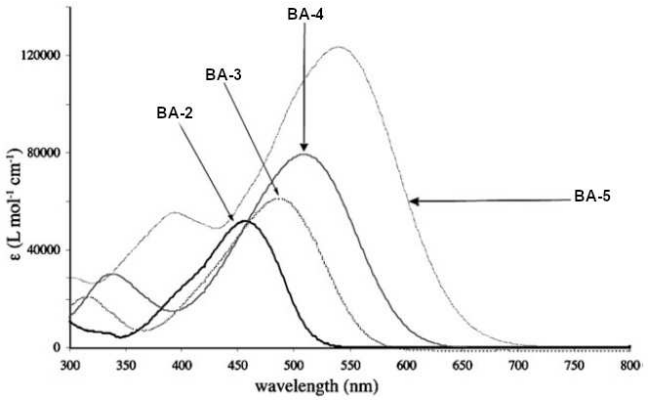

Figure 8. UV spectrum of **BA-2** to **BA-5** in chloroform.[46] Adapted with permission from Ref. [46]. Copyright 2006, Royal Society of Chemistry.

Table 3. Linear- and two-photon absorption properties of **BA1**–**BA-8**.

Molecule	λ_{abs} [nm]	$\lambda^{max}{}_{TPA}$ [nm]	$\sigma^{max}{}_{TPA}$ [GM]
BA-2	456	800	250
BA-3	486	900	325
BA-4	509	950	200
BA-5	540	–	–
BA-6	466	900	200
BA-8	503	–	–

literature reports.[47] This behavior can be explained by the extended charge transfer, which is most evident in the largest molecule. The comparison of the absorption maximum to the chain length also reveals a trend of a saturation curve which indicates that a further extension of the chain would reach a certain absorption maximum threshold.

The situation is similar for the stilbene based derivatives (Figure 9). There is also a bathochromic shift, which is more prominent for **BA-8** due to the more pronounced donor properties of the azo bridges. Although the chain length and the introduction of the stilbene groups have a clear influence on the absorption, the influence on the two-photon cross-section is only slight noticeable (Table 3).

BA-5 and **BA-8** could not be measured due to their low fluorescence, which is necessary for the up-conversion fluorescence measurement. Unfortunately, no data for **BA-7** were reported. The investigations show that the compounds **BA-2** to **BA-8** do receive a two-photon excitation, but no structuring tests were performed to determine the fabrication windows.

As mentioned above, possible cis-trans isomerization processes are one reason for a reduced performance of a photo initiator. By using other central ketones such as cyclopentanone, cyclohexanone, or substituted variants, photo initiators could be produced which have much better processability. Liska et al. met this challenge by producing photo initiators with differently sized cycloalkane ketones (including **BA-1**).[48] These are presented in Figure 10.

The change of the central acceptor ketone to cyclopentanone ketones leads to a bathochromic shift of the linear

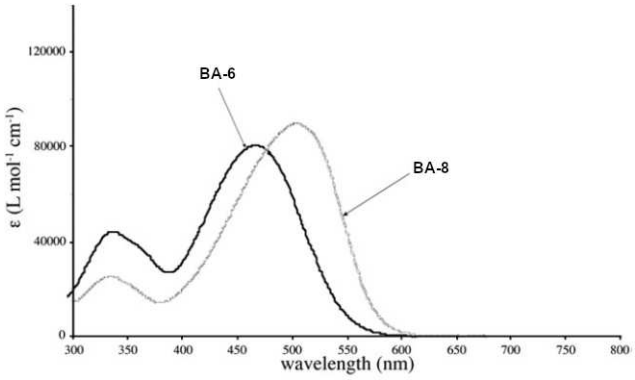

Figure 9. UV-Spectra of **BA-6** and **BA-8** in chloroform.[46] Adapted with permission from Ref. [46]. Copyright 2006, Royal Society of Chemistry.

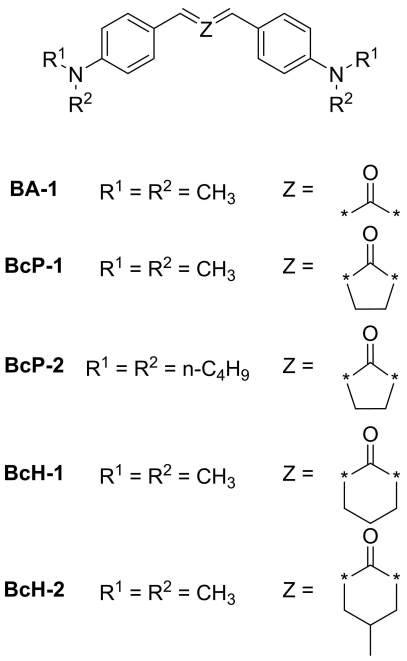

Figure 10. Schematic representation of the structure of various benzylidene photo initiators with different ring sizes.

absorption maxima of the 2PIs **BcP-1** and **BcP-2** compared to **BA-1**. Interestingly the 2PIs with a cyclohexanone central acceptor **BcH-1** and **BcH-2** reveal a hypsochromic shift of the linear absorption maxima (Table 4). Although the structure of **BcH-2** shows a methyl group in the 4-position of the cyclohexanone ring, compared to **BcH-1** the two 2PIs share the same linear absorption behavior. While the change in fluorescence quantum yield between **BA-1** and the cyclopentanone 2PIs only changes slightly, the fluorescence quantum yield for the cyclohexanone 2PIs is significantly decreased. The influence of the ring size on the two-photon cross-section differs from initiator to initiator. While the cyclopentanone derivative of **BA-1**, **BcP-1**, reveal an increase from 349 GM to 466 GM, but the σ_{TPA} value of **BcP-2** is decreased. The increase for **BcP-1** can be explained by the enhanced stiffness and the higher degree of conjugation, while the large *n*-butyl groups of **BcP-2** leads to a distortion of the molecule and, thus, to a deformation of the cyclopentanone ring. This non-planar nature of the ring could negatively influence the conjugation and thus weaken the 2PA. By replacing the cyclopentanone ring with the lager cyclohexa-

Table 4. Photophysical and polymerization data of the photo initiators **BA-1** to **BcH-2.**

Compound	λ_{max} [nm][a]	Φ_{fl}[a]	σ_{TPA} [GM]	FW [mW]
BA-1	441	0.15	349	~8 to 11
BcP-1	466	0.14	466	
BcP-2	481	0.20	327	~9 to 13
BcH-1	432	0.0095	352	
BcH-2	432	0.0095	191	~10 to 25

[a] Measured in dichloromethane.

none in **BcH-1** the σ_{TPA} value increases only slightly, however the introduction of a methyl group in the 4-position, as in **BcH-2**, decreases the σ_{TPA} drastically. Thus, Liksa et al. could show that not only the ring size of the central cycloalkane ketone but also the substitution of the ring has a decisive role on the TPA properties of a photo initiator. To determine the initiation efficiency of the initiators, whole 3D structures were abdicated under different laser intensities and different writing speeds instead of line tests. For this purpose, woodpile structures (lateral dimming: 50×50 μm, 5 μm hatch distance, 0.7 μm layer distance), made of the same polymer mixture as used with **BA-1**, were written. With the exception of **BcH-2**, which was tested with 0.2 wt%, all structures were used with a molar 2PI concentration of 6.3×10^{-6} mol 2PI/g resin. To illustrate the initiator efficiency, the results with different laser intensities (1 to 30 mW) at a writing speed of 50 μm/s are described. As mentioned above, **BA-1** has a rather small fabrication window. The change to the cyclopentanone moiety to **BcP-1** led to a drastic reduction of the solubility in the monomer, which could not be improved by the addition of different organic solvents and thus was not suitable for structuring. By exchanging the methyl substituents with *n*-butyl ones the solubility could be significantly increased and thus **BcP-2** revealed a slightly wider processing window than **BA-1**, allowing the production of structures with good stability within a laser intensity of about 9 to 14 mW. This slight increase can be attributed to the higher stiffness of the ring, which limits the possible cis/trans isomerization processes of the double bonds. Similar to **BcP-1**, **BcH-1** also shows problems with solubility, so that an exact evaluation of the initiator properties was not possible. However, the introduction of the methyl group significantly increased the solubility. Although **BcH-2** has the smallest σ_{TPA} of the mentioned initiators (191 GM) it reveals a wide processing window (approx. 10 to 25 mW). Remarkable about **BcH-2**, besides the lowest TPA, is that its fluorescence quantum yield is 5 to 10 times lower compared to that of the other initiators. Although σ_{TPA} plays a certain role in initiating efficiency, it is not the decisive factor. Low fluorescence quantum yields are essential for efficient photo initiators because this leads to lower radiation deactivations and, thus, to a higher population of the active state for initiating polymerization. This observation has also been made by other research groups.[49] In addition to the wide processing window, **BcH-2** also showed an extremely fast processability. A model F1 racing car ($285\times130\times50$ μm^3) was structured with a 0.2 wt% of **BcH-2** solution within 4 min, which corresponded to a writing speed of about 80 mm/s.[48] Recent reports revealed that **BcH-2** has been used for the fabrication of large complex 3D structures up to a volume of 292 mm^3, so called buckyballs, for cell cultivation with a writing speed of 1000 mm/s (Figure 11).[50–51]

Based on these results, several other groups investigated the influence of the ring size on the initiator performance. The 2PIs displayed in Figure 12, possess a larger π-system with more aryl moieties. Also the influence of triple bonds compared to double bonds has been investigated.[33]

The linear absorption measurements were performed in toluene and benzonitrile. Although structurally very similar, the spectrum for **BcB-2** reveals a bathochromic shift compared to **BcB-1**, in toluene as well as in benzonitrile. The installation of the stilbene unit in the different ketones shows the clear influence of the central ketone. While compared to **BcB-1/2** a small hypsochromic shift can be seen at **BcB-3**, a very clear blue shift from small to large ring size is observed (**BcB-3**- > **BcP-3**- > **BcH-3**). The photophysical data are summarized in Table 5. Looking at the values for **BcP-3** and **BcP-4** it is visible that a

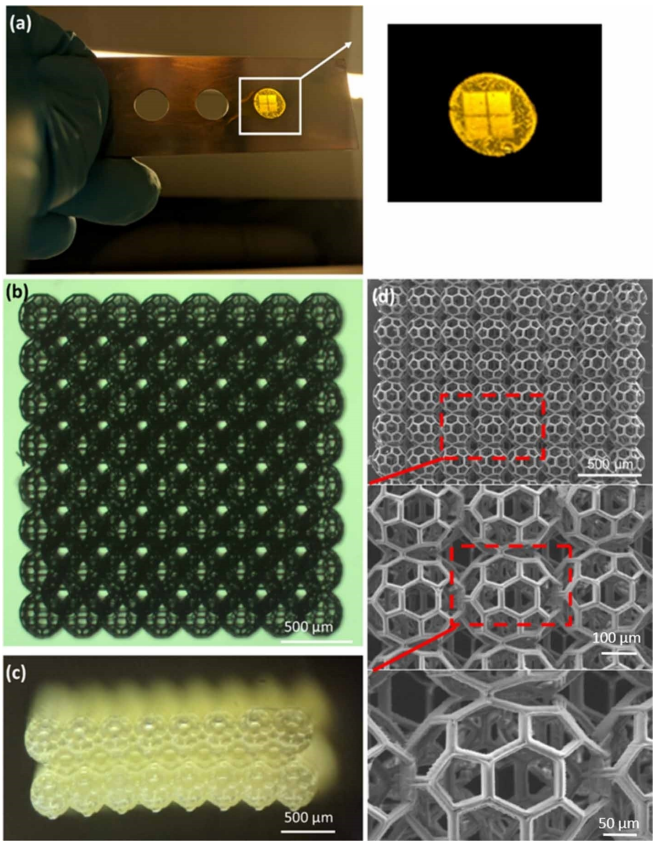

Figure 11. Fabricated scaffolds using **BcH-2**. (a) Sample holder with the polymerized structure embedded in the resin. (b) Top view and (c) side view of the fabricated buckyball scaffold. (d) SEM images of the scaffold at serval magnifications.[50] Republish with permission of Ref. [50]. Copyright 2020, IOP Publishing.

Table 5. Photophysical properties of **BcB-1** to **BcP-4** in toluene and benzonitrile.

Compound	Solvent	λ_{abs} [nm]	λ_{em} [nm]	$\Delta\nu$ [cm^{-1}]	Φ_{fl}
BcB-1	toluene	476	530	2100	0.16
	benzonitrile	488	591	3600	0.36
BcB-2	toluene	477	533	2200	0.19
	benzonitrile	503	591	3100	0.29
BcB-3	toluene	476	583	4300	0.74
	benzonitrile	488	705	6300	< 0.01
BcP-3	toluene	466	556	3500	0.72
	benzonitrile	487	764	7400	< 0.01
BcH-3	toluene	444	540	4000	0.40
	benzonitrile	460	742	8300	< 0.01
BcP-4	toluene	440	536	4100	0.14
	benzonitrile	458	793	9200	< 0.01

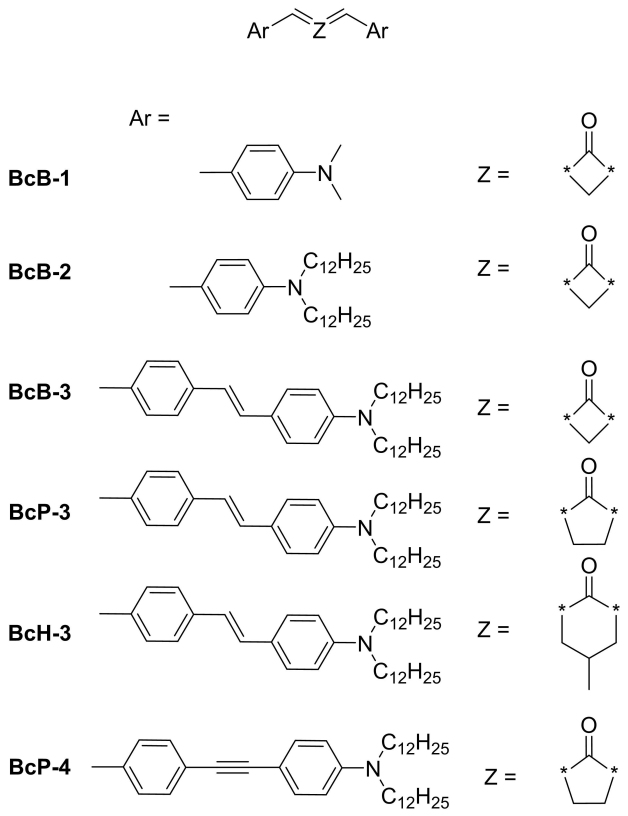

Figure 12. Schematic representation of the structure of 2PI with different ring sizes of the central ketone and various substituents reported by Nazir et al.

hypsochromic shift occurs due to the influence of the triple bond, because they are less polarizable in contrast to double bonds a reduction of the HOMO - LUMO gap is resulting.[52] The influence of the ring size can also be seen in the fluorescence quantum yields. The yields in toluene decrease with increasing ring size (Table 5). The increasing ring size gives the molecules a higher flexibility, which promotes the non-radiative relaxation of electronically excited states. It should also be noted that for **BcB-3**, **BcP-3**, **BcH-3** and **BcB-4**, fluorescence quantum yields decrease dramatically to less than 1% as the polarity of the solvent increases. These results indicate that an almost complete charge separation takes place for the 2PIs mentioned.

The σ_{TPA} values range from 50 to 370 GM and are thus many times larger compared to the frequently used **BDAB** (Table 6). Already the introduction of a longer alkyl chain leads to an increase, in this case even a doubling of the σ_{TPA}- value.[43] Compared to **BcP-1**, the cyclobutanone derivative **BcB-1** reveals a much lower value, but the two values were determined in different solvents, making comparability difficult. Compared to the studies with the 2PIs from Liska et al. (Figure 10), the results with a different π-system show another trend. Here the σ_{TPA} value increases with increasing ring size instead of decreasing. **BcP-4** with cyclopentanone as central ketone shows the highest value, which can be explained by blocking of the cis/trans isomerization in the stilbene unit with the triple bond. To determine the fabrication windows, the compounds and **BDAB** were tested at 1 wt% each with the hybrid material ZPO/MAPTMS (Figure 13).[40]

The compounds **BcP-3** and **BcP-4** display the widest fabrication windows compared to all other 2PIs. It can be assumed that an enlargement of the π-system has a positive effect on the manufacturing range. The advantage of the broad fabrication window of **BcP-4** is shown by a series of fabricated cubes where different laser intensities were used at constant writing speed (Figure 14).

Similar investigations were also carried out for the carbazole derivatives of cycloalkane ketones.[53] For this purpose, carbazole compounds were modified with 2-(ethyl)hexyl chain and reacted with cyclobutanone, pentanone and 4-methylhexanone to form the respective photo initiators (Figure 15).

As above also for carbazole benzylidene derivatives, a trend can be seen between the absorption behavior and the ring size. For example, a hypsochromic shift in the UV spectrum (chloroform) from cyclobutanone derivative with 442 nm (**BcB-4**) to 4-methyl-cyclohexanone derivative with 418 nm (**BcH-4**) is observed. The fluorescence emission spectra reveal different values for each compound (Table 7).

Concerning two-photon cross-sections the cyclobutanone **BcB-4** shows a value of 357 GM, when the ring size is increased,

Table 6. σ_{TPA} Values of the compounds **BcB-1** to **BcP-4** measured by Z-scan at 800 nm.

Compound	Solvent	σ_{TPA} [GM]	Conc. [mol L^{-1}]
BcB-1	CH_2Cl_2	70	0.05
BcB-2	CH_2Cl_2	140	0.01
BcB-3	CH_2Cl_2	50	0.01
BcP-3	CH_2Cl_2	130	0.01
BcH-3	CH_2Cl_2	200	0.01
BcP-4	CH_2Cl_2	370	0.01
BDAB	1-propanol	7	7

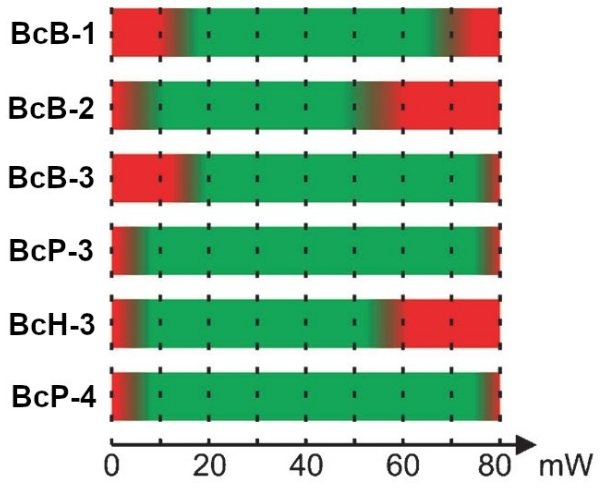

Figure 13. Fabrication windows of **BcB-1** to **BcP-4**. The low-power end shows polymerization thresholds, whereas the burning threshold is represented in the high-power end of the scale (red). The green area represents the ideal laser intensities for the fabrication of stable structures.[33] Adapted with permission of Ref. [33]. Copyright 2015, John Wiley and Sons.

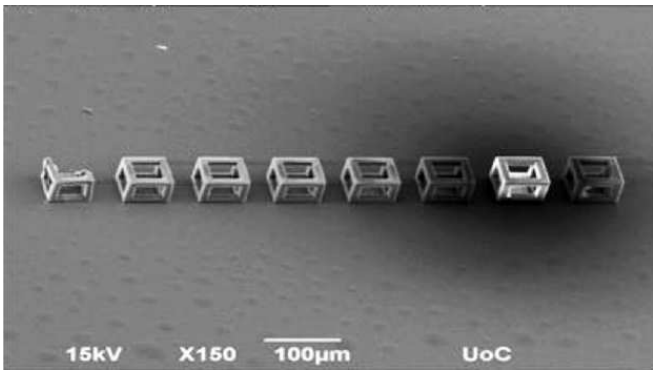

Figure 14. 3D dice structures constructed applying different laser powers, with **BcP-4**.[33] Adapted with permission of Ref. [33]. Copyright 2015, John Wiley and Sons.

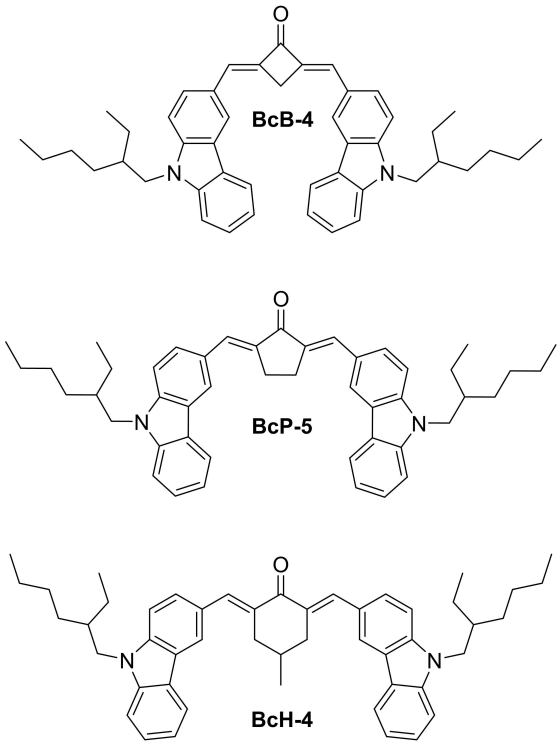

Figure 15. Schematic representation of the chemical structures of carbazole benzylidene derivatives.

Table 7. Photophysical data of the carbazole benzylidene cycloketones.

Compound	λ_{max}(< 400 nm) [nm]	λ_{em} [nm]	Stokes shift [cm^{-1}]	ε_{max} [10^4 M^{-1} cm^{-1}]	σ_{TPA} [GM]
BcB-4	442	533	3862	5.08	357
BcP-5	438	515	3413	5.16	377
BcH-4	418	560	6066	5.20	340

the σ_{TPA} rises to the highest measured value of 377 GM (**BcP-5**). Similar to the results of Liska et al.,[48] a further enlargement of the ring (**BcH-4**) lowers the σ_{TPA} value, in this case to 340 GM. To determine the fabrication window, the respective photo initiators were tested in a concentration of 1.3×10^{-6} mol/g resin in a 1:1 mixture of trimethylolpropane triacrylate (TMPTA) and ethoxylated trimethylolpropane triacrylate (TMP3EOTA). The 2PI was excited at a wavelength of 780 nm and structures were written at a speed of 750 µm/s. The initiators **BcB-4** and **BcH-4** show almost the same FW despite different GM values (approx. 12 to 28 mW for **BcB-4** and approx. 12 to 27 mW for **BcH-4**). In comparison, **BcP-5** reveals a quite extended FW of 10 to 29 mW. In addition to the structuring tests, **BcP-5** was used to write smaller and more complex structures such as a 3D microstructure of the Great Wall of China (Figure 16).

Coumarin derivatives have proven to represent promising compounds in recent years. Dyes on coumarin bases are well-known as highly efficient photosensitizers and are used in the field of UV curing. When excited by light, they are able to excite other co-initiators by electron transfer or to initiate polymerizations themselves.[54–58] Xue et al. and Nazir et al. investigated asymmetric and symmetric coumarin derivatives for their linear and two-photon absorption behavior.[32,59–60] In addition, compounds with different bridging positions were prepared to investigate their properties in more detail.[60] The obtained cumarinylated cycloketones are shown in Figure 17.

Comparing the linear absorption spectra of the coumarin containing 2PIs a bathochromic shift occurs for the symmetric structures (**BcP-7**, **BcP-9**, **BcH-5**) compared to the asymmetric ones (**BcP-6** and **BcP-8**). In case of the two-photon absorption the σ_{TPA} values differ significantly from each other. While the discrepancy between the asymmetric (**BcP-6**) and the symmetric (**BcP-7**) PI is 90 GM, the change of the bridging position (**BcP-6** vs. **BcP-8**) reveals a greater difference (Table 8). A much larger difference is observed for the cyclopentanon 2PI **BcP-9** and 4-methy-cyclohexanon 2PI **BcH-5**, in contrast to the results from Liska et al.[45] the change of the central acceptor to the larger 4-methyl-cyclohexanon ring let to a drastic increase of the σ_{TPA} value.

2PP tests with 0.4 wt% **BcP-6** and **BcP-8** showed that the threshold energy E_{th} is 99 and 198 µW respectively (Table 8). Normally, initiator concentrations of 1 to 2 wt% are common for

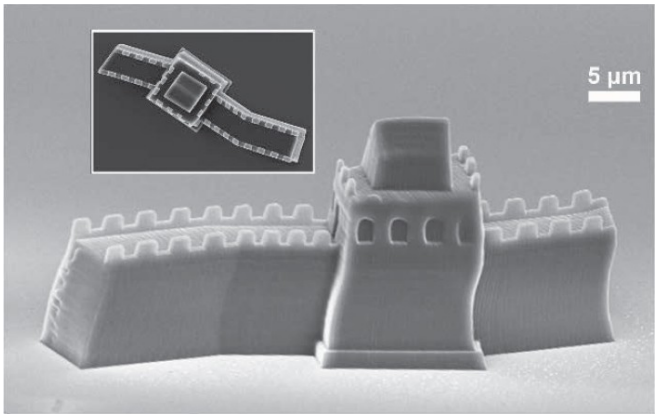

Figure 16. SEM micrograph of the Great Wall of China fabricated with **BcP-5**.[53] Adapted with permission of Ref. [53]. Copyright 2019, SPST.

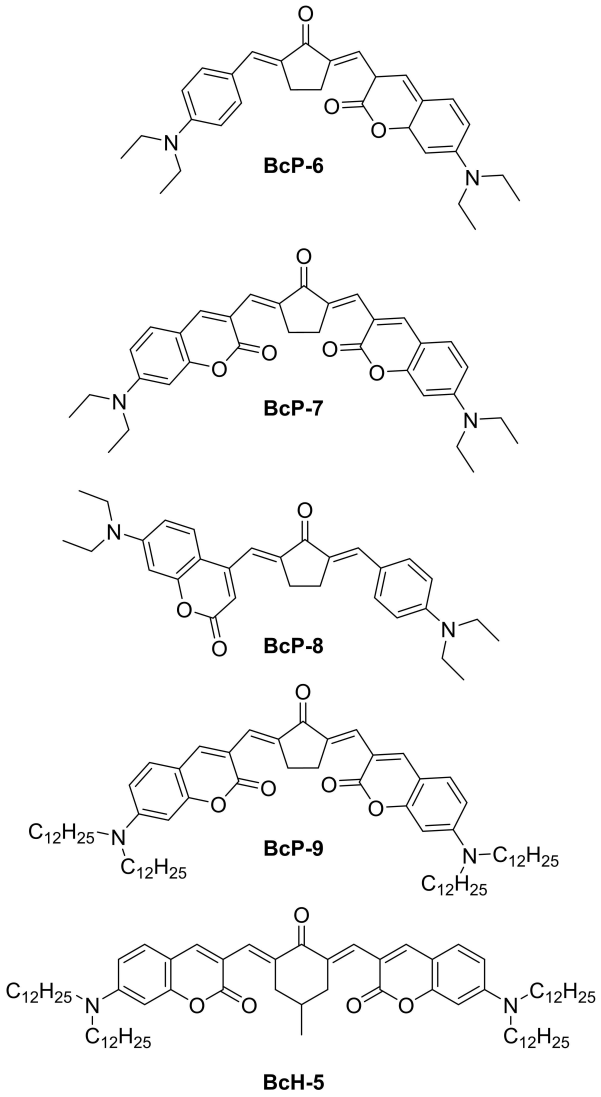

Figure 17. Schematic representation of the structures of the coumarin based benzylidene cycloketones.

Table 8. Photophysical and polymerization data of the photo initiators **BcP-6** to **BcH-5**.

Compound	λ_{max} [nm]	Φ_{fl}	σ_{TPA} [GM]	FW [mW]	E_{th} [μW]
BcP-6	500[b]	0.09	300[d]		99
BcP-7	521[b]	0.15	390[d]	1.05 to 3.39[g]	
BcP-8	471[b]	0.05	199[d]		198
BcP-9	605[a]	0.313	60.0 ± 1.2[c]	~10 to 46	
BcH-5	582[a]	0.078	401.0 ± 8.0[c]	~10 to 44	

[a] Measured in dichloromethane, [b] measured in chloroform, [c] measured via Z-scan technique at 800 nm, [d] measured at 780 nm, [e] measured with 0.1 wt% of the 2PI, [f] maximum of the σ_{TPA} measurement and [g] measured with 0.1 wt% 2PI.

2PP, but the low E_{th} of **BcP-6** and **BcP-8** allows a significant reduction of the concentration and, therefore, the amount of remaining initiator in the later structure. Thus, it was possible to write a complex microstructure (Figure 18) even with this low concentration. Although the FW of **BcP-7** is in the range of 1.05

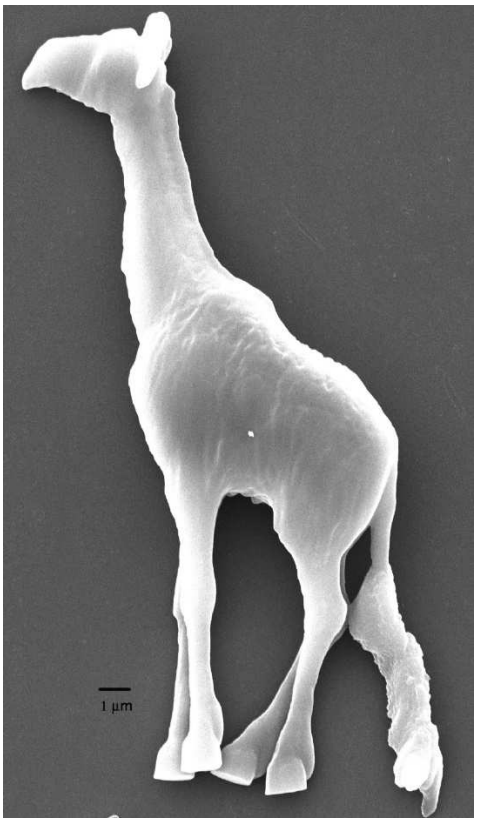

Figure 18. 3D model structure of a giraffe fabricated with **BcP-6** at 163 μW laser power and 110 μm/s writing speed.[60] Reproduced with permission from Ref. [60]. Copyright 2010, American Chemical Society.

to 3.39 mW, it has a higher E_{th}, so polymerizations could be carried out even with a small concentration of 0.1 wt%. Polymerizations were also possible with even lower concentrations but the laser power had to be increased to trigger them. Despite the high σ_{TPA} value and the low fluorescence quantum yield, **BcH-5** reveals a slightly smaller fabrication window compared to **BcP-9**. While **BcP-9** trigger polymerization between 10 to 47 mW, structures made with **BcH-5** show damage and malformations above 44 mW. Both compounds were also tested for their biocompatibility. Preosteoblastic MC3T3-E1 cells were used, which were applied to films of PLA (polylactic acid) doped with different initiators and incubated. The results show for both initiators a viability of the cells up to 100% after seven days incubation, which suggests that the compounds are biocompatible and suitable for applications in tissue engineering.

The photo initiator **BcP-10** (Figure 19) with its dimethylamino substituted naphthalene residues also has an extended π-system similar to the coumarin benzylidenes.[61] The linear absorption in dichloromethane shows two maxima at 362 nm and 502 nm. In comparison to **BcP-1** (466 nm, CH_2Cl_2) a clear bathochromic shift is observed. Furthermore, **BcP-10** reveals a very high Stokes shift of 4700 cm^{-1}, which is caused by the geometric change from non-planar in ground state to planar in the excited state. It is interesting to note that **BcP-10** has one of

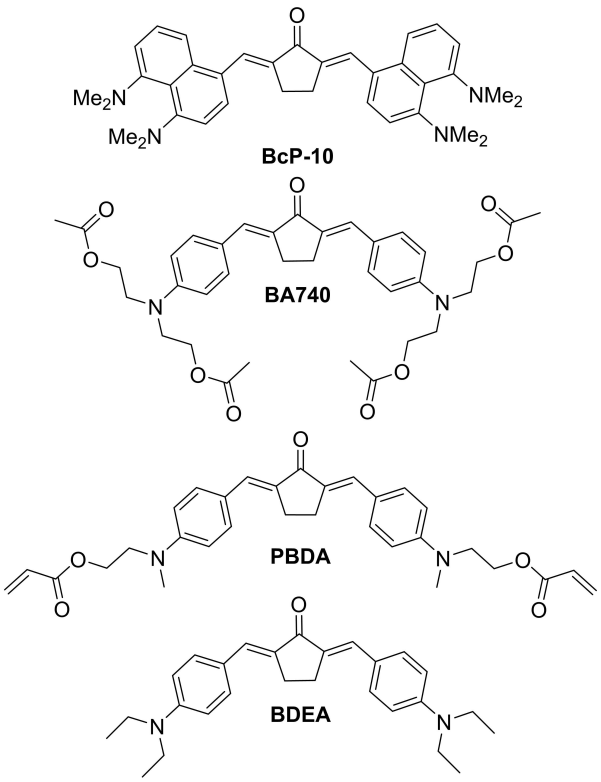

Figure 19. Schematic representation of the structures of **BcP-10**, **PBDA**, **BA740** and **BDEA**.

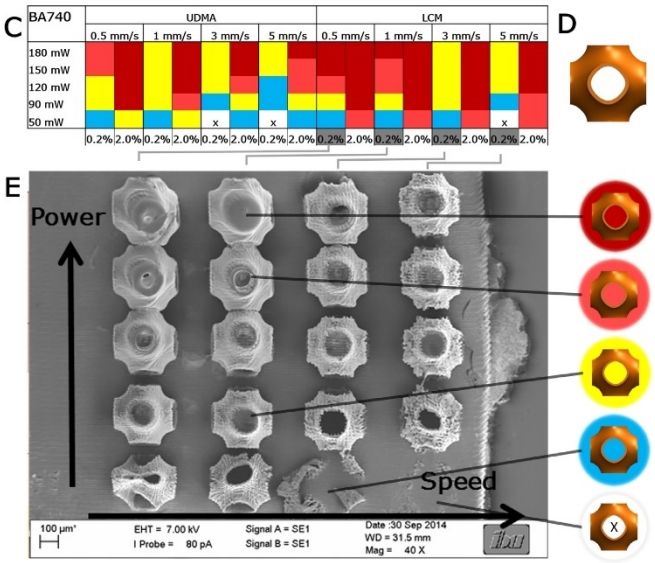

Figure 20. Structuring tests with **BA740** (0.2 %) in LCM. Representative SEM micrograph (plant view of SchwarzP unit cells with 250 µm). The colored circles represent the obtained results in the heat map. Dark red: Bulk polymerization, loss of structure. Red: Bulk polymerization is sealing the pores. Yellow: Most precise 3D SchwarzP structure, best TPP writing conditions. Blue: Polymerized structures are not stable/load bearing. With x: Not a single trace of polymerization, no TPP writing possible.[62] Reproduced with permission from Ref. [62]. Copyright 2017, John Wiley and Sons.

the lowest fluorescence quantum yields (0.11 %) among the benzylidene cyclopentanones. The two-photon absorption spectrum shows the maximum at 725 nm and the σ_{TPA} value was determined to be 600 GM. This value is significantly larger compared to the 466 GM of **BcP-1** (Figure 10), which can be explained by the different geometry of the molecule as well as the higher number of π-electrons. Polymerization tests were performed with an organic-inorganic silicate mixed with zirconium[40] and show for **BcP-10** a fabrication window of about 7 to 48 mW at a constant speed of 2 mm/s.[61] Since many photo initiators have problems with their solubility in monomer solutions, Poocza et al. developed the **BA740** photo initiator for the polymerization of the lactide-caprolactone-methacrylate (LCM)[62] system, keeping the maxim "like dissolves like". This was achieved by modifying the terminal hydroxyethylamio groups with acetic anhydride. The ester groups introduced in this way acted as solubility mediators for the LCM system. The σ_{TPA} value of **BA740** is 177 GM (805 nm, $CHCl_3$) and is smaller than that of **BcP-1** for this system (315 GM). However, the fluorescence quantum yield for **BA740** is 6.4 %, which is significantly lower compared to **BcP-1** with 12.5 %. For the structuring tests, so-called SchwarzP cells were fabricated, as this structure is a potential candidate for porous biomimetic scaffolds. Figure 20 displays the results of the writing tests at different writing speeds and laser powers. Although a higher laser power is required compared to other polymerizations and initiator mixtures, **BA740** reveals a significantly wide fabrication window of 50 to 180 mW at a constant writing speed of 3 mm/s and low 2PI concentration of 0.2 wt%. Figure 20 shows that structures can also be written at higher speeds, although the fabrication window narrows.

BA740 also was used in the fabrication of a newly introduced macromonomer based on poly(2-oxazoline)s PEtOx-DA for 2PP. In combination with the photo initiator **BA740** and the new macromonomer several investigations were performed and showed that highly precise 3D-microstructures in from of spiderwebs could be fabricated.[8,63]

Huang et al. took advantage of the easy chemical modifiability of the terminal amino residues, similar to **BA740**. The authors equipped the photo initiator **PBDA** with acryloyl groups, aiming to bind it to the produced gel during polymerization and thus limit its release or mobility.[64] For evaluation purposes **PBDA** was compared with **BDEA**, a compound which exhibits a large σ_{TPA} value of 465 GM.[49] The linear absorption spectrum of **PBDA** shows a bathochromic shift in the maximum at 473.5 nm compared to **BDEA** (Table 9). The fluorescence quantum yield of **PBDA** is 0.108 and therefore lower than the quantum yield of BDEA with 0.141. The Z-scan in DMF gave an σ_{TPA} value of 410 GM at 820 nm, which is lower than that of **BDEA**. Structuring tests with different mixtures of **PBDA/BDEA** and the monomers trimethylolpropane ethoxylate triacrylate (ETPTA) and polyethylenglycol diacrylate (PEG-DA 400) resulted in a fabrication window of 0.13 to 9.31 mW for **PBDA** and 0.09 to 5.84 mW for **BDEA**. Figure 21 shows a gear structure written with **PBDA**.

Table 9. Photophysical and polymerization data of the photo initiators **BcP-6** to **BcH-5**.

Compound	λ_{max} [nm]	Φ_{fl}	σ_{TPA} [GM]	FW [mW]
BcP-10	362/502[a]	0.011	600[d]	7–48 [g]
BA740	–	0.064	177[e]	50–180[h]
PBDA	473.5[c]	0.108	410[f]	0.13–9.31
BDEA	487[c]	0.141	465[f]	0.09–5.84

[a] Measured in dichloromethane, [b] measured in chloroform, [c] measured in DMSO, [d] measured via Z-scan at 725 nm, [e] measured via Z-scan, [f] measured via TPEF in range of 750 to 880 nm, [g] FW at a writing speed of 2 mm/s and [h] FW at a writing speed of 3 mm/s.

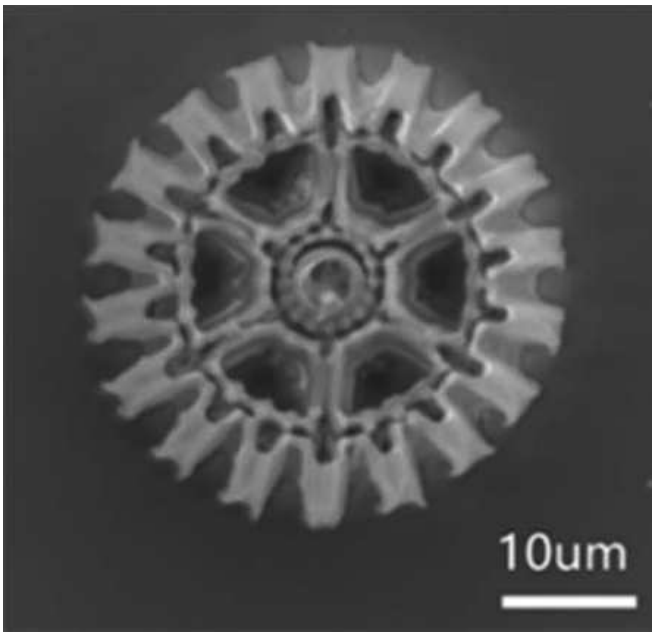

Figure 21. Gear structure fabricated with **PBDA** and PEG-DA 400 as monomer.[64] Reproduced with permission from Ref. [64]. Copyright 2019, Royal Society of Chemistry.

The migration of **PBDA** and **BEDA** was investigated by inserting polymer structures which were prepared and then crushed into DMSO. The samples were soaked for seven days and the absorbance of the extracts were measured at 480 nm. For **PBDA** the absorbance was severely lower compared to **BDEA**, which indicates that PBDA is mostly linked to the polymer backbone. Biocompatibility tests with L929 cells on polymeric tablets revealed a reduced viability of the cells grown on the structures produced with **BDEA** (~85%) after 48 h compared to the control group. The viability of the cells seeded on structures written with **PBDA** remained unchanged at 100%, indicating a significantly lower cytotoxicity due to the covalent binding of **PBDA** to the polymer scaffold.

2.3. Alkinone

As mentioned in the previous chapters (Chapters 2.1. & 2.2.), cis/trans isomerizations of double bonds are a disturbing process and the performance of the initiator might be impaired. Inspired by the good properties of 1,5-diphenylpenta-1,4-diyn-3-one (**DPD**) in single photon photo polymerization, various derivatives of **DPD** have been developed.[65–67] Several compounds with auxochromic groups have been prepared and investigated (Figure 22).

To improve the properties of **DPD** in two photon polymerization, donor groups were introduced at the terminal phenyl groups. As shown in Figure 22, the focus was mainly on amino derivatives, as these groups possesses a high donor strength.

With increasing donor property of the groups (OMe < SMe < NMe_2 < NBu_2 < NPh_2) the linear absorption maxima is bathochromically shifted (Table 10). The shifts are particularly strong for the amino-derivatives, as these have a strong influence on the system. The fluorescence quantum yields are very small for all compounds. Only **P3 K** and **O–DPD** show very weak fluorescence quantum yields, for **S–DPD** no values are reported regarding Φ_{fl} and σ_{TPA}. The two photon cross-sections reveal a clear trend, which was also observed for the linear absorptions. The σ_{TPA} value increases with increasing donor strength. **DPD** itself showed no measurable absorption in the two-photon spectrum and **O–DPD** a very low value. It is interesting to see that **P3 K** with 256 GM has a higher value than **B3 K**. Although the donor strength of diarylamino groups is smaller, their increased number of π-electrons can lead to an increase in the σ_{TPA} value.[26] Heller et al. were the first to test the 2PIs **O–DPD**, **S–DPD** and **N–DPD** for their properties in 2PP. A 1:1 mixture of Genomer 1330 (trimethylolpropane triacrylate) and Sartomer 415 (ethoxylated trimethylolpropane triacrylate) as monomer solution was used and polymerized at a constant speed of 1 mm/min (Figure 23).

The fabrication of complex microstructures with **N–DPD** was performed at different laser intensities and resulted in stable structures at any laser intensity. In comparison the

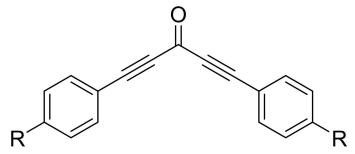

DPD R = H **S-DPD** R = SMe
O-DPD R = OMe **N-DPD** R = NMe_2
P3K R = NPh_2 **B3K** R= NBu_2

Figure 22. Schematic representation of the structures of alkinone based 2PIs.

Table 10. Photophysical data of the alkinone based 2PIs.[45,67]

Compound	λ_{MAX} [nm] (MeCN)	λ_{EM} [nm]	Φ_{fl}	σ_{TPA} [GM]
DPD	322		0.00	
O–DPD	352	526	0.02	< 10
S–DPD	375			
N–DPD	435		0.00	165
P3 K	438	650	8×10^{-4}	256
B3 K	449		0.00	238

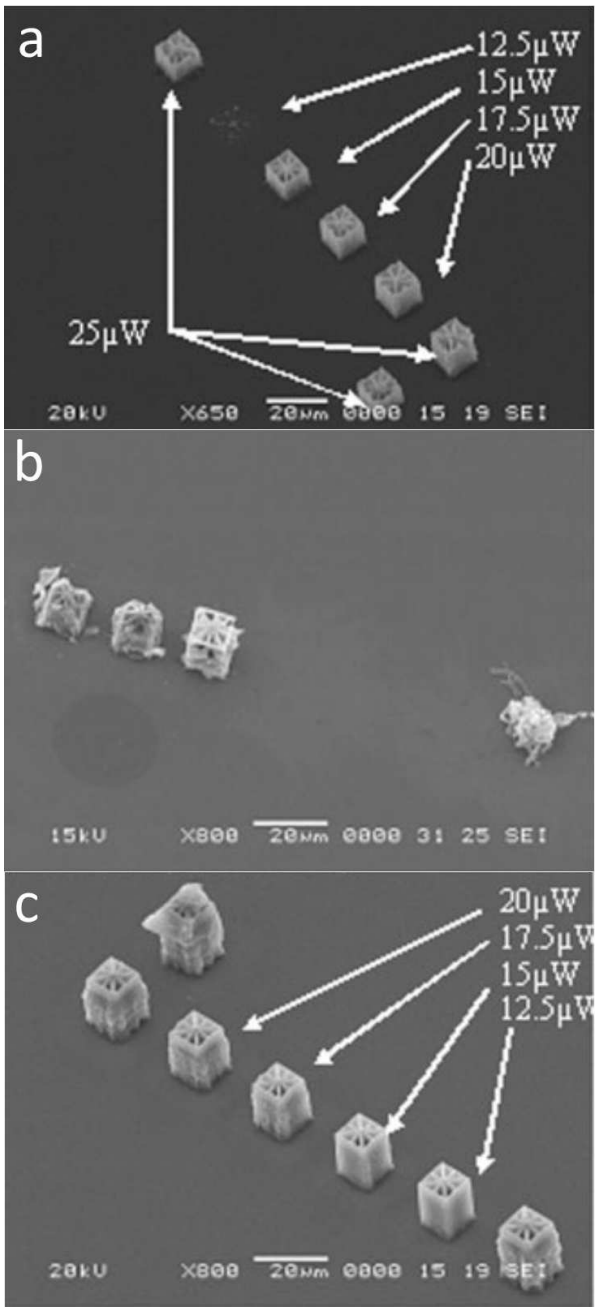

Figure 23. Fabrication tests with a) **O**–**DPD**, b) **S**–**DPD** and c) **N**–**DPD** at 0.025 wt%.[67] Adapted with permission from Ref. [67]. Copyright 2007, John Wiley and Sons.

fabrication of stable and precise structures with **O**–**DPD** was only possible at higher laser intensities. Structures fabricated with **S**–**DPD** show clear structure defects. Pucher et al. have additionally investigated the influence of longer side chains (**B3 K**) and phenyl groups (**P3 K**) on the fabrication properties.[45] The authors used the same monomer system and were able to define the fabrication windows for the respective 2PIs more precisely.[45] **S**–**DPD** was not examined more closely in this process. The resulting fabrication windows to obtain well-defined structures are listed in Table 11.

Table 11. Fabrication windows of the alkinone based 2PIs.

Compound	Laser intensity [μW]
DPD[a]	~5 to 15
O–**DPD**[b]	~40 to 65
N–**DPD**[b]	~12.5 to 35
P3 K[b]	~8 to 35
B3 K[b]	~5 to 31

[a] Polymerization at 600 nm; [b] Polymerization at 800 nm.

It is evident that all amino derivatives require significantly lower laser intensities and have a broader FW. A complex 3D model of a dragonfly was fabricated using **B3 K** as initiator (Figure 24). Thereby the overhanging wings of the dragonfly were structured without losing structural integrity.

2.4. Anthraquinone and fluorenone

Anthraquinones and fluorenone derivatives are known as dyes for a very long time. Their acceptor properties make them interesting for many different applications, for example as dyes in solar cells.[68–69] Furthermore, anthraquinone derivatives are well established in single photon photopolymerization.[70] Two-photon fluorescence dyes with an anthraquinone unit are also known to literature.[71–76] Their good chemical modifiability makes them interesting candidates as photo initiators in two-photon polymerization.

The two compounds **AQ**–**N** and **AQ**–**O** (Figure 25) represent two stilbene substituted variants of anthraquinones.[77] The effect of the different donor strength is clearly visible in the linear absorption of the two compounds. **AQ**–**N** with 492 nm reveal a clear red shift compared to **AQ**–**O** (424 nm). The determined fluorescence quantum yields show a lower yield for **AQ**–**N** ($\Phi_{fl} = 0.018$) compared to **AQ**–**O** ($\Phi_{fl} = 0.043$), can be explained by charge-transfer bimolecular quenching.

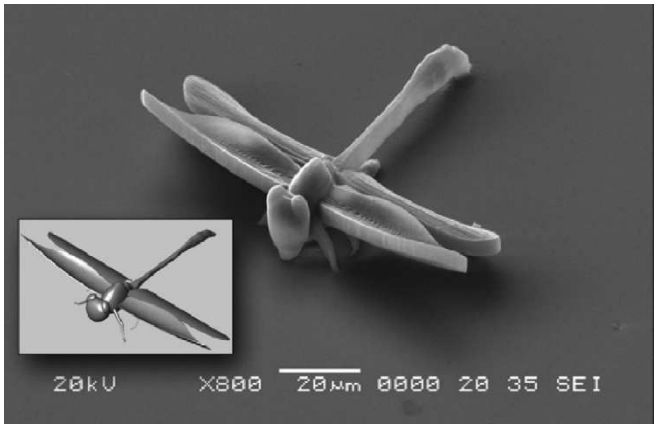

Figure 24. Dragonfly model fabricated by 2PP with **B3 K** as 2PI.[45] Reproduced with permission from Ref. [45]. Copyright 2009, American Chemical Society.

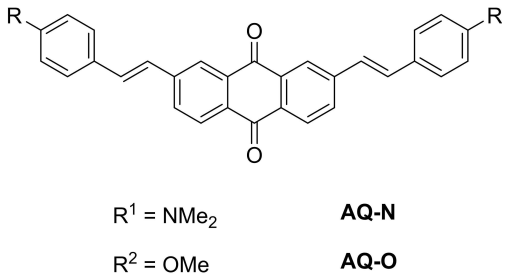

Figure 25. Schematic representation of the chemical structures of **AQ**–**N** and **AQ**–**O**.

AQ–**N** has an enormous value of 1635 GM at 800 nm, a very large value compared to other initiators, while the σ_{TPA} value of **AQ**–**O** decreases to 995 GM. Fabrication tests with 0.2 wt% **AQ**–**N** and **AQ**–**O** revealed a lower polymerization limit of 3.67 mW and 8.03 mW, respectively, at a constant speed of 10 μm/s. Line tests were carried out to determine the processability. The line sizes were examined at different laser intensities and three different writing speeds (10, 30 and 50 $\mu m\,s^{-1}$) (Figure 26). As already observed in other studies, the line width decreases with increasing speed due to the shortened exposure time. Also, the line propagation due to increasing laser intensities has been observed several times. The comparison between **AQ**–**N** and **AQ**–**O** at a laser intensity of 8.03 mW (lower polymerization limit for **AQ**–**O**) shows that with **AQ**–**N** at this power, the lines produced are wider than with **AQ**–**O**. Those results indicate that **AQ**–**N** generates more radicals at the given intensities compared to **AQ**–**O**, what can be attributed to its higher σ_{TPA} value as well as lower fluorescence quantum yield.

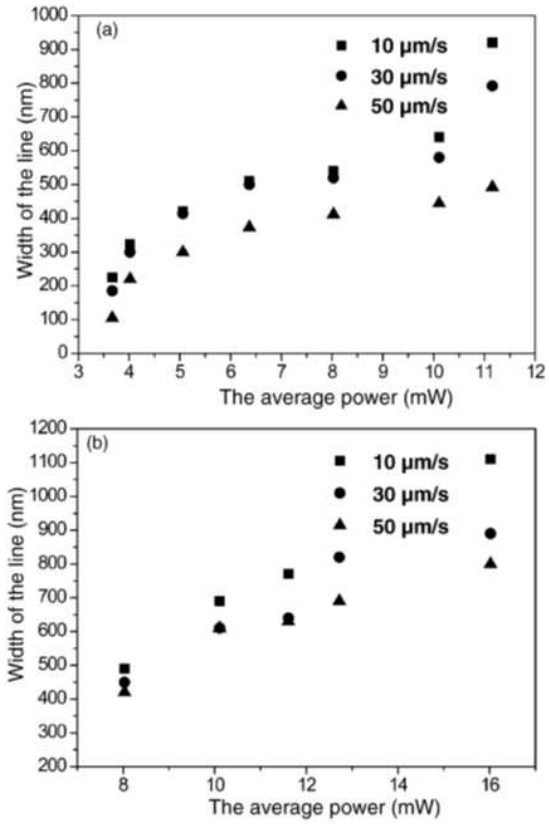

Figure 26. Line width dependence versus the average laser power for **AQ**–**N** (a) and **AQ**–**O** (b).[77] Adapted with permission from Ref. [77]. Copyright 2007, Elsevier.

Figure 27 displays the structures of **B3AN** and **BB3AN**.[43] In contrast to **AQ**–**N** and **AQ**–**O** the substitution pattern is different (positions 2 and 6 modified) and instead of a double bond triple bonds were introduced. The terminal amino groups carry *n*-butyl or a branched ethyl pentyl residue instead of methyl groups. The linear absorption spectrum of **B3AN** in dichloromethane exhibits a maximum at 485 nm. Although **B3AN** shows no visible fluorescence in dichloromethane, the fluorescence increases with increasing polarity of the solvent. Unfortunately, no linear measurements were reported on **BB3AN**. The measured two-photon cross-sections show a value of 235 GM for **B3AN** and 250 GM for **BB3AN**. In comparison to **AQ**–**N**, these values are significantly lower since the triple bond should avoid unwanted cis/trans isomerization and therefore increase the two-photon cross-section. The lower σ_{TPA} may also be due to the different substitution pattern of **B3AN** and **BB3AN**. Structuring tests were performed with a 1 : 1 mixture of TTA and ETA. It turned out that **B3AN** was not soluble in the monomer solution and, therefore, no structuring tests were possible. The introduction of branched alkyl chains resulting in **BB3AN**, revealed a slightly increased solubility, but very high laser intensities were necessary for the polymerization. Suitable structures could be fabricated with **BB3AN** only in a very narrow fabrication window of 22 to 24 mW.

Related to **B3AN** and **BB3AN**, the fluorenones **B3FL**, **BB3FL** and **3,6-B3FL** are designed in a similar way (Figure 28). Although equipped with the same substituents, they differ in their symmetry. While the anthraquinones are inversion-symmetrical, the fluorenones are mirror-symmetrical. In addition, the fluorenones are substituted in different positions. While

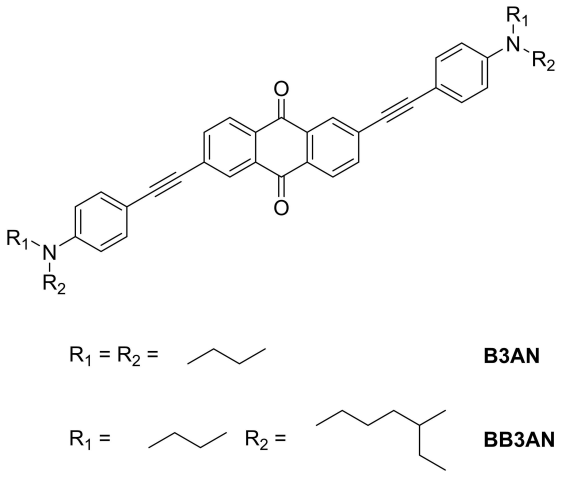

Figure 27. Schematic representation of the structure of **B3AN** and **BB3AN**.

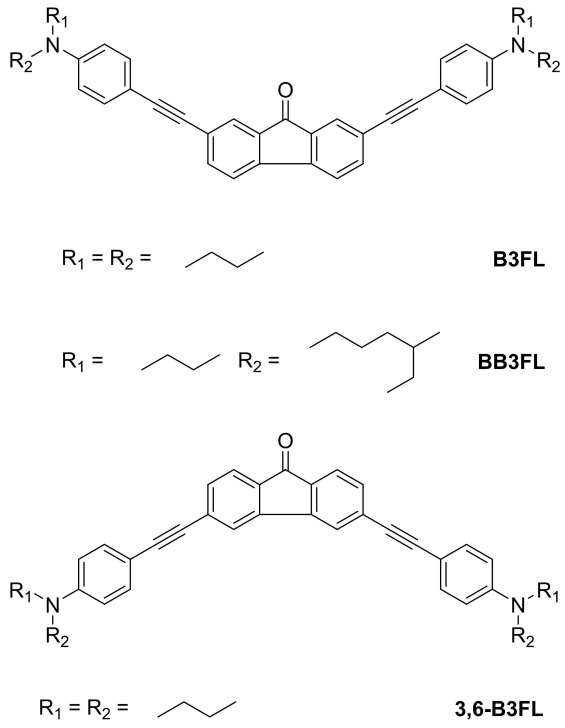

Figure 28. Schematic representation of the structures of the fluorenones **B3Fl**, **BB3Fl** and **3,6-B3FL**.

B3FL and **BB3FL** carry the substituents in positions 2 and 7, **3,6-B3FL** is modified in positions 3 and 6. The linear absorption spectrum of **B3FL** shows a maximum at 405 nm and the fluorescence quantum yield is 0.7×10^{-3}. The maximum of **3,6-B3FL** is bathochromically shifted at 460 nm, the measured fluorescence quantum yield is 12×10^{-3}. As with the anthraquinones, no absorption or fluorescence measurements were performed for **BB3FL**. The σ_{TPA} values, measured at 800 nm, reveal the highest value for **B3FL** with 440 GM. By changing to the branched alkyl chains (**BB3FL**) the σ_{TPA} value decreases to 385 GM. **3,6-B3FL** shows a much smaller σ_{TPA} value of 308 GM. This is in particular interesting because **3,6-B3FL** should facilitate the intramolecular electron transfer process by its substitution. A possible explanation for the lower σ_{TPA} value can be the redshift, which reduces absorption at the given wavelength. For the fabrication tests, the same monomer mixture was used as for the anthraquinone **B3AN**. In contrast, all fluorenones could be dissolved directly and showed a wider fabrication window. The results are summarized in Table 12.

Table 12. Experimental data of the anthraquinone and fluorenon 2PIs.

Compound	λ_{Max} [nm]	Φfl[a]	σTPA [GM][b]	FW [mW]
B3AN	485	–	235	–
BB3AN	–	–	250	22 to 24
B3FL	405	0.7×10^{-3}	440	6 to 18
BB3FL	–		385	4 to 11
3,6-B3FL	460	12×10^{-3}	308	7 to 17

[a] values measured in CH_2Cl_2. [b] Measured at 800 nm.

Figure 29 displays the great manufacturing properties of **B3FL**. Several complex 3D structures could be fabricated with an ETA/TTA 1:1 monomer mixture, such as a tarantula or the St. Stephens Cathedral.

The photo initiators **FT**–**PTAA-6** and **FT**–**CAA**–**C6** possess the same core structure as the other fluorenones (Figure 30). Instead of an aminophenyl substituent, Zhang et al. incorporated modified carbazole (**FT**–**CAA**–**C6**) or phenothiazine residues (**FT**–**PTAA**–**C6**). Both substituents were modified with an *n*-hexyl chain.[78] Carbazoles and phenothiazines are well-known donor systems of electron-rich heteroatoms (nitrogen and sulfur) and because of their optical properties are often found in areas such as organic light-emitting diodes (OLEDs),[79–82] dye-sensitized solar cells (DSSCs)[83–86] and polymeric optical fibers (POFs).[87]

Both initiators show a weak absorption above 400 nm, whereas the absorption increases strongly below it. The maxima

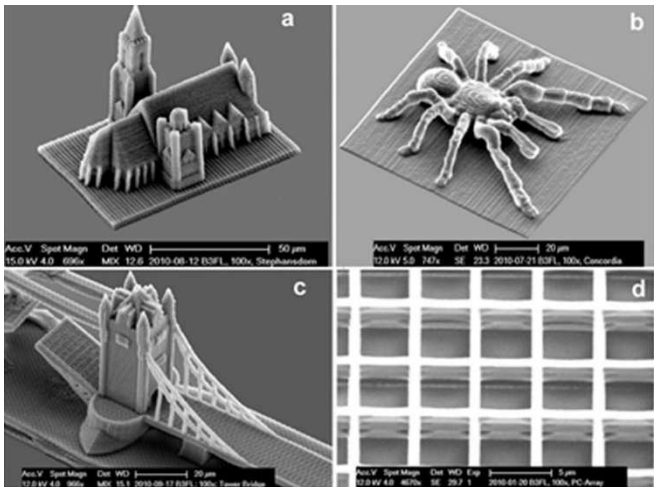

Figure 29. 3D structures: (a) St. Stephen's Cathedral, (b) Tarantula Spider, (c) detail of the London Tower Bridge and (d) detailed view of the woodpile structure.[43] Reproduced with permission from Ref. [43]. Copyright, John Wiley and Sons.

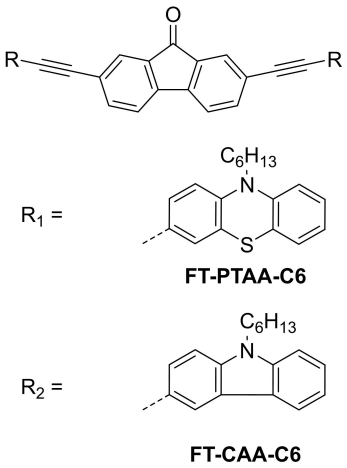

Figure 30. Schematic representation of the structures of carbazole and phenothiazine modified fluorenone 2PIs.

are very close to each other, 295 nm for **FT–PTAA–C6** and 300 nm for **FT–CAA–C6**. The fluorescence quantum yields, however, are very different. For **FT–CAA–C6** a yield of 1.65% could be obtained, for **FT–PTAA–C6** 0.01%. The two-photon-induced exited fluorescence (TPEF) method was used to determine the TPA value.[28] As a result, **FT–PTAA–C6** could not be measured due to the almost non-existent fluorescence. For **FT–CAA–C6** a value of 527 GM at 810 nm could be obtained. Successful 2PP with a 1:1 mixture of TTA and ETA were performed with **FT–CAA–C6** as initiator, but no fabrication window was reported.

2.5. Thioxanthone

Thioxanthones are well-known in the literature for their use as single photon initiators in photo polymerizations.[88–89] The electron-poor structure makes thioxanthone (**TX-1**) an interesting acceptor system, which can lead to strong two photon absorbing compounds by introducing different donor groups. By introduction of different amino donors and expanding the π-system, Nazir et al. were able to obtain various new photo initiators (Figure 31).[90]

The unsubstituted thioxantone **TX-1** itself shows little use in 2PP due to its small σ_{TPA} value (3 ±1 GM at 710 nm).[91] The performed modifications clearly demonstrates that the introduction of donor groups has a considerable influence on the two-photon absorption of the system. Table 13 summarizes the spectroscopic data.

The dialkylamino substituted initiators **TX-2** and **TX-4** reveal a strong bathochromic shift in absorption towards 500 nm. In contrast, the expansion of the π-system did not cause a significant redshift, and the initiators **TX-3**, **TX-5** and **TX-6** show an absorption maximum around 400 nm. It should be mentioned that despite the lack of redshift the molar extinction coefficient increases drastically, so that the missing redshift can be seen as an advantage when considering the two-photon absorption at 800 nm, a typical laser wavelength used in 2PP.[90] The two-photon cross-sections clearly reveal an increase of the σ_{TPA} value for the initiators with an extended π-system, in particular **TX-5** with the triple bond bridge, which shows the highest value of 128 GM. The fabrication windows of the different initiators were investigated using the same organic-inorganic hybrid material as in Ref. [40] (Figure 32).

While the initiators **TX-2**, **TX-3**, **TX-5** and **TX-4** formed structures, **TX-1** and **TX-6** revealed a seamless transition from the lower polymerization limit to the burning threshold. For **TX-2** it is clear that despite the low σ_{TPA} value, the initiator's radical yield is similar to that of 4,4′-(dimethylamino)benzophenone and its derivatives. **TX-4** behaves similarly, but a much higher laser intensity is required to write structures. The missing potential of **TX-6** to form radicals can be explained by the presence of the double bond. While radical formation via the intersystem crossing is one possibility, the cis-trans isomer-

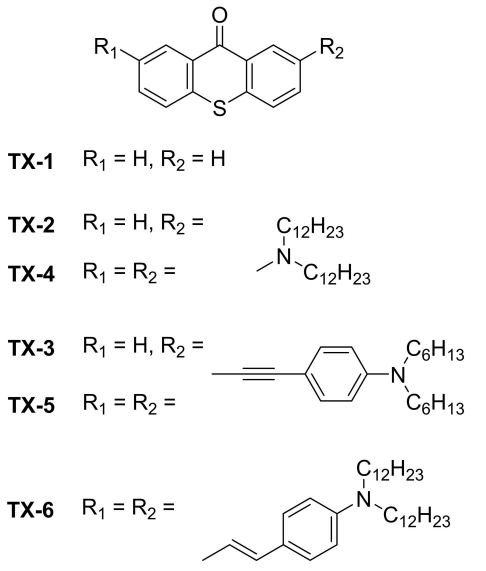

Figure 31. Schematic representation of the structures of the 2PIs **TX-1** to **TX-6** with a thioxanthone core.

Table 13. Spectroscopic properties of the thioxanthone derived 2PIs.

Compound	λ_{abs} [nm]	Φfl	σ_{TPA} [GM][a]
TX-2	463	0.25	4
TX-3	366	0.015	22
TX-4	497	0.16	9
TX-5	380	0.015	128
TX6	388	<0.01	73

[a] Measured at 800 nm.

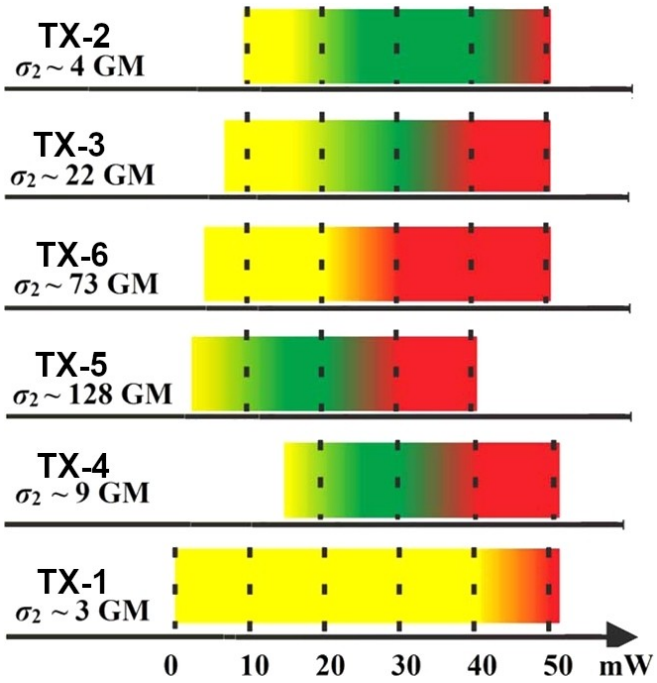

Figure 32. Fabrication windows of thioxanthone based 2PI **TX-1** to **TX-6**. Yellow area: Polymerization threshold. Green area: Stable structuring. Red area: Burning threshold.[90] Adapted with permission from Ref. [90]. Copyright 2015, American Chemical Society (https://pubs.acs.org/doi/10.1021/acs.macromol.5b00336).

ization of double bonds creates another pathway to release energy from the exited state. **TX-5** shows the best FW among the displayed initiators, this can be attributed to the relatively large σ_{TPA} value. Figure 33a displays the fabrication of squares with **TX-2** as initiator and decreasing laser power from left to right. A hollow 3D hemisphere was fabricated using **TX-3** as initiator (Figure 33b).

Similar to the fluorenone–carbazole/phenothiazine compounds, Zhang et al. also synthesized derivatives with a thioxanthone acceptor (Figure 34).[78] The linear absorption curve shows maxima at 505 nm and 523 nm for **TX**–**PTAA**–**C6** and **TX**–**CAA**–**C6**. The obtained fluorescence spectrum reveals a quantum yield of 3.56% for **TX**–**CAA**–**C6**. The TPEF performed showed an σ_{TPA} value of 72 GM. Due to the very low fluorescence quantum yield of **TX**–**PTAA**–**C6** of 0.02%, no σ_{TPA} value could be determined. So far, no structuring tests have been reported with these initiators.

Recently, a modified type of two-photon polymerization has been developed, in which polymerizations with even higher resolution should be possible. In the STED (stimulated-emission-depletion)-method, in addition to the excitation laser that excites electrons from S_0 to the S_1 state, a second laser beam is used to produce a stimulated emission from S_1 to the ground state S_0. Since a part of the electrons in the S_1 state are tripletted by ISC, the electrons in the S_1 state are converted to the S_0 state. Isopropyl thioxanthone (**ITX**) has turned into an interesting photo initiator for this type of polymerization due to its photo initiating and photo inhibiting properties.[92–93] Fischer et al. used **ITX** as initiator and were able to generate nanolines with a width of 65 nm with this new method.[92] However, the use of **ITX** requires high laser power, which is due to its low σ_{TPA} value of 3 GM.[94]

Therefore, Chi et al. developed new initiators based on the thioxanthone core moiety by expanding the π-system with various aromatic substituents and by adding a dimethylamino functionality as a donor (Figure 35).[94] While no problems during the synthesis of **DBTX** were noticed, the isolation of **DAPT**, **BDAPT** and **DANT** was difficult because of their low stability to air and light. **BDEPT**, **DEPT** and **BDANT** could be analyzed but not isolated in an amount enabling evaluation as photo initiator. Table 14 summarizes the photophysical data of the thioxanthone based 2PIs for STED-DLW (direct laser writing).

In general, all substances reveal a slight bathochromic shift compared to **ITX**. **BDAPT** shows the largest measured shift. The σ_{TPA} values could also be improved compared to **ITX**. **BDAPT** and **DANT** displayed the best values with 368 GM and 524 GM. A relatively low fluorescence quantum yield was observed in

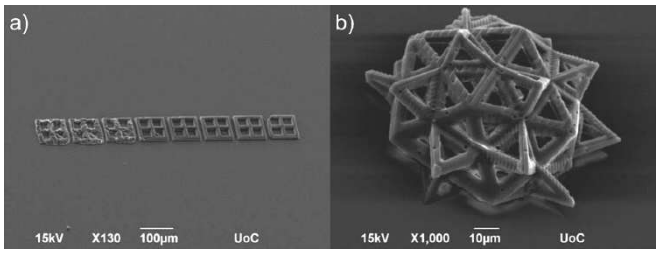

Figure 33. (a) SEM recording showing an array of microstructures fabricated with **TX-2**. (b) Hollow 3D microstructure with spikes on the surface using **TX-3** as initiator.[90] Adapted with permission from Ref. [90]. Copyright 2015, American Chemical Society (https://pubs.acs.org/doi/10.1021/acs.macromol.5b00336).

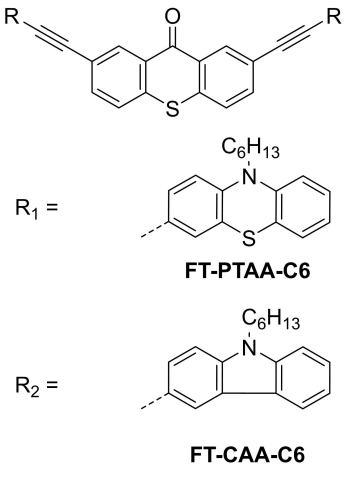

Figure 34. Schematic representation of the structures of carbazole and phenothiazine modified thioxanthone 2PIs.

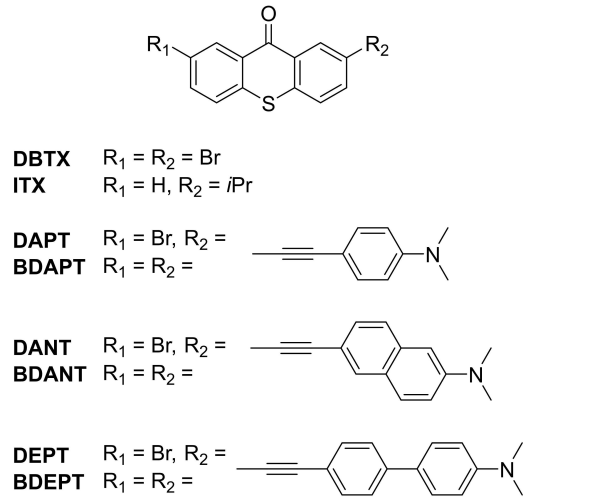

Figure 35. Schematic representation of the structures of thioxanthone based photo initiators made for the investigation in STED-DLW.

Table 14. Photophysical data of the thioxanthone based 2PI used for STED-DLW.

Compound	λ_{max} [nm][a]	Φ_{fl} [%][a]	σ_{TPA} [GM][a]
ITX	387	1.6	3 (±0.4)
DBTX	–[b]	–[b]	22 (±5)
DANT	380	4.4	524 (±61)
DAPT	–[b]	–	122 (±21)
BDAPT	408	8.1	368 (±45)

[a] Measured in PETA (pentaerythriol tri acrylate). [b] Insufficient signal in PETA.

PETA for all initiators (including **ITX**). This indicates that the nonradiative decay from the excitation is the major process and not the stimulated emission depletion process as assumed. Therefore, it can be expected that the initiators (Figure 35) follow a similar depletion pathway as **ITX**.[94] Based on the photophysical data **BDAPT** was the best candidate for STED-DLW. For this purpose, **BDAPT** was irradiated with an excitation laser (405 nm) and a trigger laser (633 nm).

A depletion of the fluorescence could be detected, which did not occur at 535 nm (depletion wavelength of **ITX**).

For demonstration purposes writing experiments with **BDAPT** in PETA were carried out. Figure 36 shows line experiments in which during writing over a length of 10 μm the depletion laser was activated without switching off the excitation laser. A total inhibition of polymerization was achieved during the exposure of the depletion laser.

Based on the previous results the same authors developed different **ITX** derivatives for the use in STED-DLW in a recent study.[95] Although the reported derivatives represents a D-π-A/D structure (Figure 37), for the purpose of comparison they will be discussed here. The initiators were equipped with electron withdrawing and donating groups to investigate their applicability in STED-DLW. In addition, initiators with phenyl or the para-fluor phenyl residues with more or less neutral electron withdrawing or donating ability were investigated.

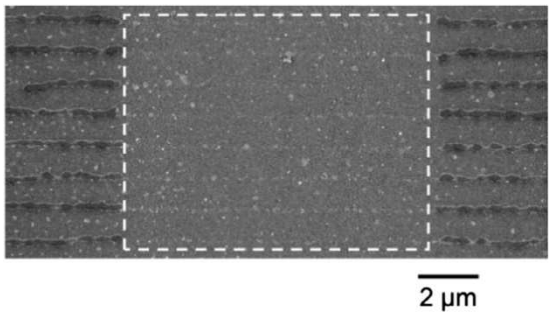

Figure 36. SEM image of photopolymerization with **BDAPT** and PETA as monomer. The highlighted box displays the area where polymerization was interrupted by the depletion laser.[94] Adapted with permission from Ref. [94]. Copyright 2019, John Wiley and Sons.

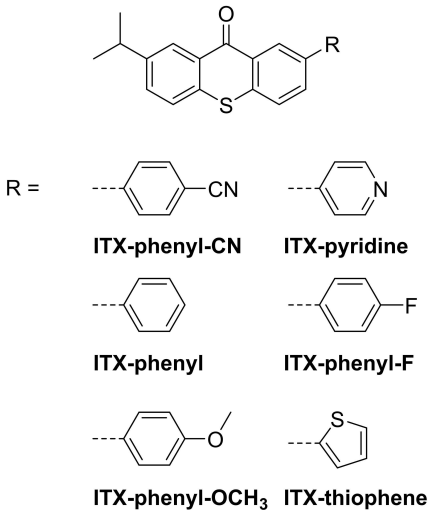

Figure 37. Schematic representation of the structures of the D-π-A/D initiators based on **ITX**.

The linear absorption maxima in toluene of the **ITX** 2PIs range in a narrow area around 391 to 402 nm, where **ITX**–**pyridine** absorbs at the lower range and **ITX**–**thiophene** at the upper area. This is clearly attributed to the electron donating effect of the thiophene. Although the authors report fluorescence emission spectra and even phosphorescence life times, no data concerning the fluorescence quantum yield is reported. The two-photon cross-sections were determined by the open z-scan method in THF at 800 nm and the results are shown in Figure 38a. In general the σ_{TPA}-values of the 2PIs are larger compared to **ITX**, but within the **ITX** derivates a clear trend is visible. While the initiators with an electron-withdrawing group exhibit only a little higher value, those equipped with an electron-donating group revealed the highest values of all initiators, investigated in this study. The writing threshold was determined by fabricating polymer lines with different laser powers at a constant writing speed of 100 μm/s. Hereby the threshold was defined as the minimum laser power, which is needed to fabricate stable structures, which survive the development process. The results are summarized in Figure 38.

Overall, the new **ITX** derivatives reveal a lower, thus more improved, writing threshold compared to **ITX**. **ITX**–**phenyl**–**OCH_3** shows the best writing threshold, although compared to **ITX**–**thiophene** it shows a lower σ_{TPA}-value. This is in good agreement with the results of other previous mentioned studies that indicate that the polymerization threshold, in this case the writing threshold, does not necessarily improve with higher σ_{TPA}-values. For the purpose to be used in STED-DLW a "new writing threshold" which depends on the power of the inhibition laser had to be investigated for the **ITX** derivatives. A better inhibition efficiency should result in increased resolution. The inhibition wavelength was set to 638 nm, which resembles the triplet absorption peak of **ITX**, thus an inhibition at this wavelength was expected.[96] Figure 39 shows the increased writing thresholds of the **ITX** derivatives.

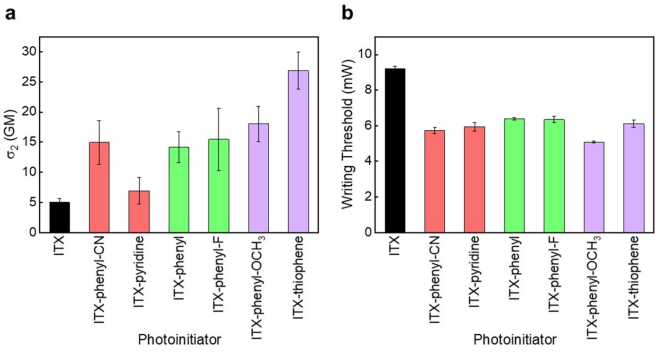

Figure 38. Bar chart of the (a) average two-photon cross-section at 800 nm and (b) average writing threshold of the 2PIs with a writing speed of 100 μm/s at 800 nm.[95] Reproduced with permission from Ref. [95]. Copyright 2021, American Society of Chemistry.

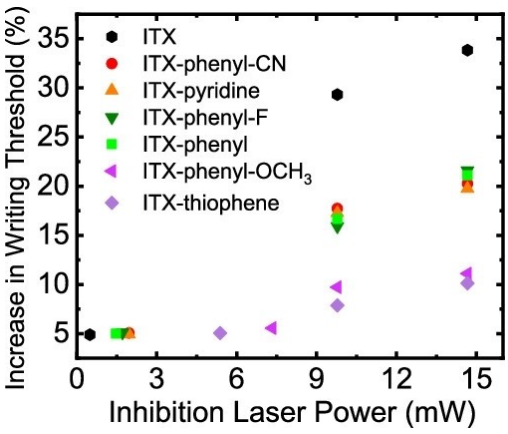

Figure 39. Writing threshold of the **ITX** derivatives in comparison to **ITX** under the exposure of the inhibition laser at 638 nm at different laser powers.[95] Reproduced with permission from Ref. [95]. Copyright 2021, American Society of Chemistry.

The best inhibition capabilities were determined for the initiators **ITX–phenyl–CN**, **ITX–pyridine**, **ITX–phenyl** and **ITX–phenyl–F** compared to **ITX**. **ITX–phenyl–OCH_3** and **ITX–thiophene** exhibit the least impressive inhibition effect, which can be attributed to the poor triplet absorption at 638 nm because of their shifted absorption by the electron donating groups. STED-DLW polymerization tests were performed by using 7% more power of the inhibition laser compared to the polymerization laser at the writing threshold of the individual initiator. In a ~70 μm^2 area the inhibition laser is turned on with a power of 9.8 mW. All **ITX** derivatives show no polymerization within that area, even **ITX–phenyl–OCH_3** and **ITX–thiophene** (Figure 40).

Although isopropyl thioxanthone (**ITX**) has a relatively low two-photon cross-section (3 GM), it was used for serval 2PP studies as initiator alone and in combination with co-initiators.[97–98] Zhang et al. used **ITX** in a process termed lithographically patterned nanostructure by chemical etching (LPNCE), where controlled etching of metal surfaces is enabled by polymerization of a protective polymer pattern onto the surface (Figure 41 & 42).[97]

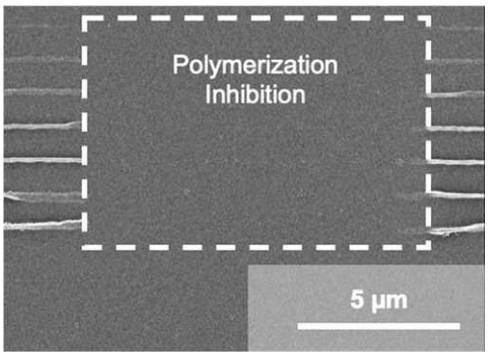

Figure 40. SEM image of fabricated lines using **ITX–phenyl–OCH_3** with the inhibition area, revealing no polymerization during the switched on inhibition laser at 638 nm.[95] Adapted with permission from Ref. [95]. Copyright 2021, American Society of Chemistry.

2.6. D-π-A-π-D photo initiators with other structures

Pyridinyl and pyridiniumyl residues are characterized by their strong electron acceptor properties. The pyridiniumyl core leads to high σ_{TPA} values, although it should be noted that the molecules under investigation are known as fluorescent dyes.[99–101] To evaluate the properties, Liska et al. synthesized two initiators **M3P** and **M3P+** (Figure 43).[45]

The linear absorption of **M3P** in acetonitrile reveals a maximum of 363 nm. By introducing a methyl group, the cationic 2PI **M3P+** shows an immense shift of absorption to 489 nm. The cationic character of **M3P+** is also evident in the fluorescence emission. While a light fluorescence with a quantum yield of 0.09 can be measured for **M3P**, for **M3P+** no fluorescence was detected. This may be due to the strong

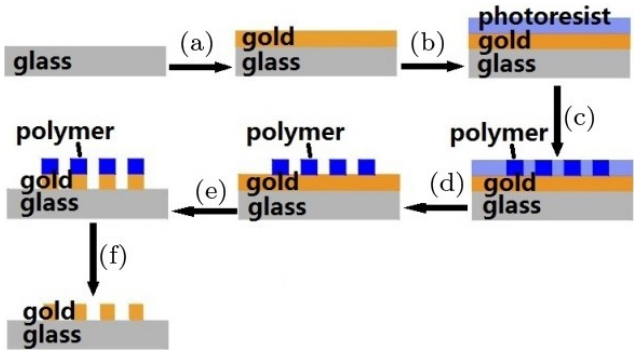

Figure 41. Overview of the LPNCE process. (a) Sputter coating, (b) dropping photoresist, (c) fabrication of polymer via 2PP using PETA as monomer, (d) removing of the unpolymerized photoresist, (e) etching of the gold with KI_3 surface and (f) dissolving of the polymer.[97] Reproduced with permission from Ref. [97]. Copyright 2014, World Scientific Publishing Co. PTE. LTD.

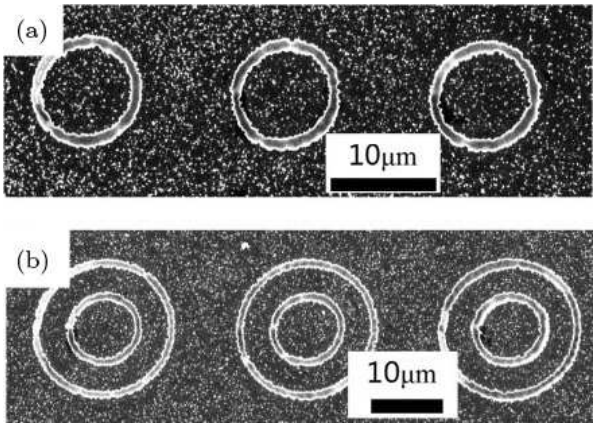

Figure 42. SEM image of fabricated micro circle via LPNCE. (a) Circles with a radius of 5 µm and a line width of 1.2 µm. (b) Outerring radius and width of 10 µm and 0.9 µm, and inner ring, 5 µm and 0.9 µm, respectively.[97] Reproduced with permission from Ref. [97]. Copyright 2014, World Scientific Publishing Co. PTE. LTD.

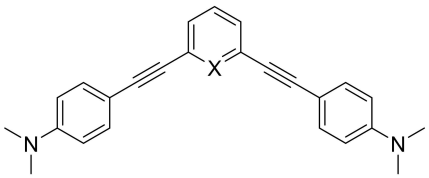

M3P X = N
M3P+ X = [N^+-Me] I^-

Figure 43. Schematic representation of the structure of the pyridinyl and pyridiniumyl based 2PIs.

acceptor of **M3P+**, which results from the methylation of the pyridine nitrogen. Due to the ionic structure of **M3P+**, Z-scan measurements could not be performed in common solvents such as *n*-hexane, THF and MeOH. **M3P** on the other hand showed a TPA of 23 GM. The determination of the fabrication window was performed with a 1:1 mixture of ETA and TTA. It turned out that **M3P** is insoluble in the monomer mixture and therefore no polymerization could be observed. Surprisingly, **M3P+** revealed low solubility in the mixture, resulting in an FW of ~18 to 29 mW.

By the reaction of dibutylaminobenzaldehyde with 2,4,6,-trimetyhl-1,3,5-triazine (**Trz**), dipolar (**BTrz**), quadrupolar (**2BTrz**) and octopolar (**3BTrz**) photo initiators were synthesized (Figure 44).[102]

The three initiators show a linear absorption around 400 nm. It should be mentioned that the absorption maximum of **2BTrz** and **3BTrz** differ only by a few nm and the fluorescence quantum yields of both are identical. The measured σ_{TPA} values using the Z-scan method at 796 nm reveal an enormous increase in the σ_{TPA} value from the D-π-A (**BTrz**) to the D-π-A- π-D chromophore (**2BTrz**). The additional expansion to an octopolar structure, represented by **3BTrz**, causes only a slight increase in the σ_{TPA} value (Table 15).

BTrz did not show any real activity in the structuring tests at 800 nm, but the activity could be improved by adjusting the laser wavelength by 15 nm. This adjustment to the maximum σ_{TPA} value of **BTrz** resulted in a significantly higher radical formation. On the other hand, **2BTrz** shows the largest fabrication window among the initiators, which could be due to the fact that its σ_{TPA} maximum is at 800 nm. **2BTrz** generates stable structures even at a high writing speed of 200 mm/s. Figure 45 displays a complex 3D structure written with **2BTrz** as photo initiator.

Searching for new heterocycles with interesting acceptor properties, recently developed thiophene based compounds exhibit high σ_{TPA} values.[103–104] By combining thiophene as a planar π-linker with several electron rich triphenylamine donors, new 2PIs (Figure 46) with broad fabrication windows were obtained.[105]

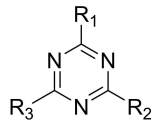

BTrz $R_1 = R_2 = Me$, R_3=
2BTrz $R_1 = Me$, $R_2 = R_3$ =
3BTrz $R_1 = R_2 = R_3$ =

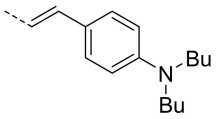

Figure 44. Schematic representation of the structures of dipolar, quadrupolar and octopolar 2PIs **BTrz**, **2BTrz** and **3BTrz**.

Table 15. Photophysical data of **BTrz**, **2BTrz** and **3BTrz**.

Compound	λ_{max} [nm]	Φ_{fl}	σ_{TPA} [GM][a]	FW [mW][b]
BTrz	412	0.055	60	–
2BTrz	432	0.20	244	18 to 120
3BTrz	434	0.20	275	18 to 100

[a] Measured in THF at 796 nm, [b] fabrication at 800 nm.

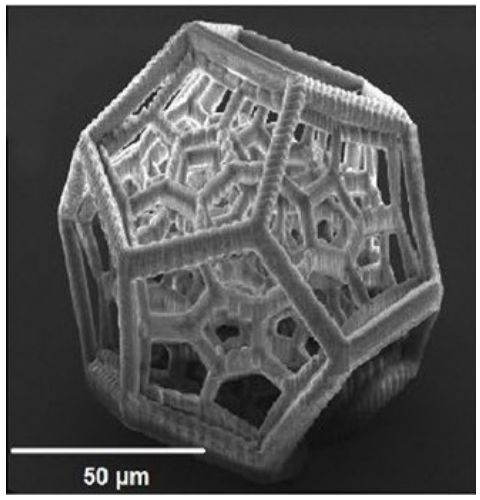

Figure 45. SEM image of a complex 3D sphere fabricated with **2BTrz** as 2PI.[102] Adapted with permission from Ref. [102]. Copyright see http://creativecommons.org/licenses/by/4.0/.

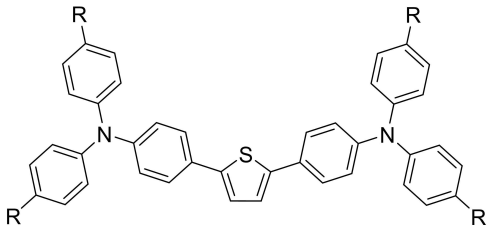

BMTOA-1T R = OCH_3
BtBuA-1T R = tBu
BMA-1T R = CH_3
BTMSA-1T R = TMS
BHA-1T R = H
BFA-1T R = F
BCNA-1T R = CN
BSO_2MA-1T R = SO_2CH_3

Figure 46. Schematic representation of the structures of the thiophene based 2PIs.

The data of the linear absorption show mostly maxima at around 400 nm (Table 16). By replacing the electron donating substituents by electron withdrawing groups a hypsochromic shift down to 345 nm occurs. Interestingly, the fluorescence quantum yields decrease when electron withdrawing groups are attached. Although a decrease occurs, the fluorescence quantum yields are in general high. The difference in substituents also has a significant influence on the σ_{TPA} value. Substances with more electron withdrawing groups, possess decreased σ_{TPA} values (from 379 GM (**BMOAT**–**1T**) to 173 GM (**BSO2MA**–**1T**), Table 16).

To estimate the fabrication windows of the 2PIs listed in Table 15 defined woodpile structures were fabricated at different laser powers and writing speeds. The well-established monomer mixture ETA/TTA was applied for the fabrication process. All of the synthesized 2PIs were able to produce well-defined wood pile structures. Although all 2PIs are able to induce polymerization in general the ones with electron donating substituents show a broader fabrication window (**BMTOA**–**1T**, **BtBUA**–**1T**, **BMA**–**1T** and **BTMSA**–**1T**) compared to those bearing electron withdrawing groups (**BFA**–**1T**, **BCNA**–**1T** and **BSO$_2$MA**–**1T**) which only gave good woodpile structures at lower laser intensities and writing speeds. Interestingly the unsubstituted initiator **BHA**–**1T** revealed the broadest fabrication window amongst the initiators (Figure 47).

Besides the mentioned heterocycles, quinoxaline compounds were investigated as sensitizers for solar cells components and as two-photon absorption dyes.[106–108] Cao et al. investigated compounds consisting of a quinoxaline and benzoquinoxaline as acceptor combined with modified triphenylamine and ethoxybenzene as donor groups (Figure 48).[109]

The four initiators show absorption maxima between 350 and 470 nm (Table 17). A significant red shift is observed for the structures containing the triphenylamine moiety (**TPAQ**, **TPABQ**) compared to the ones with the structures with the alkoxy group (**EOQ**, **EOBQ**). The same is observed between the quinoxaline and benzoquinoxaline. Here, the additional benzol ring leads to a red shift in the absorption maximum. The triphenylamine moiety as well as the benzoquinoxaline provides the system with more electrons and a larger degree of conjugation. In general, the quinoxaline compounds reveal lower fluorescence quantum yields comparted to the benzoquinoxalines. This indicates that the benzoquinoxaline is a weaker acceptor than quinoxaline. Moreover, the triphenylamine compounds show higher fluorescence quantum yields than the

Table 16. Spectroscopic data of thiophene based 2PIs in THF.

Compound	λ_{abs} [nm]	Φfl	σ_{TPA} [GM][a]
BMOA–**1T 1**	400	0.57	379
BtBuA–**1T**	396	0.44	358
BMA–**1T**	396	0.40	331
BTMAS–**1T**	394	0.40	345
BHA–**1T**	390	0.34	301
BFA–**1T**	387	0.33	301
BCNA–**1T**	352	0.39	213
BSO$_2$MA–**1T**	345	0.36	173

[a] Measured via TPEF at 800 nm.

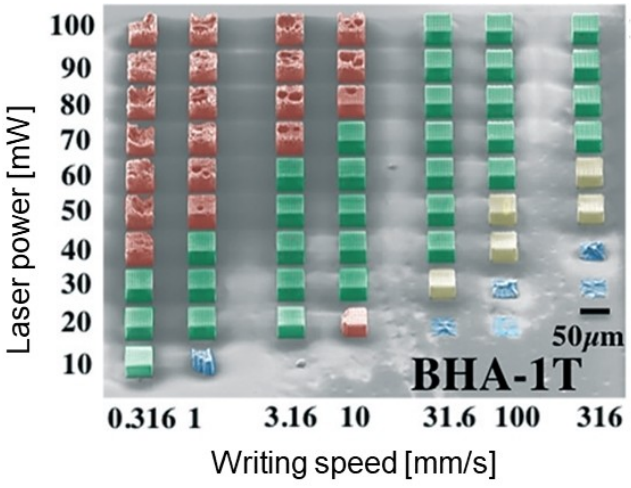

Figure 47. SEM image of the speed power screening of **BHA**–**1T**. Classification by color: (green) excellent structures, (yellow) good structures with slightly contorted shapes, (red) structures with identifiable shapes but with small errors, (blue) not identifiable structures.[105] Adapted with permission from Ref. [105]. Copyright see https://creativecommons.org/licenses/by-nc/3.0/.

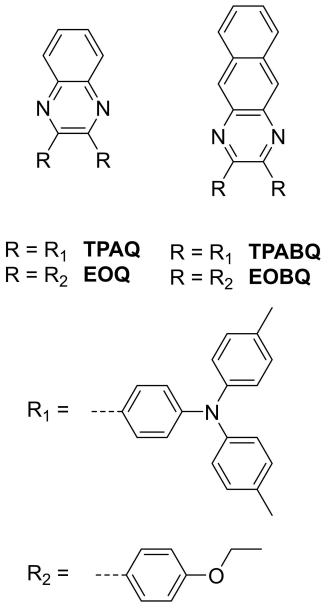

Figure 48. Schematic representation of the structures of quinoxaline and benzquioxaline based photo initiators.

Table 17. Linear and nonlinear optical properties of the quinoxalines and benzoquinoxaline based photo initiators in $CHCl_3$.

Compound	λ_{abs} [nm]	λ_{em} [nm]	Φ_{fl} [%][a]	σ_{TPA} [GM][b]
EOQ	290/371	439	11.6	15
EOBQ	330/419	483	4.5	25
TPAQ	307/419	555	14.6	160
TPABQ	304/464	573	9.8	70

[a] Compared to coumarin 307, [b] measured via TPEF, maxima at around 780 to 820 nm.

alkoxy ones. This can be attributed to the stronger donor ability of the triphenylamine moiety.

Two-photon cross-section measurements resulted in a maximum of around 15, 25, 70 and 160 GM for **EOQ**, **EOBQ**, **TPABQ** and **TPAQ**, respectively. By combining quinoxaline or benzoquinoxaline with the triphenylamine moiety the σ_{TPA} value becomes much higher than with the alkoxyaryl moiety. Although the benzoqunioxaline acceptor shows a higher degree of conjugation, it seems that an expansion of the π-conjugation, like in quinoxaline, is crucial to obtain compounds with high σ_{TPA}-values. Because of their large two-photon cross-section, polymerization tests were performed with TPAQ and TPABQ in a monomer mixture consisting of methyl methacrylic acid (MMA) and dipentaerythritol hexaacrylate (DEP-6 A) as crosslinker. Figure 49 displays fabricated lines with different laser powers at a relatively slow speed of 10 μm/s and 800 nm.

Compared to the commercial photo initiator **Benzil**, the two initiators showed lower threshold energies (0.8 mW **TPAQ**, 2.6 mW **TPABQ**, 3.2 mW **Benzil**). The polymerization rates R_p were determined according to a method developed by Katawa et al.[110] and were determined to be 5.96, 3.89 and 0.66 $\mu m^3/s$ for **TPAQ**, **TPABQ** and **Benzil**, respectively.

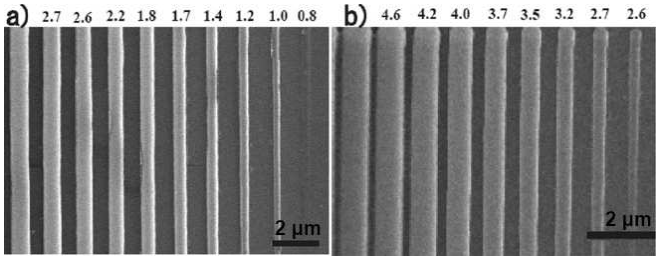

Figure 49. SEM image of the fabricated lines using (a) **TPAQ** or (b) **TPABQ** as initiators.[109] Adapted with permission from Ref. [109]. Copyright 2009, Royal Society of Chemistry.

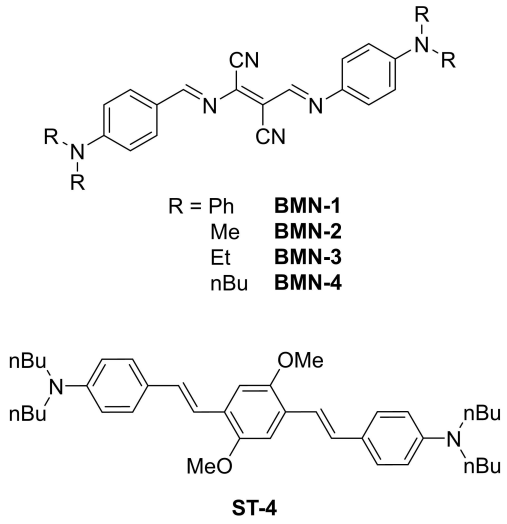

Figure 50. Schematic representation of the structures of the benzylidenediaminomaleonitrile based 2PIs.

Watanabe et al. synthesized and investigated the benzylidenediaminomaleonitrile derivatives **BMN-1** to **BMN-4** (Figure 50) for their use as photo initiators.[111] The replacement of the C–C double bond with an benzol group enhances the extent of the charge transfer from the terminal groups to the center. The two-photon cross section of the photo initiator **BMN-1** to **BMN-4** were measured via TPEF measurement (Table 18).

All photophysical measurements were performed in toluene and chloroform, except for **BMN-2** which was only soluble in chloroform. The linear absorption, the two-photon cross-section and the fluorescence quantum yield strongly depend on the solvent's polarity. For **BMN-1** the σ_{TPA} value in chloroform is decreased by more than half in comparison to the σ_{TPA} in toluene. The terminal phenyl groups decrease the polarity of the molecule, as a result **BMN-1** exhibits higher values in toluene than in chloroform. **BMN-3** and **BNM-4** reveal larger σ_{TPA} values in chloroform relative to the ones measured in toluene. The small increase of the σ_{TPA} value in chloroform can be explained by the replacement of the C–C double bond with the more polar imine group. Initiator **BMN-2** shows a large σ_{TPA} value, which can be attributed to its low fluorescence quantum yield.

Microfabrication properties of the 2PIs were tested with a monomer mixture consisting of 70 wt% multifunctional acrylate monomers (SR9008:SR368 = 1:1), 29.9 wt% of poly(styrene-*co*-acrylonitrile) as polymer binder. The 2PI concentration was set to 5×10^{-4} M. The newly synthesized 2PIs were compared to a well-known 2PI **ST-4** (σ_{TPA} = 900 GM). **BMN-1** and **BMN-2** showed low solubility in the monomer mixture and no polymerization properties could be determined. With **BMN-3** and **BMN-4** as well as with **ST-4** microgrids were fabricated and the polymerization rates R_p were determined by using the equation $\pi(d/2)^2 v_s$, where d is the width of the written protruding line and v_s is the scanning speed of 50 μm/s.

BMN-3 and **BMN-4** reveal lower polymerization rates at 755 nm, which are increasing when an excitation wavelength of 820 nm is used, although the laser power at 755 nm (5.0 mW) is higher at 820 nm (3.0 mW) (Table 19). Figure 51 shows fabricated microgrids with **BMN-3** at 755 nm (a) and 820 nm (b).

Table 18. Photophysical data of the benzylidenediaminomaleonitrile 2PIs in chloroform.

Compound	$^1\lambda_{abs}$ [nm]	$^2\lambda_{ex}$ [nm]	σ_{TPA} [GM][a][b]	Φ_{fl}
BMN-1	552	840	180	
		885	265	0.46
BMN-2	536	820	2050	0.02
		840	1910	
BMN-3	547	820	545	0.05
		840	520	
BMN-4	553	820	490	0.1
		840	480	

[a] Measured via TPEF technique with Rhodamine B as reference.

Table 19. Polymerization rates of **BMN-3** and **BMN-4** in comparison to **ST-4** at different excitation wavelength.

Compound	$^2\lambda_{ex}$ [nm]	σ_{TPA} [GM][a]	R_p [$\mu m^3/s$]	d [μm]
ST-4	730	900	395	3
BMN-3	755	390	160	2
	820	545	450	3.4
BMN-4	755	315	120	1.8
	820	490	230	2.4

[a] Measured via TPEF technique with Rhodamine B as reference.

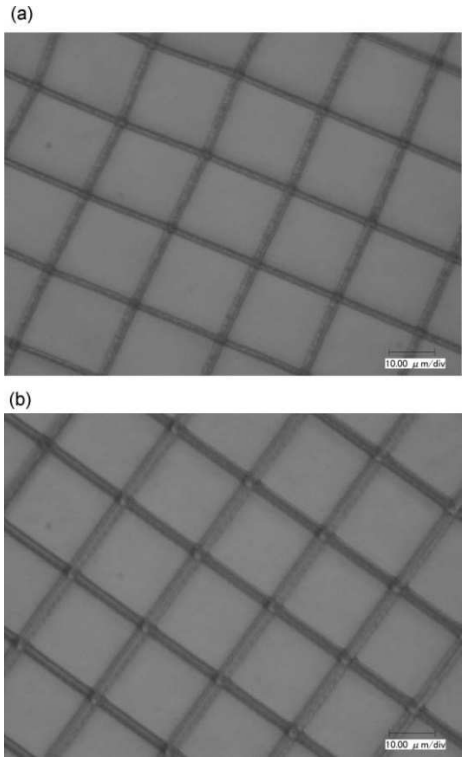

Figure 51. SEM image of fabricated microgrids with **BMN-3** at (a) 755 nm and (b) 820 nm. The scale bar is set to 10 μm.[111] Adapted with permission from Ref. [111]. Copyright 2004, Royal Society of Chemistry.

2.7. Water soluble D-π-A-π-D photo initiators

Wan et al. develop the water-soluble photo initiator **BSEA** (Figure 52) by introducing carboxylic groups to the two-photon dye 2,5-bis-[4-(diethylamino)-benzylidene]-cyclopentanone (**BDEA**).[112]

BSEA exhibits an absorption maximum at 513 nm in water and has a small fluorescence quantum yield of 0.0023 compared to Rhodamine B (in methanol) as standard. The σ_{TPA} value was measured with the nonlinear transmission (NLT) method[113] as well as with the TPEF method and showed a σ_{TPA} value of 287 GM (NLT at 800 nm)[112] and 808 GM (TPEF, maximum with the range of 750 to 840 nm).[114] This might be attributed to the difference of measuring the fluorescence quantum yield. To evaluate the fabrication properties of **BSEA**, it was compared to **Eosin Y** as a water-soluble photosensitizer.

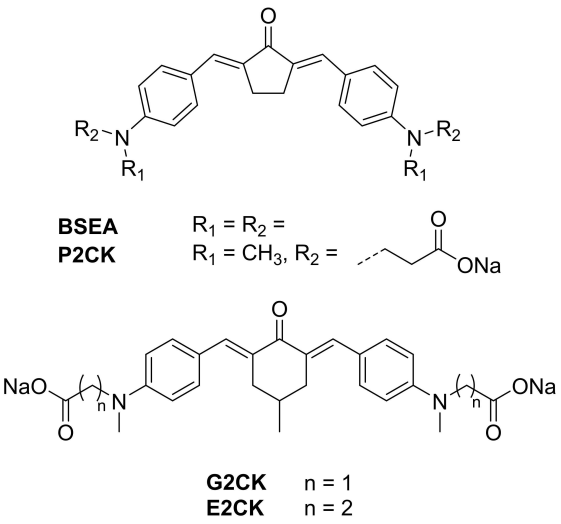

Figure 52. Schematic representation of the structures of **BSEA**, **2PCK**, **G2CK** and **E2CK**.

Both dyes were used for polymerization tests with PEGda 600 as monomer, with and without the co-initiator TEA.

The polymerization threshold of **BSEA** is much smaller, in both cases with and without TEA, compared to **Eosin Y** (Table 20). In fact, the fabrication window of **BSEA** decreased if TEA was used, although the polymerization threshold decreased. It is also interesting to see that **R**[4] reveals no E_{damage}. In fact the whole material would solidify gradually during the line scanning process. One-photon polymerization tests showed that the initiating efficiency of **Eosin Y** and TEA was much higher than for **BSEA** and TEA. Because of these results **R**[1] was chosen for the fabrication of a 3D woodpile structure (Figure 53).

Li et al. synthesized three photo initiators with carboxylic groups similar to **BSEA** but with different central ketone ring sizes (Figure 52).[115]

The three initiators exhibit a σ_{TPA}-value (Z-scan at 800 nm) over 150 GM. The σ_{TPA} value decreases first when the central ketone is changed from cyclopentanone (**P2CK**, 176 GM) to 4-methylcyclohexanone (**G2CK**, 173 GM). Because the cyclohexanone ring has a lower planarity compared to the cyclopentanone ring, the degree of conjugation in **G2CK** is lower than in **P2CK**. By extending the alkyl spacers from methylene to ethylene like in **E2CK**, an increase to 201 GM was observed, which is higher as for **P2CK**. The increase to 201 GM in **E2CK** could be attributed to the better electron donating strength of the ethylene alkyl chain. Another possibility might be that the

Table 20. Resin formulation and polymerization data.

Resin	PEGda 600 [wt%]	BSEA [wt%]	Eosin [wt%]	TEA [wt%]	E_{th} [mW]	E_{damage} [mW]
R[1]	79.87	0.16		0	0.51	4.73
R[2]	79.87		0.16	0	2.15	4.73
R[3]	78.6	0.16		1.6	0.46	4.3
R[4]	78.6		0.16	1.6	1.51	–

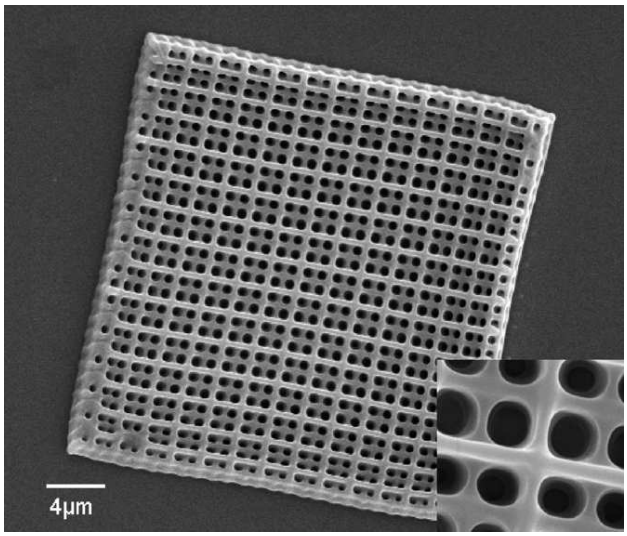

Figure 53. Fabricated woodpile structure fabricated using a writing speed of 110 µm/s, a laser power of 0.8 mW, **BSEA** as photo initiator and resin **R**[1] in water.[112] Adapted with permission from Ref. [112]. Copyright 2009, Elsevier.

red shift support a better absorption at the given polymerization wavelength. In comparison to the hydrophobic counterparts (**BcP-1** with 466 GM and **BcH-2** with 191 GM, Figure 10) the cross-sections of the water-soluble 2PIs are all lower. This discrepancy could be a solvent effect on the TPA behavior. There are several studies, which demonstrated that the absorption behavior under two-photon conditions is strongly depended on the solvent polarity. Such a drop in σ_{TPA} value is also visible in other studies of water-soluble 2PIs.[112] Evaluation of the 2PIs were performed by fabrication of 3D microstructures with PEGda 700 at different laser intensities (60 to 410 mW) and writing speeds (1 to 100 mm/s). The fabricated structures were categorized in structures with excellent integrity (green), good integrity with thick hatch-lines (yellow) and structures with identifying shapes but with mistakes (red). Like their hydrophilic counter parts, the three water-soluble 2PIs show high initiation efficiency during the 2PP screening. Figure 54 displays that the polymerization threshold of **P2CK** is lower compared to **E2CK** or **G2CK**. It is known that compounds with a central cyclohexanone core, like **E2CK** and **G2CK**, exhibit a lower fluorescence quantum yield compared to cyclopentanone compounds, like **P2CK**.[116] This may explain the lower polymerization threshold of **E2CK** and **G2CK**, because low fluorescence quantum yields are crucial for effective initiation via TPA.[43] The two cyclohexanone 2PIs show similar fabrication properties, although **E2CK** exhibit the largest σ_{TPA} value of three 2PIs. The similar efficiency of **G2CK** may lay in the methyl-substituted phenylglycine moiety, which is more active compared to other arylamines as co-initiator in UV polymerizations.[117] Therefore, it is to be assumed that the radicals formed by **G2CK** are more efficient thus compensating the lower σ_{TPA}-value. Cytotoxicity tests were performed with MG63 osteosarcoma cells and outgrowth endothelial cells (OEC), which were exposed to the 2PIs for 10 and 30 min respectively. Of all the 2PIs only **G2CK**

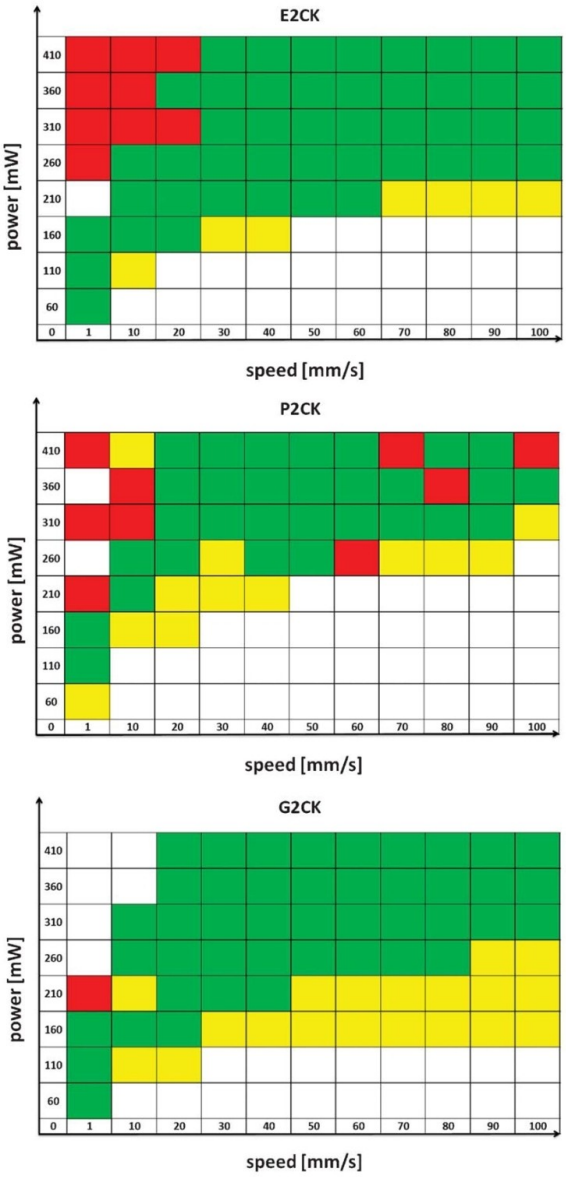

Figure 54. Fabrication windows of the water-soluble 2PIs **P2CK**, **E2CK** and **G2CK**.[115] Adapted with permission from Ref. [115]. Copyright 2013, Royal Society of Chemistry.

had a significant impact on the MG63 cells viability in both experiments. When the cell line is changed to the OEC cells a significant decrease in cell viability was observed for **E2CK** and **G2CK**. In case of **P2CK** the cytotoxicity was as low as for the reference (I2959) in the 10 min experiment. This changed when the incubation time was increased to 30 min, where **P2CK** also decreased the cell viability but not as much as the other two initiators. Although the cell viability was reduced by the photo initiators, **P2CK** and **G2CK** were successfully used in fabrication of 3D hydrogels consisting of modified gelatin with and without presence of living cells.[118–119] In a recent study from 2021, Huang et al. compared the two PIs **P2CK** and **BSEA** for their ability to fabricate scaffolds in presence of living cells.[120] The authors claim that because of the higher water-solubility of

BSEA (four carboxylic groups compared to **P2CK** with only two) the cytotoxicity is much lower. They could fabricate scaffolds using a glycidyl methacrylate modified gelatin as resin in the presents of living cells with the help of **BSEA**.

Based on the results of **BSEA** of the same group two more 2PIs with varied central cycloalkane ketones were synthesized (Figure 55).[114]

With increasing cycloketone ring size the linear absorption maximum shifts hypsochromically from 522 nm for **T1** to 478 nm for **T3** (Table 21). The fluorescence quantum yield drops when the ring size increases, as expected. Interestingly at first an increase of the σ_{TPA} value is observed from cyclobutanone (**T1**) to the cyclopentanone derivative (**T2**, **BSEA**). However, by increasing the ketone ring size to cyclohexanone (**T3**) the cross-section drops significantly, as observed in the hydrophobic 2PIs with a cyclohexanone structure (Table 4 & 5, Chapter 2.2.).

Polymerization tests were performed with three different photocurable resins SR610 (PEGda 600), BSA and a hyaluronic acid derivative (HAGM). In addition, the prepared initiators were compared to the known water-soluble initiator **Eosin Y**. The resin composition, polymerization threshold and damage threshold for SR610 are listed in Table 22.

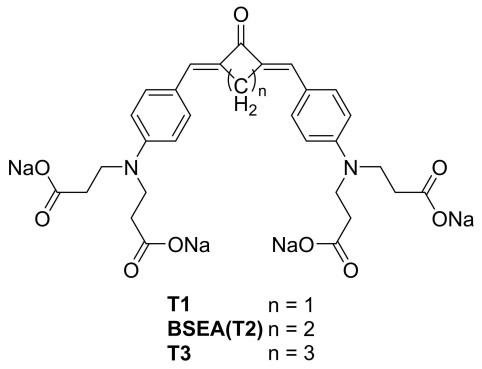

Figure 55. Schematic representation of the structure of the 2PIs **T1**, **BESA** and **T3**.

Table 21. Photophysical data of the 2PIs **T1**, **BSEA** and **T3**.

Compound	λ_{max} [nm]	Φ_{fl}[a]	σ_{TPA}[b]
T1	522	1.28	567
BSEA (T2)	513	1.10	808
T3	478	0.52	231

[a] Rhodamine B in methanol was used as reference. [b] Measured by TPEF in water. All three maxima lay around 820 nm.

Table 22. Polymerization results for the resins containing 79.87 wt% SR610 and the different 2PIs (0.16 wt% in water at 820 nm).

Resin	Initiator	E_{th} [mW]	E_{Damage} [mW]
R1	**Eosin**	0.51	5.24
R2	**T1**	0.37	5.93
R3	**T2 (BESA)**	0.08	6.94
R4	**T3**	0.43	5.65

Compared to the literature known initiator **Eosin** all three initiators exhibits broader FWs, with **T2** and **BSEA** showing the broadest FWs (Table 22). These results were also observed when the polymerizations were performed with bovine serum albumin (BSA) as photocurable material. Polymerizations with hyaluronic acid derivative (HAGM) revealed that all three initiators perform better than Eosin but it is interesting to note that **T3** in this composition exhibits the broadest fabrication window (E_{th}(**T3**): 0.38 mW, E_{br}(**T3**): 8.05 mW; E_{th}(**T2**): 0.59 mW, E_{br}(**T2**): 7.37 mW).

Biocompatibility tests were performed with MTT assay using hepatoma cells HepG2. The cells were incubated with 3 mM (2PI concentration during 2PP). After incubation for 24 h the cell viability was nearly 60 % for all 2PIs.

By combining triphenylamine motifs with a cyclopentanone core, Wloka et al. have developed the water-soluble initiator **BTABcP-1** (Figure 56) with a linear absorbance at 390 nm, nearly half the wavelength of the common polymerization wavelength of 800 nm.[8]

Z-scan measurement revealed a σ_{TPA} value of 253 GM at 800 nm (not reported in the publication, but measured after wards via Z-scan). 2PP was performed with newly introduced poly(2-oxazoline) based macromonomer (PEtOx-DA) for 2PP. A voxel array with varying laser power and exposure time was prepared (Figure 57). Also, a line array with a constant writing speed of 0.1 mm/s and laser power of 310 mW, while the z-rise of the laser focal point was increased by one micrometer per line from right to left (Figure 58).

To determine the cytotoxicity of the initiator an alamarBlue™ assay with L929 cells was performed. The cells were incubated for 24 h with various concentration (0.25 µg/mL to 1 mg/mL) and subsequently tested for their viability. From results of the assay the cytotoxic concentration (CC50) was calculated to be 740 ± 20 µg/L.

Using the host-guest interaction, a method where a molecule is incorporated into a guest molecule, Xing et al. where able to solve the hydrophobic anthracene derivative **N** in water with the help of cyclodextrin (Figure 59).[121]

By incorporating **N** into 2-hydroxypropyl-β-cyclodextrin (2-Hp-β-CD) the water-soluble complex **WI** was generated. With this the photophysical properties are influenced (Table 23).

N exhibits two linear absorption maxima at 443 nm, which corresponds to the intramolecular charge transfer and at 328 nm which can be assigned to the π-π* transition. By

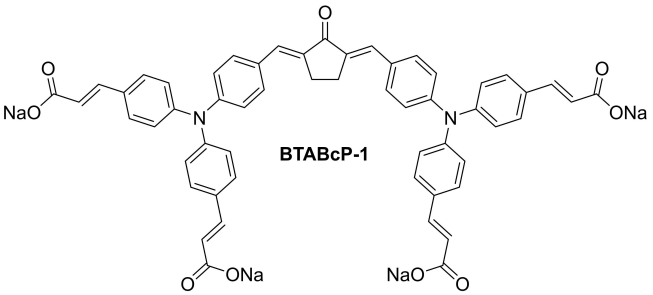

Figure 56. Schematic representation of the structure of **BTABcP-1**.

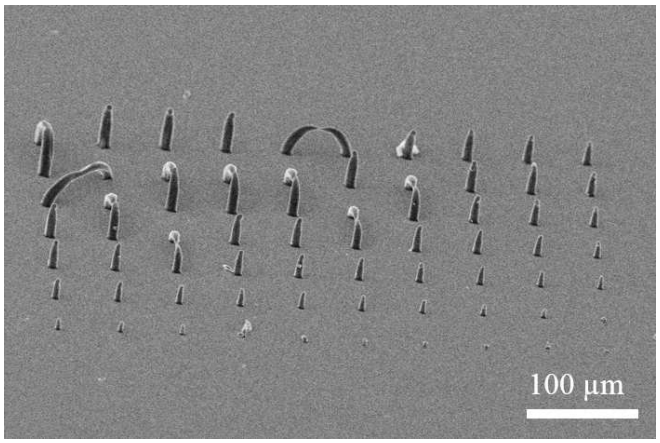

Figure 57. SEM image of a voxel array of PEtOx-DA (DP 18) and **BTABcP-1** as initiator. The exposure time ranged from 40 to 400 ms ($\Delta = 40$ ms; right to left) and the laser power ranged from 10 to 410 mw (bottom to top, $\Delta = 50$ mW).[8] Adapted with permission from Ref. [8]. Copyright 2021, Elsevier.

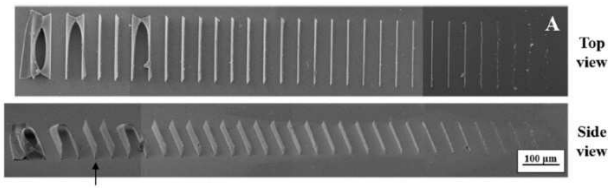

Figure 58. SEM images of the line arrays fabricated by 2PP using **BTABcP-1** and PEtOx-DA. The side view shows the fabricated lines in an 60° angle and the black arrow marks the last alone standing line.[8] Adapted with permission from Ref. [8]. Copyright 2021, Elsevier.

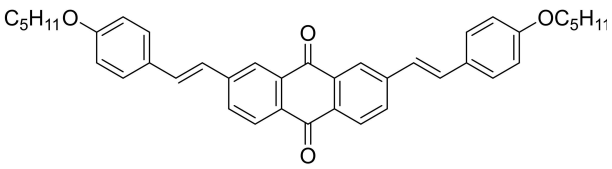

Figure 59. Schematic representation of the structure of the anthracene compound **N**.

Table 23. Photophysical data of N and N/2-Hp-β-CD complex **WI**.

Compound	Solvent	λ_{max} [nm]	Φ_{fl}[a]	σ_{TPA} [GM][b]
N	$CHCl_3$	327/443	0.023	612 (820 nm)
WI	water	290	0.007	282 (770 nm)

[a] Fluorescence quantum yield determined relative to coumarin 307. [b] Measured by TPEF at the stated wavelengths.

incorporating **N** into 2-Hp-β-CD the absorption maxima shift hypsochromically to 290 nm. This shift is mainly attributed to the decreasing polarity of the microenvironment around **N**.[122] It is also possible that **N** forms hydrogen bonds between its pentoxy groups and hydroxy groups of the cyclodextrin, which results in electron redistribution and thereby, increasing the stability of **N**.[123] The fluorescence quantum yield of **N** with 0.023 is higher compared to the water-soluble complex **WI** with 0.007. σ_{TPA} values were determined by using the TPEF technique and revealed for **N** 612 GM (chloroform) and for **WI** 282 GM. At the polymerization wavelength of 780 nm WI exhibits a σ_{TPA} of 200 GM, which is larger than common commercially available water-soluble photo initiators.[91] The decrease for **WI** compared to N is caused by the hydrogen bonds which have a major influence on the **ICT**. By polymerizing PEGda ($M_n = 700$ g/mol) the threshold energy at different writing speeds was determined by fabricating a line array. The threshold energy for WI at a writing speed of 10 µm/s was 8.6 mW, while at a higher writing speed of 50 µm/s the threshold increased to 10.2 mW. 3D woodpile microstructures with good integrity were fabricated with a writing speed of 30 µm/s at a laser power of 9.7 mW (Figure 60).

With the same technique **N** was also encapsulated in the poloxamer Pluronic F127.[124] The formed complex **WI**–**II** showed good water solubility and exhibits a linear absorption maximum of 285 nm in water, which is similar to **WI**. The maximum two-photon cross-section of **WI**–**II** lies at 760 nm and revealed a σ_{TPA} value of 260 GM. Although the σ_{TPA} value is slightly lower compared to **WI**, **WI**–**II** also exhibits 200 GM at the polymerization wavelength of 780 nm. Polymerization tests with PEGda as monomer revealed a threshold energy of 6.29 mW, which compared to **WI** is much lower. A line array performed with different laser intensities from 6.29 to 11.09 mW showed that at a laser power of 6.8 mW lines were fabricated which possessed a width of only 92 nm. The writing speed was constantly kept at 10 µm/s. 3D microstructures in form of an adenovirus were fabricated with different laser intensities to proof the suitability of the initiator complex (Figure 61). From the three SEM images displayed in Figure 61, it is visible that the structure fabricated with 7.27 mW shows the best resolution compared to the structures fabricated with higher laser power. Both **WI** and **WI**–**II** fabricate precise microstructure via 2PP, however in both studies 2-benzyl-2-

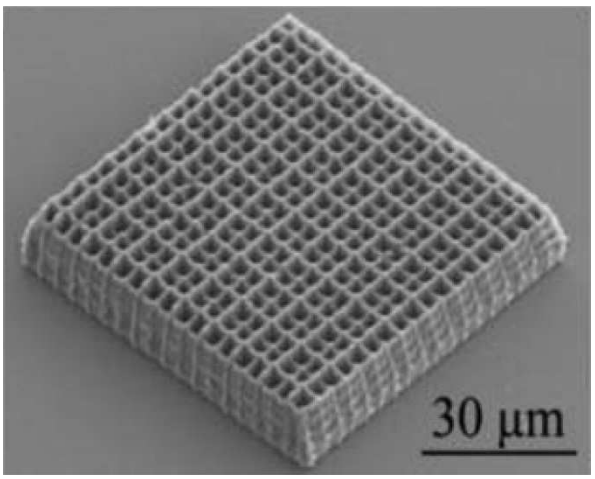

Figure 60. SEM image of a fabricated woodpile microstructure with PEGda and the N/2-Hp-b-CD complex **WI** as photo initiator.[121] Adapted with permission from Ref. [121]. Copyright 2014, Royal Society of Chemistry.

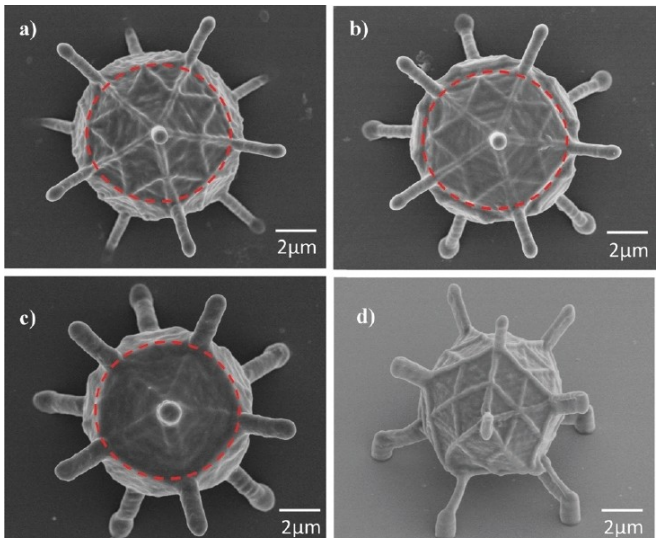

Figure 61. SEM pictures of the fabricated 3D microstructures in form of an adenovirus. (a–c) Top view of the structures fabricated with 7.27 mW, 9.46 mW and 11.27 mW. (d) Side view of fabricated adenovirus structure at 8 mW. All structures were fabricated with a writing speed of 110 μm/s.[124] Reproduced with permission from Ref. [124]. Copyright 2015, Royal Society of Chemistry.

(dimethylamino)-4′-morpholinobutyrophenone was used as photosensitizer. This compound is also known as **Irgacue 369**,), which is used as a commercial photo initiator in 2PP.[125–128] Therefore, it is not quite clear from the publication if the attendance of **Irgacure 369** in the formulations influenced the polymerization efficiencies of **WI** and **WI**–**II**.

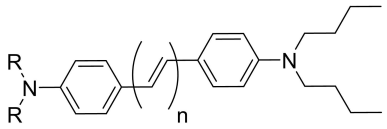

ST-1 R = nBu, n = 1
ST-2 R = Me, n = 2

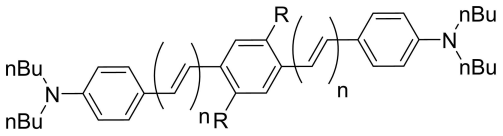

ST-3 R = H, n = 1
ST-4 R = OMe, n = 1
ST-5 R = OMe, n = 2

Figure 62. Schematic representation of the structures of the stilbene based 2PIs **ST-1** to **ST-5**.

Table 24. Optical and fabrication data for **ST-1** to **ST-5**.

Compound	λ_{abs} [nm][a]	λ^2_{abs} [nm][a]	σ_{TPA} [GM][a][b]	E_{th} [mJ]	P_{th} [μW][e]
ST-1	374	600	210	0.3[c]	
ST-2	390	645	260	0.3[c]	
ST-3	410	730	995		
ST-4	425	730	900	0.2[d]	200[f]
ST-5	448	775	1250		300[g]

[a] No solvent reported, [b] measured via TPEF technique, [c] at 600 nm, 5 ns pulses, [d] at 730 nm, 5 ns pulses, [e] power threshold P_{th}, [f] at 730 nm and [g] at 800 nm.

3. D-π-D Chromophores

D-π-D Compounds are able to transfer an electron after one- or two-photon photo excitation, because of their electron rich structure.[9] This also causes large two-photon cross-sections comparable to the before mentioned D-π-A-π-D chromophores.

3.1. Stilbene, benzene and triphenylamine photo initiators

2PIs derived from stilbene or triphenylamines are easily excited and show light induced electron transfer because of their electron rich D-π-D chromophores. They are used on their own or in combination.

Cumpston et al. investigated different stilbene based systems. Several compounds were synthesized and evaluated for their use as photo initiators in two-photon polymerization (Figure 62).[9]

In general, an enlargement of the π-system results in a bathochromic shift as well as a higher σ_{TPA} value (Table 24). The introduction of weak electron donating groups like the methoxy group to the π-backbone (**ST-4** and **ST-5**) can further enhance the initiators properties. For example, **ST-5** shows a linear absorption at 448 nm and a very high σ_{TPA} value of 1250 GM. Unfortunately, the authors did not report the solvent in which measurements where conducted.

The energy thresholds of **ST-1** and **ST-6** were compared to the commercially available UV photo initiators like 1-[4-(methylthio)phenyl]-2-methyl-2-morpholinopropan-1-one (**Irgacure 907**, **I907**, further discussed in Chapter 6.). For **I907** a E_{th} of 1.0 mJ was measured whereas **ST-1** and **ST-2** were more photosensitive with an E_{th} of 0.3 mJ. While **I907** exhibit a σ_{TPA} value lower than 10 GM, the D-π-D structures reveal a much higher value because of their electron richness.

Fabrication tests with the initiators **ST-4** and **ST-5** showed that these compounds, besides **ST-1** and **ST-2**, were able to initiate polymerization under two-photon conditions. Figure 63 displays fabricated cantilevers with 0.1% stilbene based photo initiator and 70% of reactive trifunctional acrylate monomer Sartomer SR9008 and SR368, and 29.9% poly(styrene-*co*-acrylonitrile) (75:25).

Because of their electron richness, triphenyl- or triarylamino motifs are very interesting compounds for the design of new molecules in two photon applications. The structure of **TP-1** (Figure 64) shows a biphenyl connection between two triphenylamines substituted with one methoxy group on each end.[129–130] Although, **TP-1** exhibits a lower σ_{TPA} value compared to other biphenyl centered 2PIs (Table 25) fabrication in a

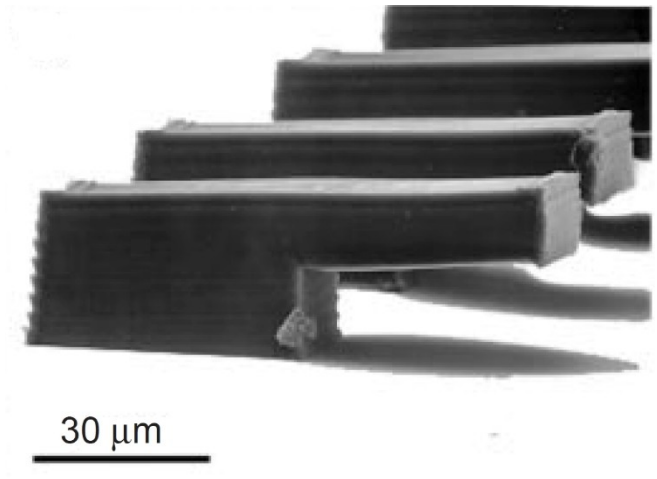

Figure 63. 2PP fabricated cantilevers with one of the stilbene based 2PI.[9] Adapted with permission from Ref. [9]. Copyright 1999, Springer Nature.

monomer mixture containing 70% tris(2-hydroxyethyl)isocyanurate triacrylate and 27% polymer binder poly(styrene-*co*-acrylonitrile) (75/25) with 3% of **TP-1** as initiator was possible. By fabrication of polymer lines the energy threshold of **TP-1** was determined to be 136 J/cm^2. While nowadays the energy threshold is reported in mW (W = J/s) Martineau and a few other authors reported their results unconventionally in mJ/cm^2, which makes the comparison to other 2PIs difficult.[129–133] Compared to **TP-1** the structure of **BTSBP** reveals an extended π-system.[131] By introducing more π-electrons to the structure, the σ_{TPA} is strongly increased to 892 GM (**TP-1** 30 GM). However, the σ_{TPA} values were obtained with two different techniques, which makes a comparison difficult. Polymerization tests in PETA with 0.4% **BTSBP** showed a polymerization threshold of 150 J/cm^2 and a burning threshold of 1600 J/cm^2 (Table 25).

Similar to **BTSBP**, Gan et al. synthesized four different 2PIs with a biphenylic core and different aminoalkyl substituents (Figure 64).[134]

All Initiators exhibit a linear absorption maximum at around 400 nm with exception of **BMHVB** with an absorption maximum of 342 nm (Table 21). This can be explained by the ethylhydroxy substituent, because its donor ability is smaller, the absorption undergoes a hypsochromic shift. The Z-scan measurement revealed for all initiators a large σ_{TPA} value. One should mention that the initiator with the highest σ_{TPA} value, **BMHVB**, interestingly is also the one, which structure contain the substituents with the lowest donor strength. Polymerization tests using bisphenyl A epoxide dimethylacrylate as monomer and 0.5% 2PI showed that all four 2PIs induce polymerization of the acrylate monomer. Figure 65 shows a fabricated micro-grid using **BDBVB** where each polymer vein has a width of 3 μm and an interval width of 10 μm. Unfortunately, the authors did not report any energy, polymerization or burning threshold.

Similar to **ST-4** the initiator **DPAMOB** uses a methoxy substituted distilbene core but with terminal diphenylamino substituents.[135] It has a linear absorption maximum of

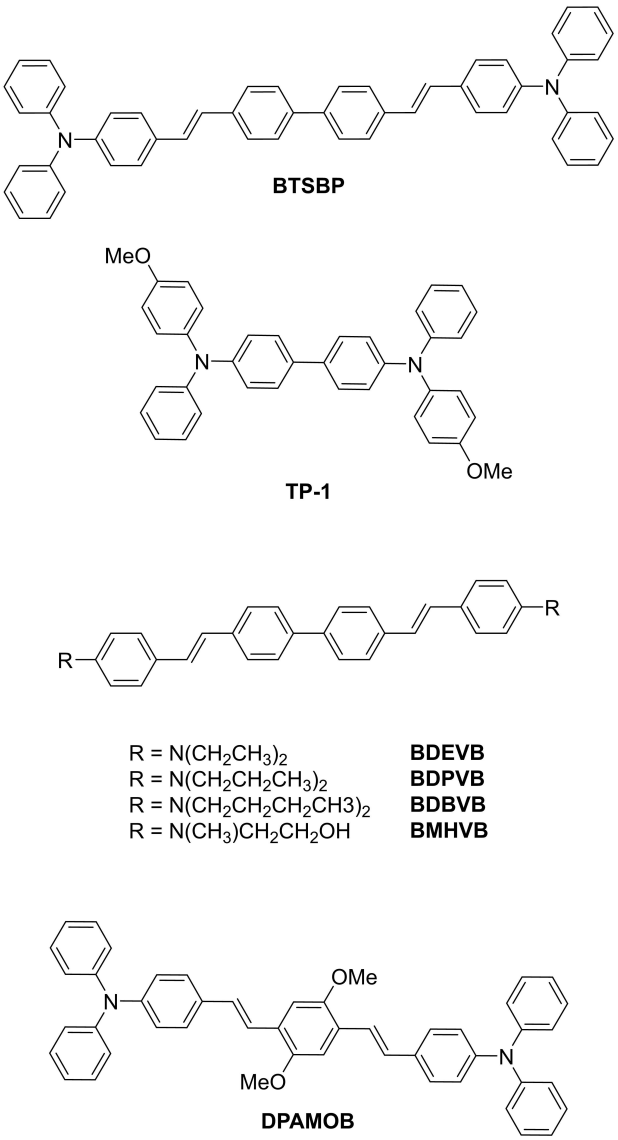

Figure 64. Schematic representation of the structures of 2PIs bearing triphenylamine moieties and biphenyl centers and the 2PA dye **DPAMOB**.

Table 25. Photophysical data and process parameters of the biphenyl centered 2PIs and **DPAMOB**.

Compound	λ_{abs} [nm]	Φ_{fl}	σ_{TPA} [GM]	E_{th} [J/cm^2]	P_{th} [J/cm^2]	E_{Damage} [J/cm^2]
TP-1	349[a]		30[d]	136[g]		2500
BTSBP	431[b]		892 ± 231[e]		150[h]	1600[h]
DPAMOB	423[c]	0.96	1007[e]			
BDEVB	380[a]		87,500[f]			
BDPVB	385[a]		100,900[f]			
BDBVB	389[a]		100,990[f]			
BMHVB	342[a]		115,700[f]			

[a] Measured in dichloromethane, [b] measured in toluene, [c] measured in a doped PMMA block, [d] measured via up-conversion fluorescence, [e] measured via TPEF-method, [f] measured via Z-scan method, [g] Laser power: 1.8 mW, Beam waist: 1.8 μm, writing speed: 30 to 500 μm/s, [h] Laser power: 270 μW, Laser wavelength: 800 nm.

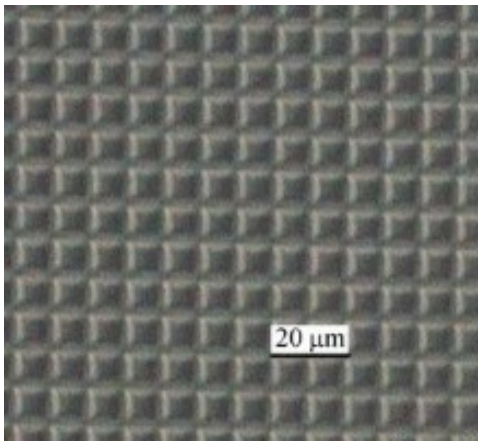

Figure 65. Micro-grid fabricated with **BDBVB** as photo initiator.[134] Reproduced with permission from Ref. [134]. Copyright 2009, Springer Nature.

423.5 nm in toluene and shows no further absorption above 500 nm. The single-photon induced emission spectrum excited with 420 nm, obtains two peaks at 479 nm and 521 nm. The fluorescence quantum yield was determined to be 0.96 for **DPAMOB** with coumarin 307 as reference. The σ_{TPA} value of **DPAMOB** was measured via TPEF in toluene and a cross-section of 1007.2 GM was obtained. Fabrication tests with the oligomer SR454 and 0.5% of the initiator showed successfully fabricated lines at 800 nm with a writing speed of 50 µm/min and a laser power of 50 mW.

The photo initiators **PVBB** and **DPVBB** represent two initiators with a modified triphenylamine structure (Figure 66).[136] The linear absorption in *p*-xylene revealed a maximum at 381 nm for **PVBB**, while for the disubstituted **DPVBB** a small bathochromic shift to 393 nm was measured. Fluorescence quantum yield was determined by the comparison to coumarin 307. **PVBB** shows a fluorescence quantum yield of 0.55 and **DPVBB** 0.14, both in *p*-xylene. By changing the solvent to methanol, the fluorescence quantum yield is strongly decreased to 0.15 and 0.041, which can be explained with the increased polarity and the twisted intramolecular charge transfer (TICT). According to the TICT model, by increasing the solvents polarity the energy level of the charge-transfer state is lowered. This causes not only a red shift of the fluorescence

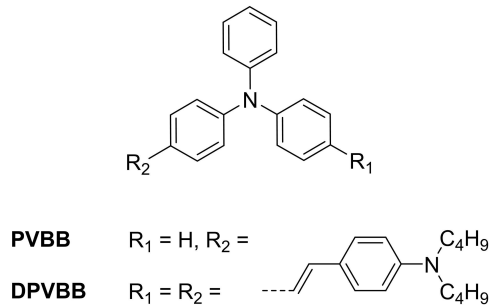

Figure 66. Schematic representation of the structures of **PVBB** and **DPVBB**.

peak, but also a rapid nonradiative transition to triplets. In turn this results in a decrease of the fluorescence quantum yield. The two-photon cross-section was determined via TPEF, and shows 12.9 GM for **PVBB** and 63.3 GM for **DPVBB** in *p*-xylene ($c = 1 \times 10^{-2}$ mol/L).

To evaluate the polymerization properties of the two initiators the polymerization rates (R_p) were compared. The R_ps were determined by a method established by Youmei et al. with SR454 (ethoxylated trimethylolpropane triacrylate) as monomer and 0.6% of initiator.[111] For **DPVBB** the R_p was 471 $\mu m^3/s$ and 180 $\mu m^3/s$ for **PVBB**. With a higher σ_{TPA}-value and lower fluorescence quantum yield it is not surprising that **DVPBB** has a higher photosensitivity along with a higher R_P.

Similar to **2BTrz** and **3BTrz** (Chapter 2.6.) Arnoux et al. synthesized two new initiators bases on an oligo(phenylene–ethynylene) structure. The structures show a two branched quadropolar (**V-Shape**) and three branched octapolar (**Oct**) structure (Figure 67).[137]

The linear absorption spectra in dichloromethane revealed that both compounds exhibit the same absorption maxima at 386 nm. However, the measured fluorescence quantum yields differ around 10%, showing a quantum yield of 66% for **V-Shape** and 79% for **Oct**. This difference becomes even larger for the σ_{TPA} values. z-scan measurements at 532 nm revealed a more than two times higher two-photon cross-section for V-Shape, with 1500 ± 200 GM compared to Oct with 740 ± 150 GM. Polymerizations were performed in a monomer mixture consisting of 20 wt% 1,10-decanediol diacrylate (DDA)

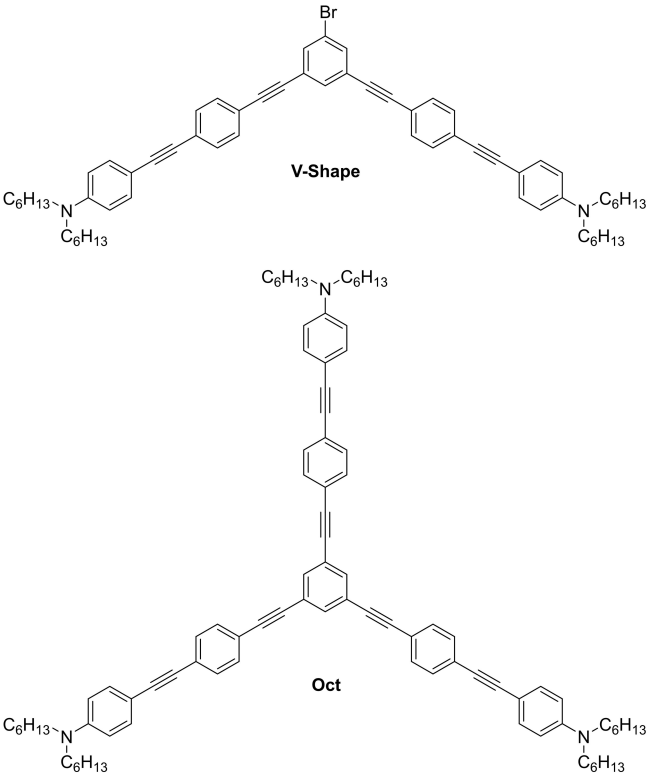

Figure 67. Schematic representation of the structures of the two-branched (**V-Shape**) and the three-branched (**Oct**) 2PIs.

and 80 wt% dipentaerythriol penta-/hexa-acrylate (DPPHA). **V-Shape** was used in a 1 wt% concentration, while Oct was used in a concentration of 0.66 wt% due to its poor solubility in the formulation. For the determination of P_{th} polymer lines were fabricated with different laser powers. The polymerization thresholds for **V-Shape** and **Oct** were 120 μW and 90 μW, respectively. Unfortunately, the authors do not report a fabrication window for the 2PIs.

3.2. Fluorene derivatives

The fluorene core provides a larger electron delocalization because of the increased π molecular orbital overlap, compared to the diphenylic core systems. This structural feature enhances the molecular polarity and by increasing the planarity leads to an optimized charge transfer.[138–139]

Martineau et al. investigated the influence of the fluorenyl core in comparison to the biphenylic core structure.[129–130] The structure containing the fluorenyl core (**FL-1**, Figure 68) shows a bathochromically shifted absorption maximum compared to the structure with the biphenylic core (**TP-1**, Figure 64, Table 24 & 25). 2PA spectra were measured by up-conversion fluorescence measurement and the σ_{TPA} value was determined using 1,4-bis(2-methylstryryl)benzene as reference.[140–141] The fluorenyl structure of **FL-1** exhibit a more then two times higher σ_{TPA} value compared to the biphenylic structure of **TP-1**. This result is in good agreement with an increased charge transfer due to the higher planarity in the fluorenyl core. Threshold energies of the two 2PIs were determined by fabrication of line arrays with different writing speeds. Polymerization was performed with a monomer mixture of 70% tris(2-hydroxyethyl) isocyanurate triacrylate, 27% poly(styrene-*co*-acrylonitrile) (75/25) as polymer binder and 3% of the initiator. **FL-1** revealed an energy threshold of 95 J/cm^2, showing a higher photosensitivity then **TL-1** with 163 J/cm^2. Both of the initiators showed a damage energy of 2500 J/cm^2.

By altering the terminal substituents with an electron donating (triphenylamine) and an electron withdrawing (phthalimide) group Fitilis et al. investigated the 2PIs **F(TPA)$_2$** and **F(PHT)$_2$**.[142–144] Different to **FL-1** the terminal end groups in the structures of **F(TPA)$_2$** and **F(PHT)$_2$** were linked to the fluorene core by a double bond bridge (Figure 68). The linear absorption maximum showed that triphenyl amine containing **F(TPA)$_2$** is higher redshifted compared to the phthalimide containing **F(PHT)$_2$**. Both 2PIs reveal a larger σ_{TPA} value compared to **FL-1** (Table 26). Polymerization tests were performed with bisphenol A ethoxylate diacrylate as monomer and 0.12 wt% of the initiator and revealed a polymerization threshold of 5.6 mW and 3.2 mW for **F(PHT)$_2$** and **F(TPA)$_2$**, respectively. The threshold was further decreased by adding the co-initiator 2,6-diisopropyl-*N*,*N*-dimethylaniline. Fitilis et al. considered that the rate of the free radical polymerization is not only depending on the σ_{TPA} value and the fluorescence quantum yield, but also the radical generation quantum yield as well as the initiation efficiency of the generated radicals are important.[142] To initiate polymerization with such types of photo initiators it is know that an electron transfer must occur after the TPA.[9] In the case of **F(TPA)$_2$** the electron donating substituent makes the molecule more chemically active compared to **F(PHT)$_2$**.

Park et al. developed the initiator **FL-2** with a similar structure to **F(TPA)$_2$** (Figure 68).[145] The linear absorption of **FL-2** reveals a maximum of around 400 nm and the two-photon cross-section at 780 nm shows a σ_{TPA} value of 470 GM (the solvent and method of σ_{TPA} determination not reported). The performance of **FL-2** was tested in a concentration of 0.1 wt% with SCR resin (urethane acrylate mono- and oligomers). To produce a 2D-micro object out of a bitmap image, raster graphics type voxel matrix scanning (VMS) was used. Figure 69

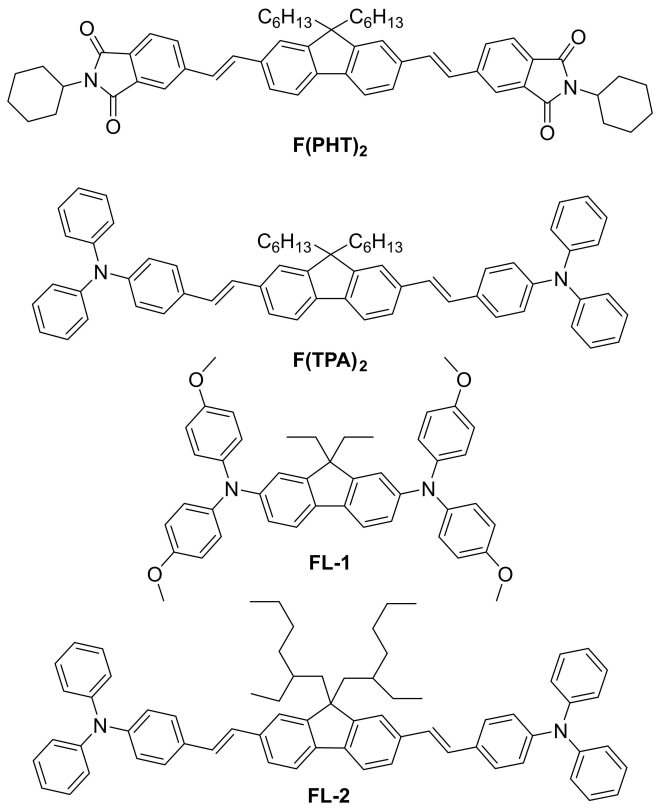

Figure 68. Schematic representation of the structures of the fluorenone based 2PIs **F(PHT)$_2$**, **F(TPA)$_2$**, **FL-1** and **FL-2**.

Table 26. Photophysical data and process properties of the 2PIs containing a fluorenyl core.

Compound	λ_{abs} [nm]	Φ_{fl}	σ_{TPA} [GM]	E_{th} [J/cm^2]	P_{th} [mW]	E_{Damage} [J/cm^2]
FL-1	374[a]		80[d]	95 [g]		2500[g]
FL-2	400[b]		470[e]			
F(PHT)$_2$	378[c]	0.36	835[f]		5.6 [h]	
F(TPA)$_2$	447[c]	0.65	243[f]		3.2 [h]	

[a] Measured in dichloromethane, [b] the authors did not provide the solvent, [c] measured in THF [d] measured via up-conversion fluorescence, [e] determination method not stated, [f] measured via TPFE in THF at 800 nm, [g] Laser power: 1.8 mW, Beam waist: 1.8 μm, Writing speed: 30 to 500 μm/s, and [h] Laser power: 270 μW, Laser wavelength: 800 nm.

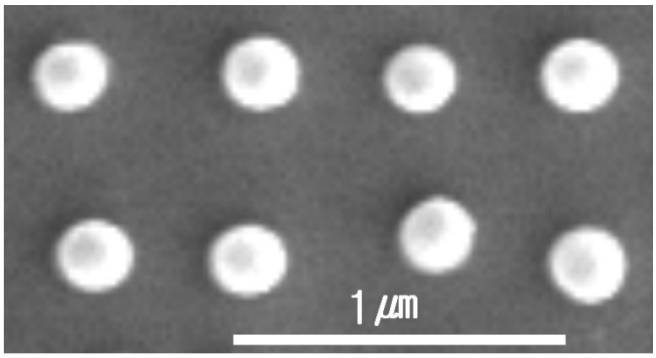

Figure 69. Voxel array fabricated using **FL-2** as initiator with a laser power of 5 mW and an exposure time of 2 ms.[145] Reproduced with permission from Ref. [145]. Copyright 2004, Korean Chemical Society.

displays an array of voxels with 200 nm diameter using this VMS technique.

Figure 70 shows a fabricated 2D structure and its corresponding bitmap image, proofing that with VMS it is possible to translate a bitmap image to an almost identical 2D micro structure.

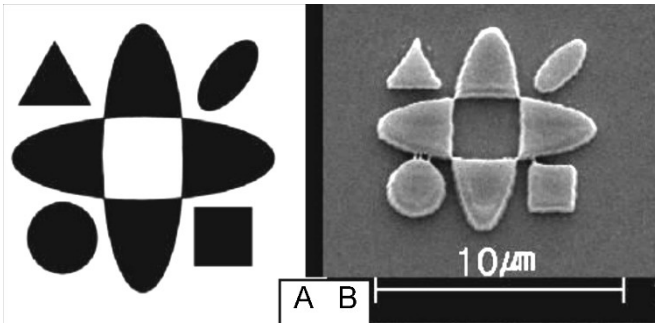

Figure 70. Fabricated micro structure using **FL-2** (B) and its corresponding bit map image (A).[145] Reproduced with permission from Ref. [145]. Copyright 2004, Korean Chemical Society.

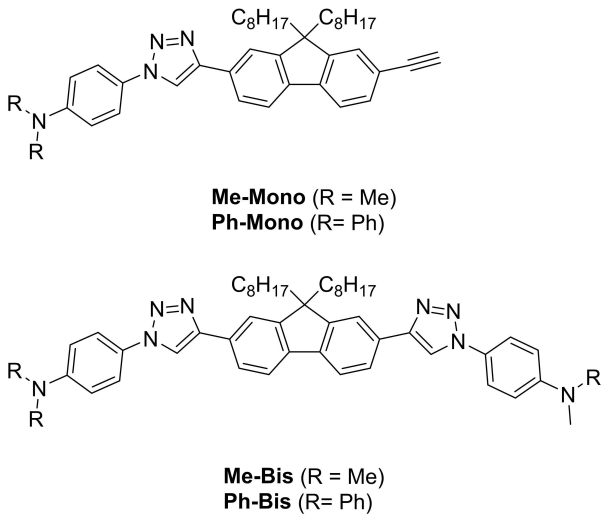

Figure 71. Schematic representation of the structures of the triazole bridged fluorene 2PIs.

In order to develop new and efficient photo initiators Henning et al. reported the first triazole containing photo initiators for use in 2PP.[146] The authors used the copper catalyzed azide/alkyne cycloaddition (CuAAC) reaction for the synthesis, because of its wide use in organic chemistry and high yields.[147] It is also known that the also called "click reaction" was used to synthesize UV photo initiators as well as organic dyes and fluorophores.[148–150] With this approach the authors created mono- and difunctionalized photo initiators with a octanyl modified fluorene core (Figure 71).

From the linear absorption spectra, it is evident that the change from the mono- to the disubstituted structure has only a slight influence on the absorption maxima. The maxima also only shift very little if the methyl group is substituted by the phenyl group (Table 27). However, the phenyl substituted 2PIs **Ph**–**Mono** and **Ph**–**Bis** show generally lower fluorescence quantum yields compared to the methyl substituted ones. But in total the here reported 2PIs show quite high fluorescence quantum yields compared to other photo initiators for 2PP. The two-photon absorption spectra were measured via TPEF method and revealed that the σ_{TPA} values did not differ munch comparing the asymmetrical (**Me**–**Mono**, **Ph**–**Mono**) and symmetrical (**Me**–**Bis**, **Ph**–**Bis**) initiators (Figure 72). But overall the phenyl containing 2PIs showed higher σ_{TPA} values, which can be attributed to the higher number of π-electrons.

For the determination of the fabrication windows arrays of small cubes (5×5×5 μm) were fabricated with two different monomers, PEG-DA and PETA. All initiators were able to initiate polymerization in PEG-DA, although **Me**–**Bis** and **Ph**–**Bis** showed poor solubility. **Ph**–**Mono** was performing best. The polymerization tests in PETA revealed lower polymerization thresholds compared to PEG-DA, which indicate that PETA needs lower laser power to polymerize. However, the FW in PETA were narrower compared to the ones in PEG-DA. For **Me**–**Bis** and **Ph**–**Bis** no fabrication window was determined because of solubility problems.

For comparison complex 3D structures in form of buckyball domes were fabricated with all of the 2PIs (Figure 73). The structures fabricated with **Me**–**Bis** and **Ph**–**Bis** show collapsed structures, due to the poor solubility of the photoinitator. More stable structures were obtained with **Me**–**Mono** and **Ph**–**Mono**,

Table 27. Photophysical data in toluene and process properties of triazole containing 2PIs.

Compound	λ_{abs} [nm]	Φ_{fl} [%]	FW [mW][a]	FW [mW][b]
Me–**Mono**	340	50.8	18 to 39	14 to 24
Ph–**Mono**	338	30.0	16 to 40	13 to 25
Me–**Bis**	343	67.3	17 to 31	–
Ph–**Bis**	352	58.3	13 to 31	–

[a] Fabrication windows with PEG–Da as monomer, writing speed = 20 mm/s, Laser wavelength = 780 nm, 2PI concentration 4 mM, [b] Fabrication window with PETA as monomer, writing speed = 20 mm/s, Laser wavelength = 780 nm, 2PI concentration 4 mM.

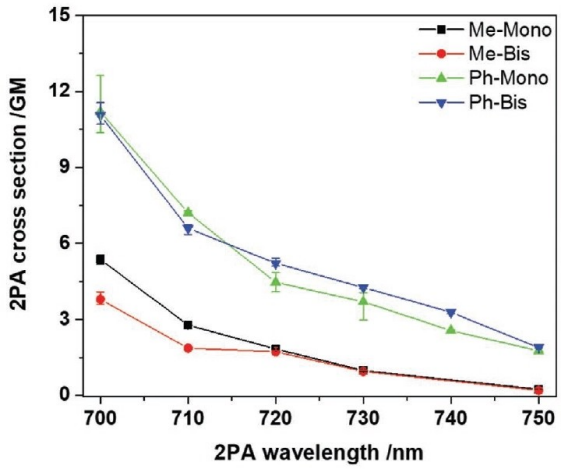

Figure 72. Two-photon absorption spectra for the triazole containing fluorene 2PIs.[146] Adapted with permission from Ref. [146]. Copyright 2020, John Wiley and Sons.

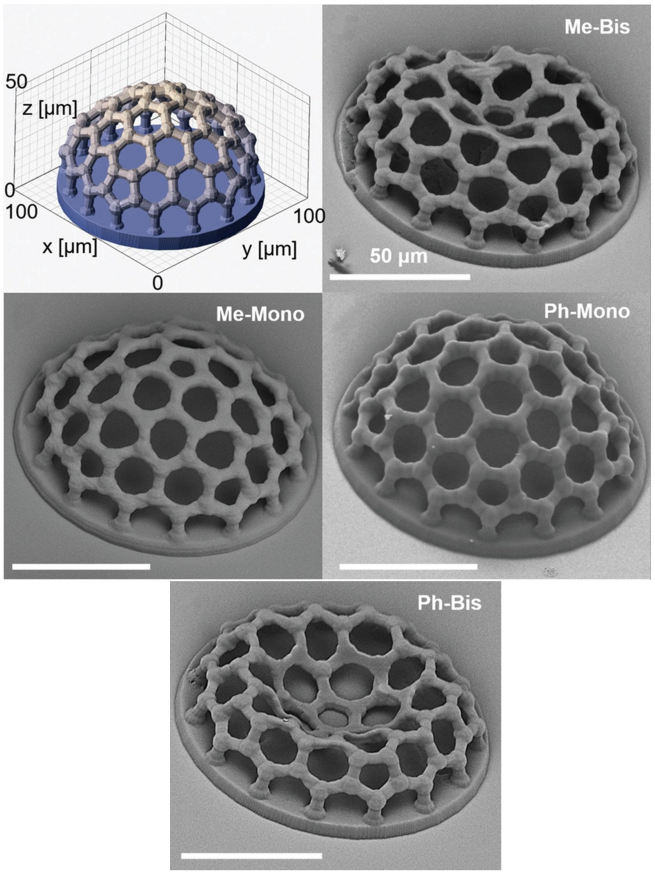

Figure 73. SEM images of complex 3D structures in form of a buckyball dome fabricated with the triazole containing fluorine based 2PIs.[146] Adapted with permission from Ref. [146]. Copyright 2020, John Wiley and Sons.

with a stable top part of the dome. Thus, making **Me**–**Mono** and **Ph**–**Mono** promising candidates for 2PP.

3.3. Anthracene derivatives

Anthracene derivatives have been widely investigated as UV photosensitizers or -initiators.[151–152] TPA properties of molecules containing anthracene as a central π-system were thoroughly investigated by several groups.[153–156] Yang et al. synthesized serval anthracene derivatives, investigated and compared them to known TPA dyes.[157] The authors were able to synthesize anthracene derivatives with an σ_{TPA} value up to 2490 GM and also showed that the overall TPA properties increased by changing the phenyl center to an anthryl one.[157]

Xing et al. synthesized three 2,7-substituted anthracene derivatives (Figure 74) and investigated their ability as photo initiators in two-photon polymerization.[132–133]

Table 28 summarizes the influence of a strong electron donating substituent (**AN-1**) to a weak (**AN-2**) and an electron withdrawing group (**AN-3**). Compared to **AN-1** with its $N(CH_3)_2$ groups, **AN-2** and **AN-3** show a hypsochromic shift in the absorption maxima. Interesting about that is that **AN-2** with a weak electron donating group reveals a larger hypsochromic shift compared to **AN-3** with a nitrile group. The fluorescence quantum yield measurement shows that **AN-3** has the largest yield, **AN-2** the second largest and **AN-1** the smallest. The TPEF measurement revealed that **AN-1** has the largest value with 466 GM, followed by **AN-3** with 121 GM and at last **AN-2** with 78 GM. This strong enhancement of the σ_{TPA} value of **AN-1** is mainly attributed to the strong electron donating groups, since it leads to a large intramolecular charge transfer (ICT).

Polymerization tests were performed with methacrylic acid (MAA) as monomer and dipentaerythritol hexaacrylate (DEP-6 A) as crosslinker. The laser wave length was set to 800 nm and the writing speed was 10 µm/s.

AN-1 reveals the lowest polymerization threshold as well as the 2PP threshold (E_{th}) of all the tested initiators (Table 29). The sensitivity of the initiators follows the order **AN-1** > **AN-2** >

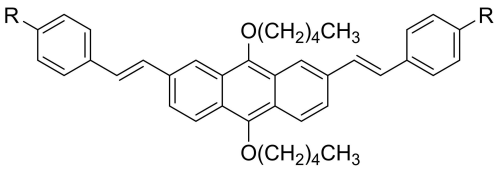

AN-1 R = $N(CH_3)_2$
AN-2 R = CH_3
AN-3 R = CN

Figure 74. Schematic representation of the structures of the anthracene based photo initiators **AN-1** to **AN-3** synthesized by Xing et al.

Table 28. Photophysical properties of **AN-1** to **AN-3** in $CHCl_2$.

Compound	λ_{max} [nm]	Φ_{fl}	$^2\lambda_{max}$ [nm]	σ_{TPA} [GM][a]
AN-1	396	0.17	750	466
AN-2	347	0.36	700	78
AN-3	355	0.22	700	121

[a] Measured via TPEF.

Table 29. Resin formulations and photopolymerization data of **AN-1** to **AN-3** compared to the common used 2PI **Benzil**.

2PI	MAA [wt %]	DPE-6 A [wt %]	MR [%][a]	P_{th} [mW][b]	E_{th} [mJ/cm^2][c]
AN-1	66.47	32.59	0.18	0.64	2.77×10^7
AN-2	66.53	32.61	0.18	1.60	6.93×10^7
AN-3	66.50	32.61	0.18	8.37	3.56×10^8
Benzil	66.89	32.80	0.18	6.37	2.82×10^8

[a] Molar ratio of initiator in resin, [b] threshold power of the initiator in resin and [c] exposure intensity at threshold power.

Benzil > **AN-3**. Line arrays of the polymerization tests are displayed in Figure 75.

To investigate the influence of the concentration of the 2PI on the polymerization threshold several resin formulations with **AN-1** as initiator were prepared (Table 30). The results show that a lower concentration of **AN-1** results in a higher P_{th}, which indicates a fewer generated radicals. In addition, the dependence of the polymerization threshold to the writing speed (10 to 1000 μm/s) was investigated using the resin formulation **R**[1]. By increasing the writing speed, the exposure time was decreased from 40 ms (10 μm/s) to 0.4 ms (1000 μm/s) and the P_{th} increased from 0.64 to 2.53 mW.

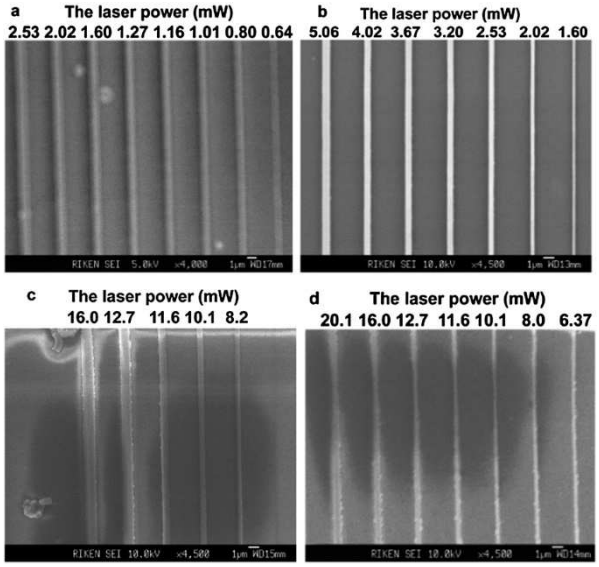

Figure 75. SEM pictures of fabricated line arrays using (a) **AN-1**, (b) **AN-2**, (c) **AN-3** and (d) **Benzil**.[132] Reproduced with permission from Ref. [132]. Copyright 2012, Royal Society of Chemistry.

Table 30. Polymerization and 2PP thresholds at different concentrations of **AN-1**.

Resin	MAA [wt %]	DPE-6 A [wt %]	MR [%][a]	P_{th} [mW][b]	E_{th} [mJ/cm^2][c]
R[1]	66.47	32.59	0.18	0.64	2.77×10^7
R[2]	66.78	32.75	0.09	1.01	4.37×10^7
R[3]	66.94	32.82	0.045	1.60	6.93×10^7
R[4]	67.02	32.86	0.023	2.02	8.74×10^7
R[5]	67.06	32.88	0.012	5.06	2.19×10^8

[a] Molar ratio of initiator in resin, [b] threshold power of the initiator in resin and [c] exposure intensity at threshold power.

3.4. Water-soluble photo initiators with a D-π-D structure

Although D-π-A-π-D chromophores show great potential, other structural chromophores, like D-π-D structures, also have been successfully used as water-soluble initiators. **WSPI** is a D-π-D chromophore, which has a distyrylbenzene core with terminal amino alkyl groups (Figure 76). Frist synthesized by Woo et al.[158] as a TPA chromophore **WSPI** was later used as a water-soluble photo initiator in 2PP by the group of Liska et al.[159–160]

WSPI exhibits a linear absorption maximum at 423 nm and a σ_{TPA} value of 360 GM measured with the TPEF method at 730 nm.[158] The fluorescence quantum yield was determined to be 0.40 for **WSPI** with fluorescein and 9,10-diphenylanthracene as references.

Stampfl et al. were able to fabricate successfully hydrogel structures with **WSPI** as 2PI and PEGda (700 Da) and embed the living organism *Caenorhabditis elegans* into a scaffold during 2PP structuring.[159] Therefore, several test structures were fabricated to investigate the fabrication window of this monomer/2PI system. Two formulations were tested, both of them with a 2PI concentration of 2 wt%, one with a water content of 50 wt% and the second with 80 wt%.

Intact structures were obtained at 60 mW at 1 mm/s, 100 mW at 4 mm/s, 140 mW at 7 mm/s, and 220 mW at 10 mm/s, respectively (Figure 77). By increasing the water content to 80 wt% the polymerization threshold shifts to higher laser powers and the threshold for the writing speed is reduced. Polymerization at 300 mW and 10 mm/s occurred but a stable structure was not obtained.[159] Besides PEGda as monomer, fabricating structures from a binary monomer mixture consisting of gelatin hydrolysate vinyl esters (GH-VE) and reduced derivatives of bovine serum albumin was achieved with **WSPI** as 2PI.[160]

For a long time aryl diazosulfone compounds are known to initiate free radical polymerization under thermal conditions, forming phenyl- and sulfonyl-based radicals.[161] Although such initiators have not been used in 2PP, some exhibit a strong absorption within the visible range. Therefore, an absorption under two-photon conditions around 800 nm was assumed. On

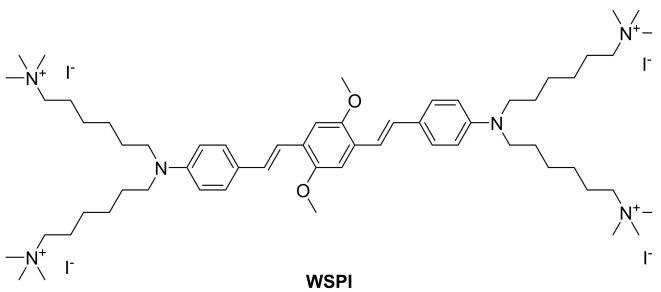

Figure 76. Schematic representation of the structure of **WSPI**.

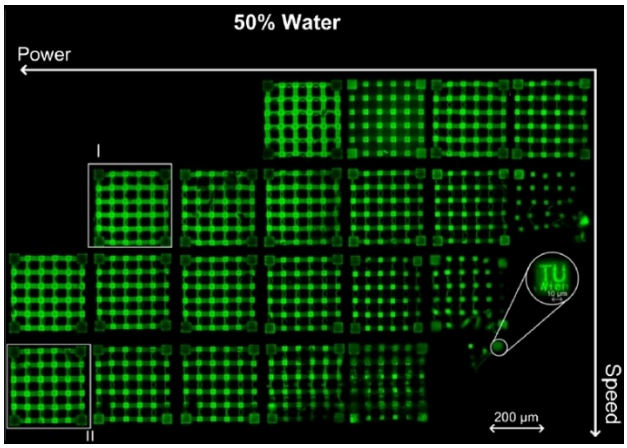

Figure 77. Woodpile structures of PEGda with **WSPI** as photo initiator at a water content of 50 wt%. The laser power range was 10 to 300 mW ($\Delta = 40$ mW) and the writing speed was 1 to 10 mm/s ($\Delta = 3$ mm/s).[159] This image was adapted with the permission of the publisher and the authors of Ref. [159]. Copyright 2012, SPIE.

this basis the water-soluble initiator **DAS** (Figure 78) was developed.[162]

DAS exhibits a linear absorption maximum at 370 nm in water, which is strongly blue shifted in comparison to the literature known initiator **P2CK** (507 nm, Figure 52). This strong shift of **DAS** is due to the absence of electron donating groups and by the electron withdrawing ability of the azosulfones. To determine the two-photon cross-section the white light continuum (WLC) Z-scan method, developed by Ajami et al., was used.[163] It shows a σ_{TPA} value of 40 GM and 140 GM for **DAS** and **P2CK**, respectively. Fabrication tests of **DAS** and **P2CK** with gelatin methacrylamide revealed that, although **DAS** has a low σ_{TPA} value the polymerization initiation efficiency is high enough. The low σ_{TPA} value is compensated by doubling the concentration. The polymerization thresholds for both initiators were tested between 20 to 100 mW laser power and 100 to 1000 mm/s writing speed at different concentrations (Figure 79).

The tests show that, although **P2CK** has a lower polymerization threshold, **DAS** can be used as a suitable photo initiator at higher concentrations. Latter is interesting in particular because cytotoxicity tests using the Presto Blue assay revealed that **P2CK** reduced the cell viability above a concentration of 0.5 mM immensely (< 50 % cell viability). With **DAS** the cell viability remain also at higher concentrations (> 50 % cell viability).

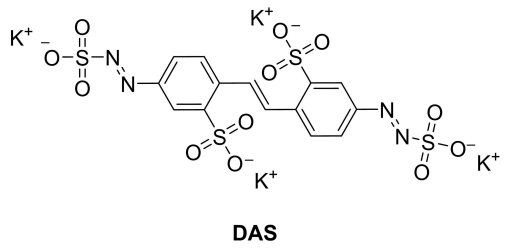

DAS

Figure 78. Schematic representation of the structure of **DAS**.

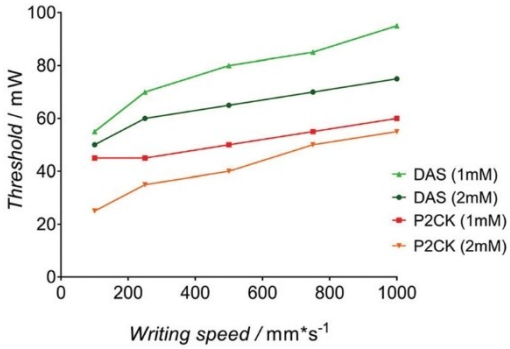

Figure 79. Polymerization thresholds of **DAS** and **P2CK** at concentrations of 1 mM and 2 mM.[162] Adapted with permission from Ref. [162]. Copyright 2018, Royal Society of Chemistry.

4. A-π-D-π-A and D-π-D-π-D Chromophores

Besides the D-π-A-π-D chromophores, also chromophores with the inverse structure motif A-π-D-π-A exhibit large σ_{TPA} values. But only a limited number of these compounds were investigated as photo initiator for 2PP.

4.1. Carbazole and phenothiazine based initiators

Among these chromophores carbazole based chromophores have been investigated intensively. Figure 80 displays the V-shaped photo initiators (**BAC-1** to **BAC-4**) with carbazole as central core.[110]

Compared to the aldehyde derivatives **BAC-1** and **BAC-2**, the nitro substituted initiators **BAC-3** and **BAC-4** exhibit very low fluorescence quantum yields. Additional measurements of the fluorescence quantum yield in THF of **BAC-3** and **BAC-4** revealed a slight increase, which results from the difference in

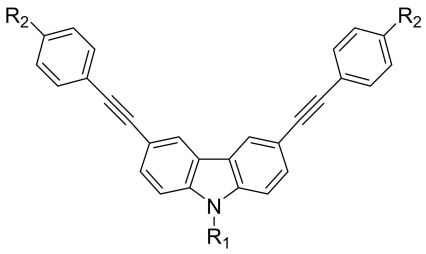

BAC-1	$R_1 = C_5H_{11}$	R_2 = CHO
BAC-2	$R_1 = CH_2Ph$	R_2 = CHO
BAC-3	$R_1 = C_5H_{11}$	$R_2 = NO_2$
BAC-4	$R_1 = PhCH_2$	$R_2 = NO_2$
BNMBC	$R_1 = CH_2Ph(4\text{-}OMe)$	$R_2 = NO_2$

Figure 80. Schematic representation of the structures of V shaped photo initiators based on carbazole.

contact charge transfer (Table 31). **BAC-1** and **BAC-2** revealed a σ_{TPA} value in chloroform of around 300 GM, while **BAC-3** and **BAC-4** showed a value of 645 GM and 916 GM in THF, respectively. Due to the high σ_{TPA} values and the low FQ **BAC-3** and **BAC-4** should be promising candidates for initiating 2PP. Polymerization tests were performed with MAA as monomer and DEP-6 A as crosslinker, at 800 nm laser wavelength and 10 μm/s writing speed.

As displayed in Table 32 the polymerization thresholds of the initiators are quite different. **BAC-1**, with a P_{th} of 10.11 mW, revealed a much higher threshold compared to the commercial initiator **Benzil** with a P_{th} of 6.37 mW. Initiator **BAC-3** shows the third largest P_{th}, followed by **BAC-2** with 1.60 mW. Due to its high σ_{TPA} value and low fluorescence quantum yield compared to the other initiator, **BCA-4** reveals the smallest Pth with 0.80 mW. Therefore, concentration tests with **BAC-4** were performed. The 2PI concentration was decreased from 0.18 wt% to 0.012 wt%. By decreasing the 2PI concentration, the P_{th} was increasing to a value of 3.20 mW at a 2PI concentration of 0.012 wt%. In addition, the 2PP threshold for different concentrations was calculated, which were for 0.18 wt% and 0.012 wt% values of $E_{th} = 3.0 \times 10^7$ and 1.2×10^8 mJ cm^{-2}.

Since the resolution of fabricated structures via 2PP is strongly depended on the radicals generated in the focal spot of the laser, a possible way to further enhance the resolution of 2PP is by combining a radical quencher with an existing photo initiator with good initiating properties. Such a chromophore should terminate the photoinduced radicals around the focused spot. Lu et al. developed such a photo initiator (**BNMBC**) by introducing *p*-methoxybenzene (PhOMe, Anisol) into the structure of photo initiator **BAC-4** (Figure 80).[164]

The linear absorption maximum of **BNMBC** in THF is at 384 nm and is nearly exact the same as for **BAC-4**. Although the maxima are quite the same **BNMBC** exhibit with 0.17 a much larger fluorescence quantum yield in comparison to **BAC-4** with 0.077. Two-photon cross-sections were determined by the TPEF as well as the Z-scan method. σ_{TPA} values obtained via TPEF revealed for **BNMBC** and **BAC-4** a cross-section of 262 and 500 GM, respectively. Because of the difference in fluorescence quantum yield, an additional measurement with the Z-scan method was performed. The cross-sections received from Z-scan were 2367 and 2285 GM for **BNMBC** and **BAC-4** respectively, showing that these compounds possess a large σ_{TPA} value. Polymerization tests were performed by using MAA as monomer, pentaerythriol triacrylate (PE-3 A) as crosslinker and the photo initiator systems **BAC-4**, **BAC-4**/PhOMe (molar ration 1 : 1) and **BNMBC**. The resin formulations are listed in Table 33.

To investigate whether the intermolecular (**BAC-4**/Anisol) or the intramolecular (**BNMBC**) system performs better at radical quenching, different resins were prepared. Thereby, fibers were fabricated and the obtained heights and widths were compared (Figure 81).

Table 31. Photophysical data of the carbazole based photo initiators **BAC-1** to **BAC-4**.

Compound	Solvent	λ_{max} [nm]	Φ_{fl}[a]	σ_{TPA} [GM][b]
BAC-1	$CHCl_3$	383	0.63	337 (730 nm)
BAC-2	$CHCl_3$	378	0.66	308 (730 nm)
BAC-3	$CHCl_3$	396	0.005	–
	THF	390	0.065	645 (770 nm)
BAC-4	$CHCl_3$	385	0.007	–
	THF	384	0.065	916 (780 nm)

[a] Fluorescence quantum yield determined relative to coumarin 307. [b] TPEF measurement. The numbers in parentheses are the wavelengths of the maximum TPA.

Table 32. Polymerization results and formulation conditions for **BAC-1** to **BAC-4** and **Benzil** as reference.

2PI	MAA [wt %]	Initiator [wt %]	DPE-6 A [wt %]	MR [%][a]	P_{th} [mW][b]
BAC-1	66.62	0.72	32.66	0.18	10.11
BAC-2	66.60	0.75	32.65	0.18	1.60
BAC-3	66.59	0.77	32.64	0.18	2.02
BAC-4	66.57	0.80	32.63	0.18	0.80
Benzil	66.90	0.31	32.79	0.18	6.37

[a] Molar ratio of initiator in resin, [b] threshold power of initiator in resin and [c] exposure intensity at threshold power.

Table 33. Resin composition for 2PP polymerization tests.

Resin	2PI	MAA [wt%]	Initiator [wt%]	PE-3 A [wt%]	MR [%][a]	P_{th} [mW]
R^1	**BAC-4**	80.02	0.47	19.51	0.1	
R^2	**BAC-4**/Anisol	79.95	0.57	19.49	0.1	
R^3	**BNMBC**	80	0.5	19.5	0.1	
R^4	**BAC-4**	80	0.1	19.9	0.02	4.02
R^5	**BAC-4**/Anisol	80	0.1	19.9	0.02	4.82
R^6	**BNMBC**	80	0.21	19.9	0.02	5.53

[a] Molar ratio of the initiator.

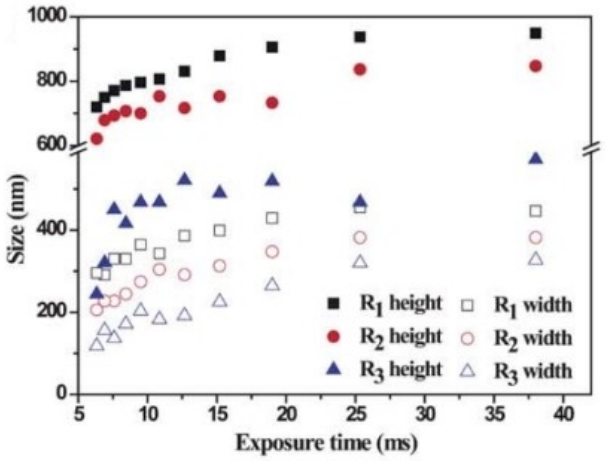

Figure 81. Plot of the fabricated fiber versus the exposure time for the resins R^1, R^2, R^3. The fabrication was performed at a laser power of 3.67 mW.[164] Adapted with permission from Ref. [164]. Copyright 2011, Royal Society of Chemistry.

From the plot is evident that the heights and widths are decreasing from **R**[1] to **R**[3], what means that **BNMBC** has a higher radical quenching effect than the **BAC-4**/PhOMe system in **R**[2]. In the resin with **BNMBC** an intramolecular quenching of radicals during the polymerization takes place, while the bimolecular system **BAC-4**/PhOMe acts in an intermolecular way, which is much slower compared to the intramolecular process. Similar results were obtained by decreasing the molar ratio of the initiator system to 0.01 %. The polymerization thresholds were investigated with a higher concentration of the initiators, resulting in 4.02, 4.28 and 4.53 mW for **R**[4], **R**[5] and **R**[6] respectively. Despite the small differences in the σ_{TPA} values **BNMBC** shows a similar polymerization initiating efficiency comparable to **BAC-4**. In addition, **BNMBC** revealed radical-diffusion control due to the *p*-methoxybenzyl group. To demonstrate the potential of **BNMBC** a complex 3D structure in from of a fly was fabricated using **R**[6] as resin. The fabricated fly has a height of 6.47 µm and a width of 17.61 µm and is 20.90 µm long (Figure 82).

Li et al. developed four carbazole based photo initiators using classical aldol-conditions. The initiators **CRB-1** and **CRB-2** show a A-π-D-π-A structure, and were compared to **CRB-3** and **CRB-4** which possess a D- π-D- π-D structure (Figure 83).[165]

CBR-1 and **CBR-2** exhibit a linear absorption maximum at 415 nm and 394 nm in chloroform, respectively. Both absorption maxima from **CBR-3** and **CBR-4** reveal a bathochromic shift to 350 nm and 360 nm, respectively (Figure 84).

The two-photon cross-sections were measured using open aperture Z-scan analysis at 800 nm in DMSO. Both **CBR-3** and **CBR-4** show a relatively low σ_{TPA} value of 20 and 18 GM, respectively. On the other hand, the σ_{TPA} value increases by a factor of 10 when the terminal donor groups are exchanged by acceptor groups like nitro or nitrile groups. Therefore **CBR-1** and **CBR-2** exhibit a value of 280 and 220 GM. This increase is attributed to the ICT which is well-known to be the "driving force" of the two-photon absorption process.[165–167] Fabrication tests were performed with a 1:1 mixture of TMPTA and TMP3EOTA resin at 800 nm with a writing speed of 60 µm/s. Y shaped structures were fabricated at different laser powers to evaluate the fabrication windows. Figure 85 displays the fabricated structures using **CRB-4** at different laser powers.

The fabrication windows for all initiators are displayed in Figure 86. **CBR-2** and **CBR-4** reveal the broadest fabrication windows. Although **CBR-4** has the lowest σ_{TPA} value of all, it seems to compensate this disadvantage with its electron richness. As shown in Chapter 3. D-π-D chromophores initiate polymerization by electron transfer,[9] it seems that **CBR-4** follows a similar pathway in the initiating polymerization. By introduction of the nitro groups the solubility of **CBR-1** was significantly decreased so that no reasonable results were obtained. These results indicate again that although a high σ_{TPA} value is desirable, the initiator efficiency is not only depending on that.

Although many neutral compounds have been discussed, there are several research groups which also investigated ionic

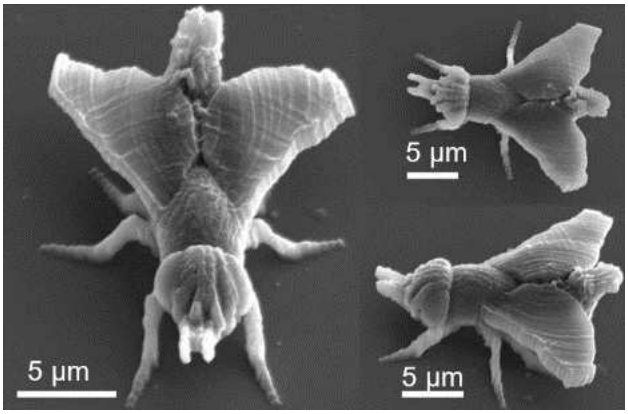

Figure 82. SEM image of a fly fabricated via 2PP using **BMNBC** as initiator.[164] Adapted with permission from Ref. [164]. Copyright 2011, Royal Society of Chemistry.

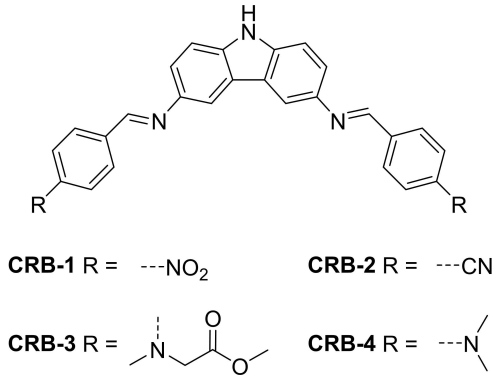

Figure 83. Schematic representation of the structures of carbazole based photo initiators **CRB-1** to **CRB-4**.

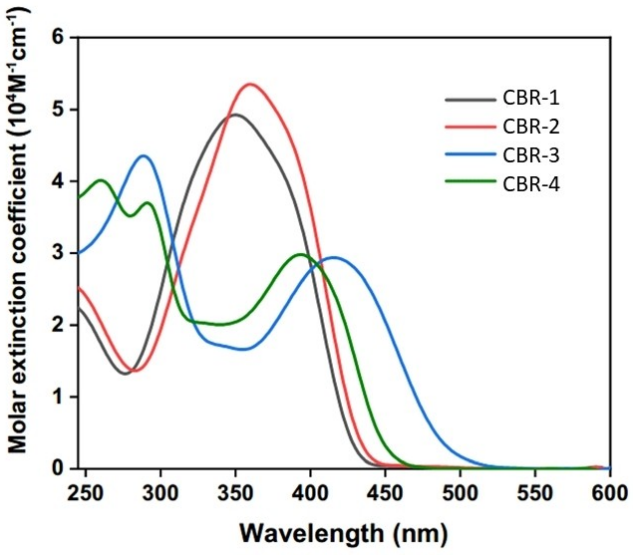

Figure 84. UV-Vis absorption spectra of **CBR-1** to **CBR-4** in $CHCl_3$.[165] Reproduced with permission from Ref. [165]. Copyright 2018, John Wiley and Sons.

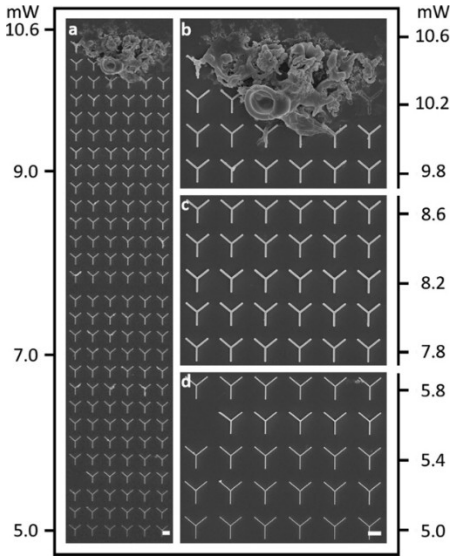

Figure 85. SEM image of the fabricated Y structures evaluating **CBR-4** as photo initiator, (a) full view of the structures along the laser power gradient and (b)–(d) enlargement of different segments of (a).[165] Reproduced with permission from Ref. [165]. Copyright 2018, John Wiley and Sons.

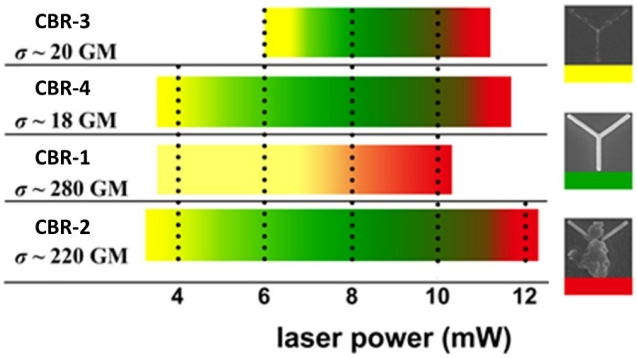

Figure 86. Display of the fabrication windows of the initiators **CBR-1** to **CBR-4**.[165] Adapted with permission from Ref. [165]. Copyright 2018, John Wiley and Sons.

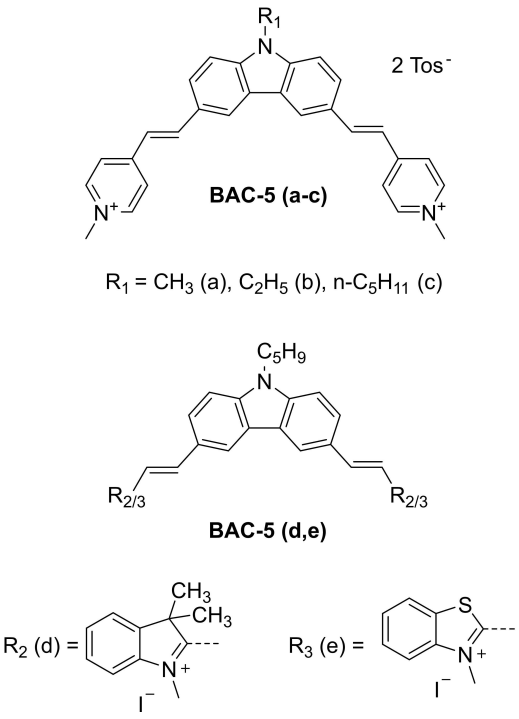

Figure 87. Schematic representation of the structures of **BAC-5**(a–e).

Table 34. Photophysical data of the initiators **BAC-5**(a–e) in methanol.

Compound	λ_{max} [nm]	Φ_{fl}	σ_{TPA} [GM][a]
BAC-5a	456	0.011	1737[c]
BAC-5b	456	0.013	1740[c]
BAC-5c	458	0.013	1650[c]
BAC-5d	510	0.007	474[b][d]
BAC-5e	495	0.039	151[e]

[a] Measured via TPEF, [b] measured in glycerol, [c] TPA maximum at 800 nm, [d] TPA maximum at 880 nm and [e] TPA maximum at 840 nm.

compounds for their TPA properties.[99,168–172] Gu et al. developed carbazole based organic salts with an elongated π-system.[173] Pyridinium, indolium and benzothiazolium derivatives (**BAC-5a** to e, Figure 87) have also been reported.

The photophysical properties of the different compounds are listed in Table 34. The linear absorption maxima of **BAC-5**(a–c) show that the length of the aliphatic chain in the R_1 position shifts the absorption maxima only slightly to higher wavelengths. In addition, the impact on the fluorescence quantum yield is only marginal. The σ_{TPA} values are high with around 1700 GM but decrease when the pentyl substituent is used. By changing from the pyridinium to either an indolium (d) or a benzothaizolinium (e) substituent the linear absorption shifts to higher wavelengths, while the fluorescence quantum yields and the σ_{TPA} decreases.

From the above-mentioned photo initiators **BAC-5c** was chosen for further polymerization tests. 0.1 wt% of **BAC-5c** were mixed with 49.9 wt% MAA as monomer and 50.0 wt% DEP-6 A as crosslinker. The threshold energy of polymerization for **BAC-5c** was calculated by analyzing polymer spots fabricated via single-spot exposures and a value of 3.0 mW was determined. In addition, a microgrid structure was fabricated using **BAC-5c** with a laser power of 10 mW and an exposure time of 2 ms (Figure 88).

To investigate the influence of the core structure, Li et al. synthesized four different photo initiators, two with a carbazole core and two with a phenothiazine core.[174] In addition, the structures of the initiators showed two different acceptor groups, a thiophen aldehyde and quinoline group, which are linked to the core via triple bond bridges (Figure 89).

In the linear absorption measurement, the compounds revealed that the change of the carbazole to the phenothiazine core shifts the absorptions maxima to higher wavelengths. In addition, also the fluorescence quantum yield of the phenothiazine based initiator are lower in comparison to the carbazole

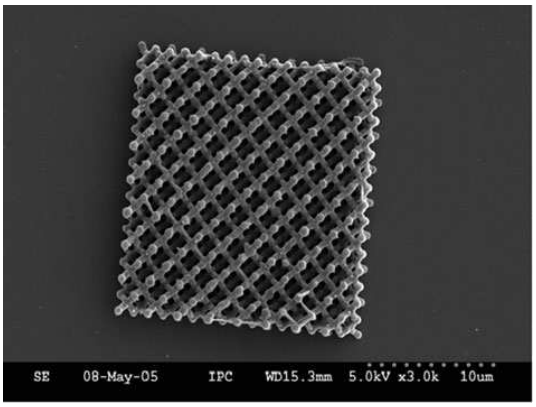

Figure 88. Microgrid structure fabricated via 2PP using 0.1 wt% **BAC-5 c** as 2PI.[173] Reproduced with permission from Ref. [173]. Copyright 2007, Royal Society of Chemistry.

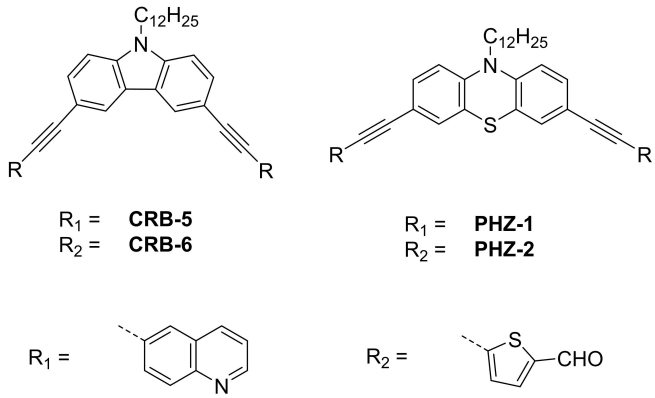

Figure 89. Schematic representation of the structure of the carbazole (**CRB-5** and **CRB-6**) and phenothiazine (**PHZ-1** and **PHZ-2**) based 2PIs.

2PIs, in particular **PHZ-2**. From the σ_{TPA} values it can be anticipated that the higher donor strength of the thiophen aldehyde group leads to a stronger ICT, which can be seen in the higher σ_{TPA} value as well as the red shifted absorption maxima (Table 35). Because of their absorption maxima the 2PIs **CRB-6**, **PHZ-1** and **PHZ-2** may be potential candidates to efficiently initiate polymerization at a wavelength at 780 nm, in particular **PHZ-2** with its high σ_{TPA}-value and its low fluorescence quantum yield.

For the polymerization tests all 2PIs were dissolved in TTA and fabrication was performed with different laser intensities and writing speeds. In this report the laser intensity was set to 30 mW which was declared as 100%. The tests revealed that the thiophen aldehyde containing initiators **CRB-6** and **PHZ-2** successfully initiated polymerization. However, the authors did not report weather **CRB-5** or **PHZ-1** initiate polymerization under the reported conditions. Initiator **PHZ-2** was able to initiate polymerization at higher writing speeds up to 14,000 μm/s at 100% laser intensity, but with lager deformations of the structure. However, this was avoided by decreasing the writing speed. In comparison **CRB-6** was not able to initiate polymerization at 100% laser intensity at a writing speed of 1000 μm/s.

Besides the A-π-D-π-A chromophores Gu et al. also prepared a series of D-π-A chromophores with the same donor-acceptor system but none of them were used in fabrication tests.

Since type I photo initiators generate radicals by α-cleavage most of the known initiators, especially commercially available UV-initiators, contain carbonyl groups. However, also oxime esters are other functional groups, which generate radicals under irradiation.[175–176] Hereby, the N–O bond is cleaved thus generating active radials.[177] This is followed by decarboxylation which reduces the probability of recombination of the generated radicals and thus leading to better initiation performance. With this in mind, Hu et al. developed photo initiators with a A-π-D-π-A structure with a carbazole core containing oxime esters.[178] Besides the initiation properties of the oxime esters, the authors also investigated the influence of the substitution pattern (2,7 and 3,6 position on the carbazole core) as well as the influence on the generated radical by using phenyl and vinyl esters (Figure 90).

Table 35. Photophysical data of the carbazole and phenothiazine based 2PIs measured in dichloromethane.

Compound	λ_{abs} [nm]	Φ_{fl} [%]	σ_{TPA} [GM][a]
CRB-5	364	84.28	–
CRB-6	398	51.52	198
PHZ-1	385	41.75	65
PHZ-2	419	0.86	1315

[a] Measured via TPEF at 780 nm.

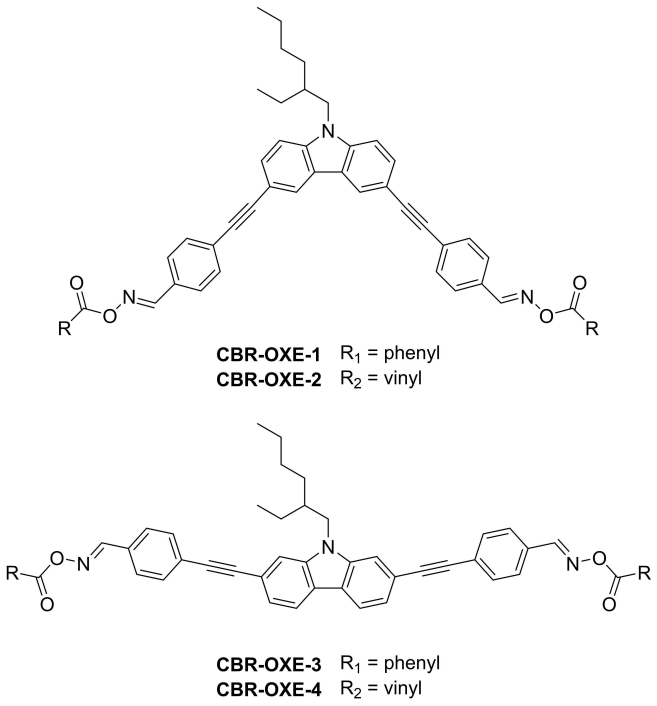

Figure 90. Schematic representation of the oxime ester containing 2PIs with carbazole core.

All four 2PIs reveal a broad absorption band between 250 and 400 nm. The results summarized in Table 36 indicate that the changes in the absorption maximum depending on the substitution pattern is only marginal. However, comparing the derivatives substituted in 3,6-position (**CBR–OXE-1 & -2**) to the the ones functionalized in 2,7-position (**CBR–OXE-3 & -4**) the molar absorption coefficient (ε) is increased. This trend is also visible in the measured two-photon cross-sections. The σ_{TPA}-values show an increase when the position of the substituents is changed from 3,6 to 2,7. This can be related to the enhanced absorption properties of **CBR–OXE-1** and **-2**. Steady-state photolysis experiments revealed that all initiators undergo α-cleavage at the oxime ester position when irradiated. For 2PP polymerization tests a doughnut shaped structure was fabricated at a writing speed of 750 µm/s and polymerization wavelength of 800 nm with various laser intensities (Figure 91). For this a 1:1 mixture of trimethylolpropane triacrylate (TMPTA) and ethoxylated trimethylolpropane triacrylate (TMP3EOTA) with a 2PI concentration of 1.3×10^{-3} mol/g resin was used.

CBR–OXE-4 exhibits the broadest FW of all four initiators and the lowest polymerization threshold. Comparing **CBR–OXE-1** and **-2** the vinyl residue seems to have a advantageous influence compared to the phenyl substituent. This may be attributed to the better initiation efficiency of the released vinyl radical in contrast to the phenyl radical. **CBR–OXE-3** showed poor polymerization behavior due to its decreased solubility in the monomer mixture. It is commonly known that UV photo initiators suffer from pot life issues, due to the N–O bond. Thermal stability in the dark is essential for those compounds, therefore the new photo initiators had been investigated by thermal gravimetric analysis (TGA). The results are listed in Table 36 and reveal that the decomposition temperatures (T_d) ranges from 160 to 200 °C. Compared to the commercially available UV photo initiator Irgacure OXE01 with a T_d of 185 °C the investigated initiators are sufficient for daily storage.

Table 36. Photophysical data and thermal stability of **CBR–OXE-1** to **CBR–OXE-4**.

Compound	λ_{abs} [nm][a]	σ_{TPA} [GM][a][b]	T_d [°C][c]
CRB–OXE-1	377	122	163
CRB–OXE-2	377	102	185
CRB–OXE-3	371	125	201
CRB–OXE-4	371	136	190

[a] Measured in chloroform. [b] Measured via z-scan at 800 nm. [c] Decomposition temperature.

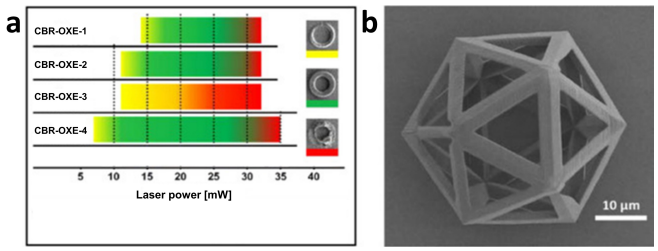

Figure 91. (a) Fabrication window of the investigated carbazole 2PIs containing oxime ester moieties and (b) complex 3D-structure fabricated with **CBR–OXE-4**.[178] Adapted with permission from Ref. [178]. Copyright 2020, John Wiley and Sons.

4.2. Triphenylamine based initiators

Based on the work of Prasad et al. and Goodson et al., who reported that triphenylamine-cored branched structures (**TPA-1**) exhibit large TPA cross-sections,[179–180] Jiang et al. developed several initiators (**TPA-2** to **TPA-6**, Figure 92) and evaluated their properties for initiating 2PP.[181]

UV-measurements in different solvents revealed that the investigated compounds exhibit solvatochromic behavior. Nearly all of the linear absorption maxima, except the one of **TPA-4**, undergo a redshift when the polarity of the solvents is increased. This observation indicates a better stabilization of the excited state in polar solvent compared to the ground state. Table 37 lists the photophysical data of the initiators in toluene and DMF, as well as the two-photon cross-sections in DMF. All

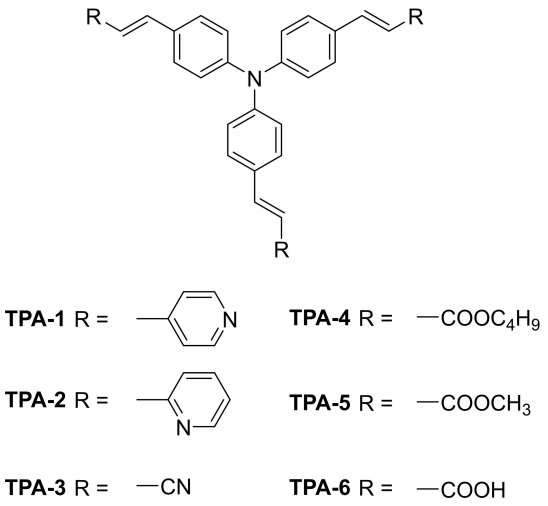

Figure 92. Schematic representation of the structures of the tri-dentrical initiators **TPA-1** to **TPA-6**.

Table 37. Photophysical properties of the initiators **TPA-1** to **TPA-6**.

Compound	Solvent	λ_{max} [nm]	Φfl[a]	$^2\lambda_{max}$ [nm]	σTPA [GM][b]
TPA-1	Toluene	379	0.15	492	
	DMF	396	0.06	536	330.8
TPA-2	Toluene	387	0.21		
	DMF	387	0.10	527	38.4
TPA-3	Toluene	397	0.57		
	DMF	387	0.20	510	57.9
TPA-4	Toluene	402	0.47		
	DMF	398	0.38	522	19.8
TPA-5	Toluene	387	0.39		
	DMF	397	0.16	530	66.1
TPA-6	Toluene	387	0.03		
	DMF	388	0.11	523	19.4

[a] Fluorescence quantum yields were determined by comparison to coumarin as standard and. [b] Measured via TPEF.

initiators exhibit their lowest fluorescence quantum yield in ethanol, due to the hydrogen bond interactions between ethanol and the excited state of the molecules.

Using 0.5 wt% **TPA-4** and 99.5 % of the commercial monomer SR349 (ethoxylated bisphenol-A dimethacrylate) a microgrid structure was fabricated at 780 nm laser wavelength, 500 μW laser power and a writing speed of 50 μm/s (Figure 93). The distance between the fabricated lines is about 10 μm.

In search of new potential initiators with low fluorescence quantum yields Whitby et al. investigated branched triphenylamine derivates with aromatic ketones.[182] The carbonyl groups of the aromatic ester have two advantages: 1. They act as strong electron acceptors and 2. are efficient spin-orbit coupling agents, which promote intersystem crossing.[46,183–184] In addition, the influence of the degree of substitution of the triphenylamine derivatives (Figure 94) was investigated.

The linear absorption maxima of the three derivatives show, that by increasing the degree of substitution the absorption maxima are red shifted, indicating a stabilization of the ICT. From **TPA-7** to **TPA-8** the shift is larger than compared to from **TPA-8** to **TPA-9**, suggesting that the third substituent does not have a strong stabilizing effect on the ICT (Table 38). However, the structures containing more than one substituent (**TPA-8** and **TPA-9**) exhibit a drastically lower fluorescence quantum yield. This decrease of fluorescence quantum yield is well-known in literature.[185] The σ_{TPA} values reveal a linear increase with increasing number of substituents. The increase is 232 GM per substitution. This "branching effect" of multibranched triphenylamine derivatives is well reported in the literature.[26,186]

Polymerization tests were performed with the acrylate resin (50 : 50 wt% SR415/SR351) at 800 nm laser wavelength, 50 μm/s writing speed and different laser intensities. Figure 95 displays the fabrication windows for the 2PIs at different laser powers with a color code displaying the integrity of the fabricated structures.

The obtained polymerization thresholds at 50 μm/s writing speed were 45 μW, 61 μW, and 27 μW for **TPA-7**, **TPA-6** and **TPA-9**, respectively. From Figure 96 one can see that good structures were obtained for **TPA-7** at about 40 to about 150 μW. For **TPA-8** the window starts at about 50 μW and goes up to 160 μW. Although **TPA-9** reveals the lowest polymerization threshold, it exhibit the smallest FW from about 20 to 100 μW. An example of an excellent fabricated structure is displayed in Figure 96.

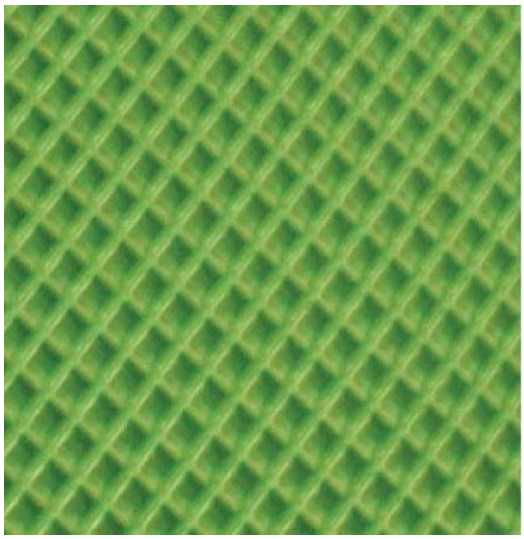

Figure 93. Optical micrograph of the microgrid fabricated with SR349 and 2PI **TPA-4**.[181] Reproduced with permission from Ref. [181]. Copyright 2007, Royal Society of Chemistry.

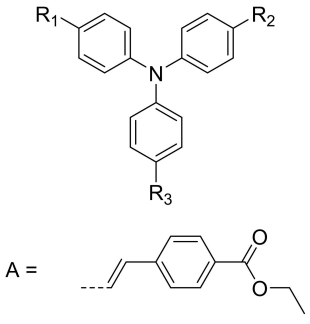

TPA-7 R_1 = H, R_2 = H, R_3 = A
TPA-8 R_1 = H, R_2 = A, R_3 = A
TPA-9 R_1 = A, R_2 = A, R_3 = A

Figure 94. Schematic representation of the structures of the different branched initiators **TPA-7** to **TPA-9**.

Table 38. One- and two-photon photophysical properties of the initiators **TPA-7** to **TPA-9**.

Compound	Solvent	λ_{max} [nm]	Φfl[a]	σ_{TPA} [GM][b]
TPA-7	Methanol	384	0.198	126[b]
TPA-8	Methanol	404	0.021	358[b]
TPA-9	Methanol	410	0.019	590[b]

[a] Fluorescence quantum yields were determined by comparison to quinine bisulfate as standard and [b] Measured by open Z-scan method at 780 nm in $CHCl_3$.

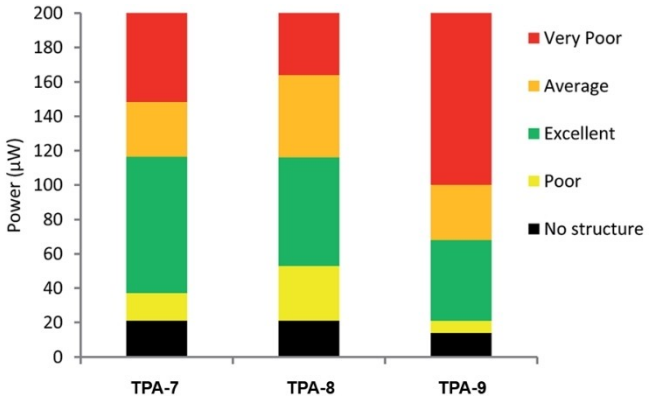

Figure 95. Fabrication windows of **TPA-7** to **TPA-9** at 50 μm/s writing speed.[182] Reproduced with permission from Ref. [182]. Copyright 2017, Royal Society of Chemistry.

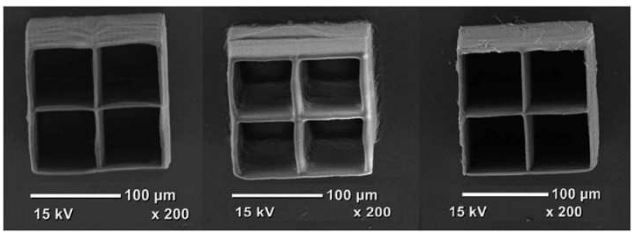

Figure 96. SEM images showing fabricated structures produced via 2PP (from left to right with the initiators **TPA-7** to **TPA-9**).[182] Reproduced with permission from Ref. [182]. Copyright 2017, Royal Society of Chemistry.

4.3. Water-soluble photo initiator with A-π-D-π-A structure

Zheng et al. were able to develop a new water-soluble photo initiator system by the host-guest method as mentioned before.[187] Hereby a complex consisting of vinylpyridine substituted carbazole **BMVPC** (guest) with a A-π-D-π-A structure and cucurbit[7]uril **CB7** (host) was established (Figure 97). Cucurbit[n]urils are known for their ability to incorporate neutral and cationic molecules.[188]

The linear absorption spectrum of pure **BMVPC** in water exhibits a maximum at 418 nm, which shifts to 471 nm by adding **CB7** to the solution. The addition does not affect the absorption, which indicates the non-covalent interaction of **BMVPC** and **CB7**. The successful incorporation of BMVPC into **CB7** was proven by isothermal titration calorimetry, which revealed that the host-guest complexation represents an exothermic process with a calculated free Gibb's energy of −32.9 kJ/mol. The addition of CB7 also had a second effect, which is the enhancement of the fluorescence quantum yield of BMVPC. Within the host-guest complex with a 10-fold amount of CB7 the fluorescence of BMVPC enhances to $\Phi_{fl} = 0.0463$. By restricting the torsional motion of biscyanines through the inclusion interaction, the nonradiative decay is inhibited thus enhancing the fluorescence quantum yield. The measured 2PA spectra in water via TPEF revealed a σ_{TPA} value of 613 GM and 2999 GM for **BMVPC** and the **BMVPC/CB7** (1:10) complex, respectively. The increase of the cross-section by a factor of 4.9 is due to the change of the intramolecular charge transfer (ICT) by the interaction between **BMVPC** and **CB7**.[189] Fabrication tests with PEGda as monomer revealed that the 2PI complex exhibits a polymerization threshold of 4.5 mW at a writing speed of 10 µ/s and at a laser wavelength of 780 nm. It was possible to construct lines with small structural deformation with a width of 180 nm. A hexagonal grid scaffold was fabricated using those conditions for biological investigations (Figure 116a/b). HeLa cells were co-incubated with the fabricated scaffold for 48 h and were afterwards stained with the mitochondrial dye MitoTracker™ Deep Red. Figure 98c shows the confocal fluorescence image of the stained cells. The scaffolds with good mechanical performance were noncytotoxic and the cells maintained their morphology. These results indicate that the fabricated scaffolds display good biocompatibility and low cytotoxicity.

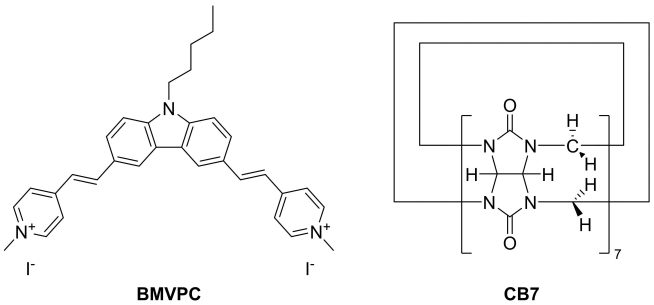

Figure 97. Schematic representation of the structures of **BMVPC** as the guest, and **CB7** as the host.

5. D-π-A Chromophores

α,β-Unsaturated ketones like benzylidene cycloalkanes (Chapter 2.2.) are well-known for their good modifiability and large σ_{TPA} values. In those D-π-A-π-D systems mostly ketones are used as strong electron withdrawing groups, which are required to reach large σ_{TPA} values. Based on the work of Lalevée et al., who worked on 1,3-diketone-based photo initiators for cationic- and UV photopolymerization, Nazir et al. developed D-π-A structured photo initiators with 1,3-diketones as a strong electron withdrawing groups (Figure 99).[61,190–192] The 1,3-diketone group has the advantages of broadening the absorption spectrum, therefore adjusting the laser wavelength for 2PP if necessary. Also, those structures show a decrease of fluorescence quantum yield, which is favorable in 2PP.[61,192] In addition, Nazir et al. combined two large π-system bridged by a double- or triple-bond to the central anthracene core system.

The cyclohexane-1,3-diketone based 2PIs **DA-1** and **DA-3** show a blue shift compared to the indene-1,3-diketone based **DA-2** and **DA-4** (Table 39). While the structures containing the cyclohexane-1,3-diketone (**DA-1**, **DA-3**) reveal only a marginal

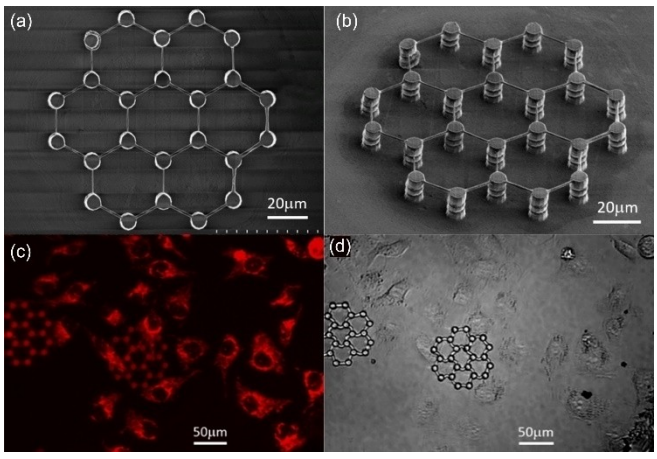

Figure 98. (a) Top view of the SEM image of the hexagonal grid scaffold fabricated using the **BMVPC/CB7** complex. (b) Tilted view in the hexagonal grid scaffold. (c) Confocal fluorescence image of the stained HeLa cells and (d) bright-field image.[187] Reproduced with permission from Ref. [187]. Copyright 2019, American Chemical Society.

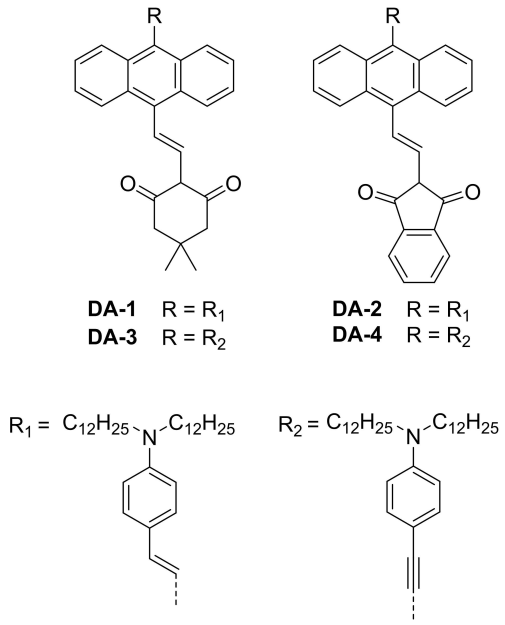

Figure 99. Schematic representation of the structures of the 1,3-diketone based photo initiators **DA-1** to **DA-4**.

Table 39. Photophysical properties of the photo initiators **DA-1** to **DA-4** in dichloromethane.

Compound	λ_{max} [nm]	Φfl [%]	σ_{TPA} (Z-scan) [GM][a]	σ_{TPA} (TPEF) [GM][b]
DA-1	435 511	0.020	700	< 8000
DA-2	395 542	0.010	970	< 2000
DA-3	470 521	1.010	1000	200
DA-4	439 561	< 0.001	2500	n.d.

[a] Measured at 725 nm and [b] Measured at 970 nm (**DA-1**), 710 nm (**DA-2**, **DA-3**), n.d. = not detected.

shift in the absorption spectrum by changing from the C–C double bond bridge, the indene-1,3-diketones experience a much larger shift (**DA-2**, **DA-4**). All fluorescence quantum yields were in general below 0.1 % except **DA-3** with a yield of 1.01 %. This is in good agreement with the theory that 1,3-diketones reduce the fluorescence quantum yield as mentioned before. The Z-scan measurements show that the 2PIs with the indene moiety possess larger σ_{TPA} values compared to the ones with the cyclohexane moiety. Also, the structures equipped with the triple bond exhibit a large σ_{TPA} value compared to the ones with a C–C double bond. In addition, the two-photon cross-sections were measured via TPEF to investigate how reliable this technique works for compounds with low fluorescence quantum yields. Because the TPEF method compares the TPA emission spectrum with a reference, a low or even zero fluorescence results in a large error. Therefore, the σ_{TPA} values from Z-scan and TPEF vary extremely. In case of **DA-4** the σ_{TPA} value could not be measured by TPEF because of the low fluorescence quantum yield, showing that the Z-scan method is the technique of choice for those compounds. Polymerization tests were performed with a hybrid material consisting of MAPTMS, MAA and ZOP, and the fabrication windows of the 2PIs at 800 nm were determined (Figure 100).

All initiators reveal broad FWs from around 10 to 55 mW. More complex structures in form of hollow pyramids were fabricated using **DA-3** as initiator with increasing laser power from left to right (Figure 101). The three left pyramids were prepared with a laser power of 15, 25 and 40 mW and display a well-defined structure. By increasing the average laser power the structures begin to show deformation and over-polymerization until total collapse of the structure at around 50 mW (pyramids on the right).

While one of the most popular ways to tune the efficiency of a photo initiator is to modify the electron donating or withdrawing substituents or to expand the conjugation, Li et al. chose a different approach. Since the polymerization initiation depends on the generated radicals, Li et al. developed silicon-based photo initiators (Figure 102) based on studies which describe the photolytically cleavage of the Si–Si bond.[193]

All compounds show an absorption band in THF of around 450 nm. The modification of 3-hydroxy-4-diethylamino-4′-nitro-

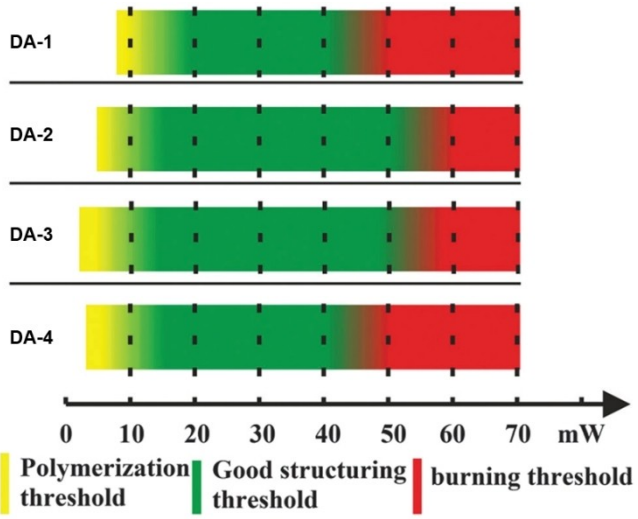

Figure 100. Determination of the fabrication windows of **DA-1** to **DA-4** using 800 nm as polymerization wavelength.[61] Adapted with permission from Ref. [61]. Copyright 2016, Royal Society of Chemistry.

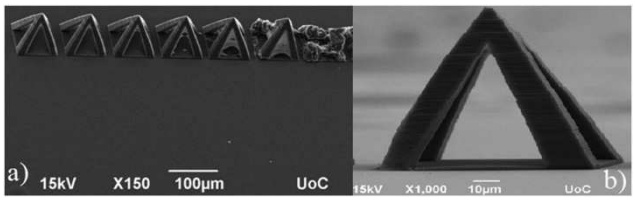

Figure 101. (a) SEM image of the fabricated hollow pyramids with increasing laser power using **DA-3** as initiator. (b) Hollow pyramid fabricated at a laser power of 30 mW with **DA-3**.[61] Reproduced with permission from Ref. [61]. Copyright 2016, Royal Society of Chemistry.

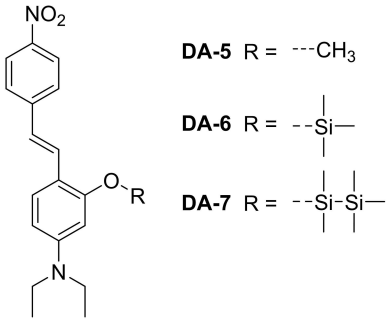

Figure 102. Schematic representation of the structures of the silyl modified 2PIs **DA-5** to **DA-7**.

stilben (**DA-5**) shifts the absorption maxima only slightly when a silyl group is used (Table 40). The same was observed with the fluorescence quantum yields, which increased slightly from 0.38 for **DA-5** to 0.41 for **DA-6** and **DA-7**, respectively. Two-photon cross-sections have been determined by an approach of Rebane et al., in which the cross-section is estimated purely from one-photon spectral properties.[194–195] The authors demonstrated that the σ_{TPA} value can be calculated, when in case of non-centrosymmetric dipolar molecules, the TPA transition between the ground and the first excited electronic state appears without involving any intermediate states. To determine the fabrication windows of the photo initiators, a 1:1 mixture of TMPA and ETA was used. Y-structures were fabricated at 800 nm and 50 μm/s writing speed at different laser intensities.

DA-5 shows the broadest FW of those three initiators, with the lowest polymerization threshold as well with the highest burning threshold (Figure 103). Both of the silyl-based initiators exhibit a lower FW with higher polymerization thresholds as well as lower burning thresholds. Although the Si–Si bond is a known functionality which undergoes fragmentation induced by light to produce silyl radicals,[196–197] the results indicate that neither the cleavage of the Si–O nor of the Si–Si bond occurred under TPA. This could be achieved by increasing the laser intensity, however the risk of over polymerization and damage to the structure is possible.

It is known that also cationic polymerization under 2PA condition can be performed. Such photo acid generators (PAG) generate protons upon excitement and thus initiate the cationic polymerization. Such PAG initiators have been reviewed recently.[24] However, some of the PAGs can also generate radicals under 2PA conditions by photolysis, like compounds with sulfonium salts.[198] Chen and coworkers developed three different photo initiators for cationic polymerization under 2PA conditions, but also tested them for their ability to initiate radical polymerization under 2PA conditions. Therefore they chose a 1,3,5-triphenyl-2-pyrazoline structure for their initiators (Figure 104), because their interesting non-linear optical behavior.[198–199]

The 2PIs show a linear absorption maximum between 340 and 375 nm in acetonitrile. Steady state fluorescence measurements revealed that all three initiators exhibit a fluorescence quantum yield of under 1%. The z-scan measurements of the 2PIs showed that **PI–H** and **PI–CF$_3$** exhibit a σ_{TPA}- value of 75 and 105 GM, respectively. For **PI–EtO** no σ_{TPA} -value was reported. The larger cross-section of **PI–CF3** compared to **PI–H** can be explained by the stronger D-π-A character between the CF_3-group and the pyrazoline ring. Polymerization tests were performed with PETA as monomer at 780 nm polymerization wavelength with different laser powers and writing speeds. Hereby solid lines were fabricated with a 2PI concentration of 1 wt%. Both initiators initiate polymerization, however the polymerization threshold of **PI–CF$_3$** is lower compared to the of **PI–H**. The fabrication window of F and **PI–H** at 100 μm/s was observed to be 4.5 to 14 mW and 7.5 to 18 mW, respectively. Figure 105 displays the 2PP experiments with **PI–CF3**.

Coumarin based initiators are a well studied compound class which, are known to generate radicals under 2PA conditions as mentioned before. Oxime esters are a new interesting functional, which generate radicals by α-cleavage as shown before. Qiu et al. investigated 2PIs with a coumarin core

Table 40. Photophysical properties of the photo initiators **DA-5** to **DA-7** in tetrahydrofuran.

Compound	λ_{max} [nm]	Φ_{fl}	σ_{TPA} [GM][a]
DA-5	458±2	0.38	90
DA-6	453±2	0.41	90
DA-7	453±2	0.41	90

[a] Measured at 725 nm.

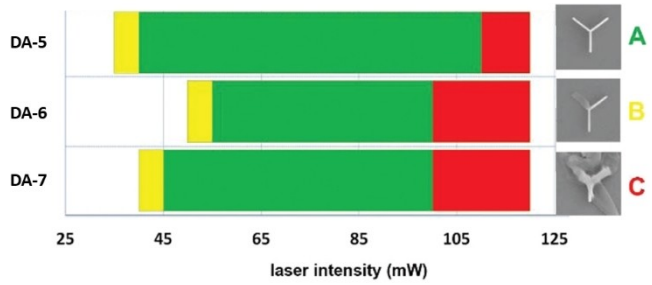

Figure 103. Fabrication windows of the silylated 2PIs **DA-6**/**DA-7** and **DA-5** (2PI concentration 6.3×10–6 mol 2PI/g resin).[193] Adapted with permission from Ref. [193]. Copyright 2017, Royal Society of Chemistry.

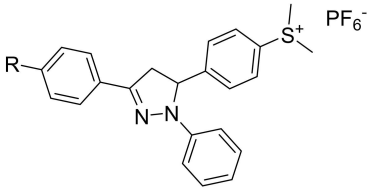

PI-H R = H
PI-CF$_3$ R = CF_3
PI-EtO R= O-CH_2CH_3

Figure 104. Schematic representation of the structures of the 1,3,5-triphenyl-2-pyrazoline 2PIs.

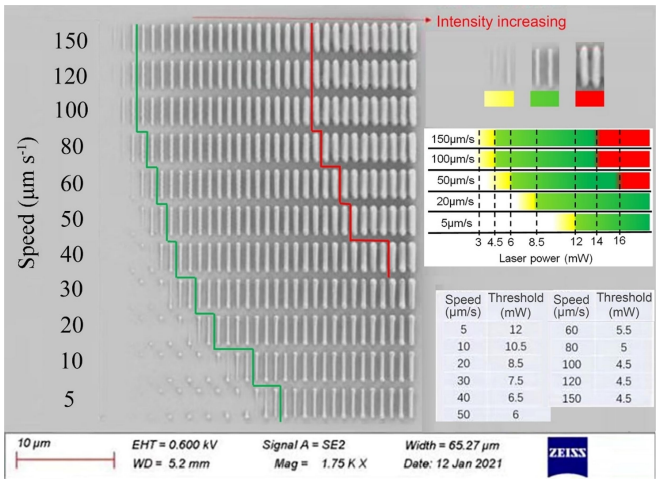

Figure 105. SEM image of the fabrication array prepared with **PI–CF_3** at a concentration of 1 wt% in PETA.[198] Adapted with permission from Ref. [198]. Copyright 2021, Elsevier.

equipped with different oxime esters (vinyl- & phenylester) at different positions (Figure 106).[200]

The measured UV/Vis-absorption spectra in acetonitrile revealed that **OEC3-1 & -2** possess absorption maxima at around 405 nm. **OEC4** shows a slightly red shifted maximum at 421 nm. Although the change in the absorption maxima seems to be only marginal, by changing the position from 4 to 3 the molar absorption coefficient increases, in case of **OEC4** and **OEC3-1** ε it is doubled. A study by Wu et al. reports that a coumarin derivative substituted in 4-position adopted a twisted conformation. In contrast, coumarines substituted at position 3 show a more planar conformation, thus explaining the higher

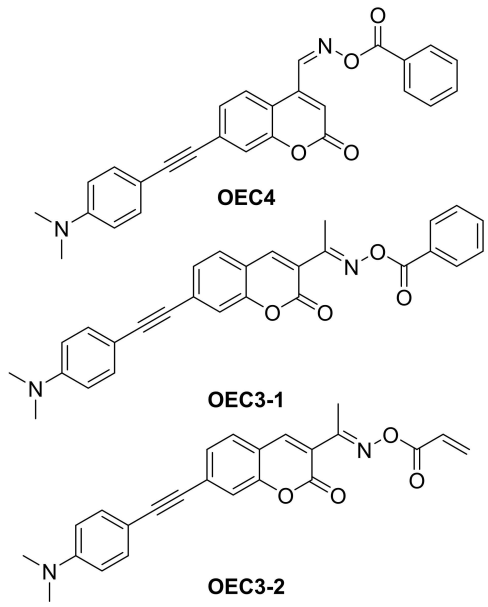

Figure 106. Schematic representation of the oxime esters substituted coumarin 2PIs.

ε.[60] This is also reflected in the two-photon absorption behaviour (at 800 nm). While **OCE4** exhibits a two-photon cross-section of 208 GM, **OEC3-1** and **OEC3-2** reveal values of 486 and 536 GM. Steady state photolysis experiments showed that all three initiators undergo photolysis by α-cleavage of the oxime ester, hereby **OCE3-2** shows the fastest photolysis rate. 2PP fabrication experiments were performed using a 1:1 mixture of trimethylolpropane triacrylate (TMPTA) and ethoxylated trimethylolpropane triacrylate (TMP3EOTA) with a PI concentration of 1.1×10^{-5} mol/g resin using 800 nm as polymerization wavelength. The fabrication window was determined by polymerizing doughnut shaped structures using different laser intensities at a writing speed of 750 µm/s.

While **OEC4** exhibit a poor fabrication window due to poor solubility in the monomer mixture, **OEC3-1** and **OEC-2** reveal broad fabrication windows. The best results were achieved with **OEC3-2** as initiator with a fabrication window of 12 to 28 mW (Figure 107). The fabrication of complex 3D-strucutres was possible with **OEC3-2** as 2PI. As discussed above, it seems that the generated vinyl radical has a higher initiation efficiency compared to the phenyl radical. Since the thermal stability of oxime esters compounds are an issue, TGA measurements were performed. The investigated photo initiators revealed a T_d between 189 to 220 °C which is above the T_d of the commercial available initiator Irgacure **OXE02** showing that the new 2PIs are sufficient for daily storage.

OXE is another carbazole based initiator equipped with a oxime ester functionality. This chevron-shaped initiator was develop by Zhou et al. and investigated for its use in 2PP (Figure 108).[201]

The linear absorption spectrum of **OXE** in acetonitrile revealed an absorption maximum of 374 nm. The determined two-photon cross-section via the z-scan technique revealed a σ_{TPA} value of 87 ± 13 GM, which compared to other carbazole based 2PIs with an oxime ester group is quite low. Steady state photolysis experiments showed that the oxime ester group in **OXE** undergo cleavage under one photon and two photon conditions. To determine the polymerization threshold of the initiator, polymer lines were fabricated with a formulation of

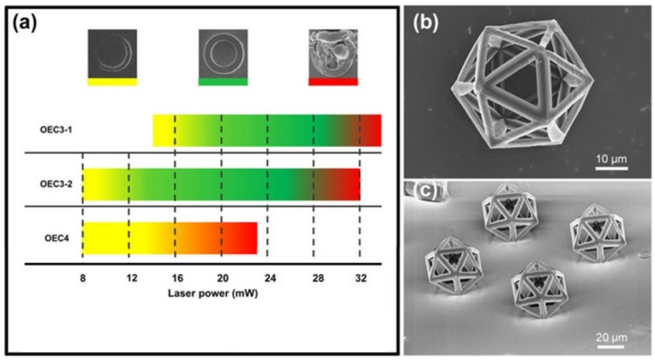

Figure 107. (a) Fabrication window of the oxime ester substituted coumarin initiators. (b),(c) 3D complex structures fabricated using **OEC-2** as photo initiator.[200] Adapted with permission from Ref. [200]. Copyright 2019, John Wiley and Sons.

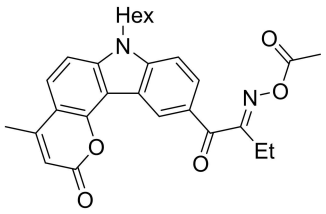

OXE

Figure 108. Schematic representation of the structure of the carbazole based 2PI **OXE** with an oxime ester group.

PETA and 2.5 mM **OXE**. The 2PP were performed at 800 nm polymerization wavelength and revealed a P_{th} of 0.73 mW. This low polymerization threshold shows the great potential of **OXE** and it was possible to fabricate complex 3D-strucutres in form of pyramids.

6. Photo Initiators without Extended π-Systems

Most of commercially available photo initiators are well-known compounds for single photon photopolymerization. Most of the initiators lack on high two-photon cross-sections, which means that higher intensities of the laser power are required to initiate polymerization under 2PP conditions. Schafer et al. investigated the two-photon cross-sections of several initiators from the Irgacure and Darocure family (Figure 109).[91] Most of these initiators induce polymerization via the Norrish Type I mechanism, where an α-cleavage reaction generates the desired radicals. The typical structures are based on α-aminoketones, α-hydroxyketones and acylphospine oxides.

The linear absorption measurements in methanol revealed that the absorption maxima range from 242 to 328 nm.

The two-photon cross-sections vary from 4 to 28 GM (Table 41). Although the σ_{TPA} values are rather low, the application of commercial 2PI is often reported in literature. **Irgacure 2959** (**I2959**) (Figure 110) is one of the most used commercial initiators for 2PP throughout literature. **I2959** is mostly used in fabrication of hydrogels based on different materials like methacrylamide-modified gelatin,[202–203] modified hyaluronic acid[204–205] and methacrylated carbohydrates.[206]

Käpylä et al. investigated newly synthesized polymerizable amino acids (polyAA) for the use as extracellular matrix (ECM) mimicking material.[207] For this purpose, polyAAs based on methacrylolated (PHEG–MA) and acrylolated (PHEG–A) poly[N^5-(2-hydroxyethyl) L-glutamine]s (PHEGs) were synthesized with different degrees of functionalization (D_f). 2PP was applied to fabricate hydrogels with high integrity by using **Irgacure 2959** as initiator. Besides the fabrication also the polymerization threshold (P_{th}) and damage threshold (P_D) were investigated. Figure 111 shows the dynamic range (defined as the quotient of P_D/P_{th}) of **I2959** in different polyAAs and different PEGda monomers.

The dynamic range clearly depends on the used monomer system. In case of **I2959** with the modified polyAAs and PEGda the dynamic range is much broader with PHEG–MA as well as PHEG–A compared to PEGda. In addition, Käpylä et al. estimated the σ_{TPA} value of **I2959** to be between 0.001 to 0.01 GM, which agrees with the σ_{TPA} values of other commercial photo initiators.[91]

Irgacure 369 (**I369**, Figure 109) is also a frequently used initiator for 2PP fabrication of structures for different applications. Fabricated microneedles, doped with gentamine sulfate,

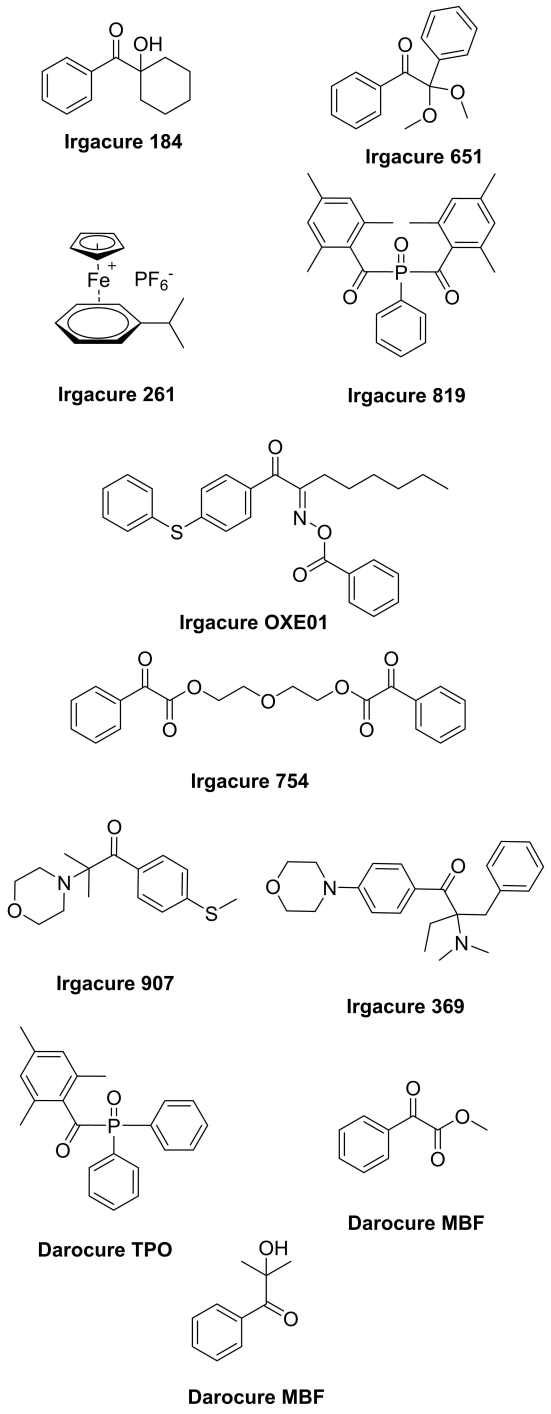

Figure 109. Schematic representation of the structures of the commercially available photo initiators investigated in the studies of Schafer et al.

Table 41. Photophysical data of selected commercially available photo initiators.

Compound	λ_{max} [nm]	$\lambda^{(2)}_{max}$ [nm]	σ_{TPA} [GM][a]
Irgacure 184	246	265	23
Irgacure 261	242	265	<20
Irgacure 369	324	335	7
Irgacure 651	254	265	28
Irgacure 754	253	265	21
Irgacure 819	295	300	<4
Irgacure 907	306	300	4
Irgacure OXE01	328	330	31
Darocure TPO	299	300	<4
Darocure MBF	255	265	27
Darocure 1173	244	265	<20

[a] Measured by Z-scan technique.

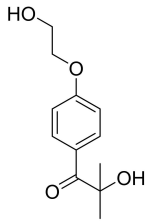

Irgacure 2959

Figure 110. Schematic representation of the structure of **Irgacure 2959**.

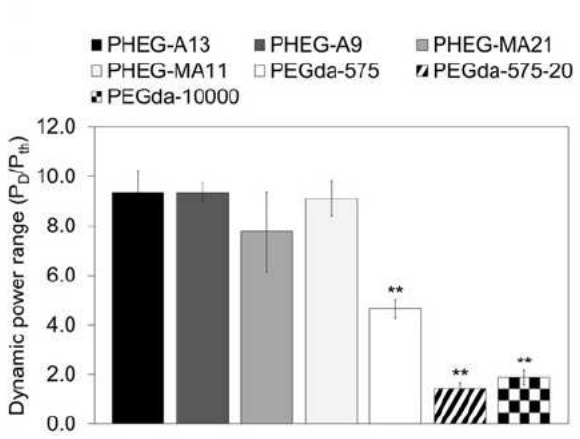

Figure 111. Dynamic range of **I2959** in different polyAAs and different PEGda monomers. PHEG–A13 (D_f = 12.9), PHEG–A9 (D_f = 9.4), PHEG–MA21 (D_f = 20.7), PHEG–MA11 (D_f = 11.2).[207] Adapted with permission from Ref. [207]. Copyright 2014, Elsevier.

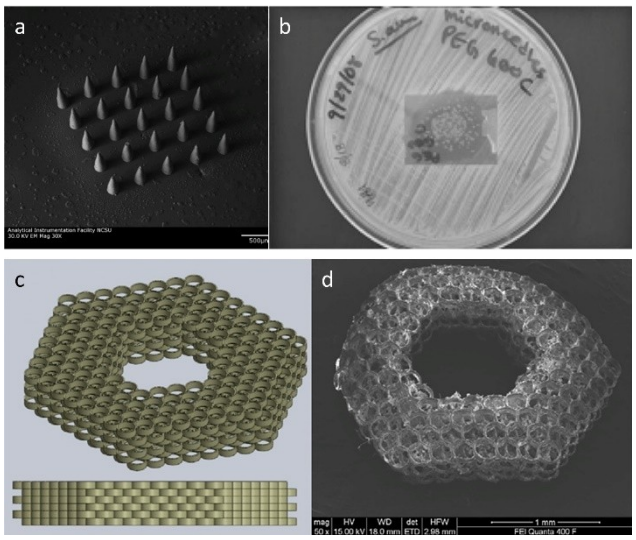

Figure 112. (a) SEM image of microneedle array fabricated with gentamicin-doped SR610 (Sartomer, Paris France) and **I369**. (b) Fabricated microneedle array against Staphylococcus aureus. Growth inhibition area around the array was 26.8 mm large.[125] Adapted with permission from Ref. [125]. Copyright 2010, John Wiley and Sons. (c) CAD design for the hydrogel scaffold structure. (d) SEM image of the scaffold fabricated by using **I369** and PEGda.[208] Adapted with permission from Ref. [208]. Copyright 2010, IOP Publishing.

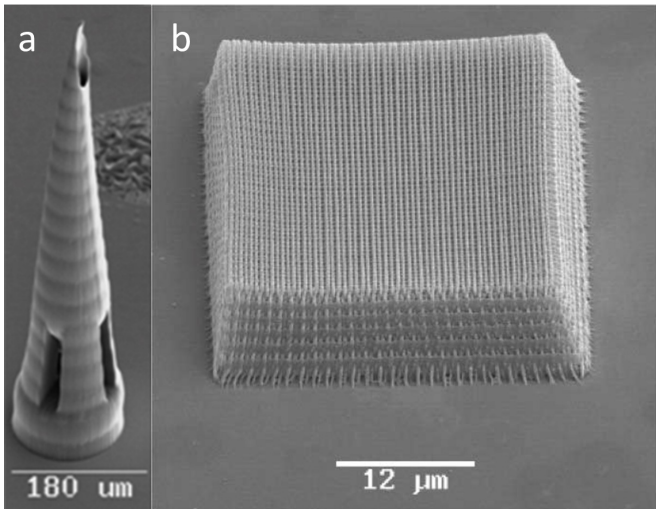

Figure 113. (a) Hypodermic needle.[126] Adapted with permission from Ref. [126]. Copyright 2007, John Wiley and Sons. (b) Micro grid structure fabricated by 2PP using **I369** as 2PI.[128] Adapted with permission from Ref. [128] ©The Optical Society.

successfully inhibited the growth of *Staphylococcus aureus* bacteria (Figure 112 a and b).[125] Ovsianikov et al. successfully fabricated scaffolds in the presents of living cells (Figure 112 c and d).[208] Scaffolds for tissue engineering and hypodermic needles, which successfully penetrate cadaveric procine adipose tissue, were fabricated by using the same organic-inorganic photoresist as in Ref. [15] and 16 (Figure 113).[126,128,209–211] Furthermore Koroleva et al. fabricated 3D-scaffolds out of methacrylate PLA and **I369**, which enabled and supported the proliferation of Schwann cells.[127] Iron platinum nanoparticle based 3D microrobots for potential applications in medicine, as well as light- induced reconfigurable smart materials based on liquid crystalline elastomers were also fabricated with I369.[212–213]

Although **I369** is used in many applications, no data of fabrication windows is reported.

A representative of the acylphosphine oxide initiators is **Irgacure 819** (**I819**, Figure 109). Despite its low σ_{TPA} value of

< 4 GM (Table 41) **I819** is capable to successfully initiate polymerization via 2PP. For example, a monomer mixture of PETA and BisGMA (bisphenol A glycidyl methacrylate) was used to fabricate polymer scaffolds to seed mesenchymal progenitor cells and to stimulate them to produce bone-forming cells for tissue engineering (Figure 114).[214] By using high molar mass PEGda monomers Scarpa et al. were able to fabricate 3D pH-responsive microstructures for soft tissue applications.[215]

Harnisch et al. investigated the fabrication windows of several commercial initiators including **I819**.[216] To evaluate the FW, **I819** was used at a concentration of 1 wt% in the commercial hybrid monomer mixture OrmoComp®. The resulting FW of 16 to 32 mW for **I819** was determined by fabricating microstructures with different laser intensities (Figure 115).

Zandrini et al. investigated the influence of the viscosity of the monomer solution on the dynamic range. Therefore, different resin formulations were prepared and **I819** was used as photo initiator.[217] The resin solutions consisted of the two monomers dipentaerythritol pentaacrylate and 1,3-butylene glycol oxide diacrylate (Table 42).

To estimate E_{th} and E_{damage}, 20 μm long lines were fabricated at a writing speed of 50 μm/s and the laser energies varied from 0.03 nJ/pulse to 0.45 nJ/pulse. Table 43 shows that with decreasing viscosity the energy threshold increases, what leads to a lower dynamic range. Although a large dynamic range is desirable in 2PP to fabricate microstructures, it is also important to have a low viscosity to achieve high resolutions and prevent damage of the structures by overpolymerization. The results indicate that the viscosity of the monomer solution represents another parameter which has to be considered while fabrication of 3D microstructure by 2PP.

Besides **I819**, **Irgacure TPO–L** (formally known as Luricin TPO, Figure 116) is another well-studied initiator of the acylphosphine oxide class.

Two-photon absorption measurements performed by Mendonca et al. revealed that **Irgacure TPO–L** has a σ_{TPA} value of 1.2 GM at 610 nm. Figure 117 shows the linear absorption spectrum and two-photon absorption cross-section spectrum.[218]

To exhibit high σ_{TPA} values a molecule requires a high conjugation and molecular planarity.[166] Quantum mechanical calculations revealed that **Irgacure TPO–L** has a non-planar structure due to the phosphorus atom in the center of the molecule and a low conjugation length, which results in a low σ_{TPA} value. Detailed investigations of the initiator concerning the polymerization performance were conducted by Baldacchini et al.[219] and De Marco et al.[220] Baldacchini et al. investigated the polymerization and damage threshold in dependence to

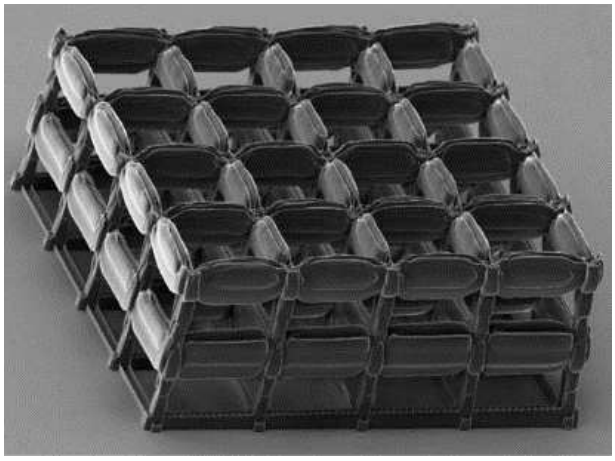

Figure 114. SEM image of a three-level cage structure fabricated with PETA/BisGMA (80/20) and **I819** as 2PI. The square pore sizes are 35 μm.[214] Adapted with permission from Ref. [214]. Copyright 2016, John Wiley and Sons.

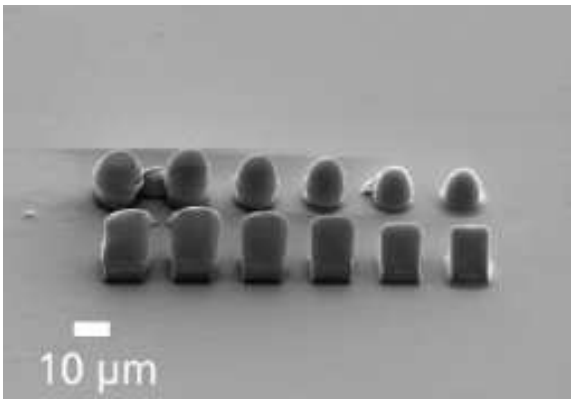

Figure 115. SEM image of fabricated microstructures with **I819** as 2PI. The laser intensity was increased from 16 to 32 mW in 4 mW steps (left to right).[216] Adapted with permission from Ref. [216] ©The Optical Society.

Table 42. Composition of monomer solutions with corresponding viscosity.

Resin	DPEPA [mmol]	BGDA [mmol]	I819 [mol %]	Viscosity, n [mPa-s]
A	11.4	0	3.8	10,400
B	6.8	12.5	2.3	116
C	3.9	19.8	1.9	23
D	0.5	28.9	1.6	15

Table 43. Threshold energies and dynamic ranges of the different resins from Table 42.

Resin	E_{th} [nJ/pulse]	E_{damage} [nJ/pulse]	Dynamic range [%]
A	0.04	0.49	91.8
B	0.06	0.52	88.5
C	0.09	0.50	82.0
D	0.19	0.53	64.2

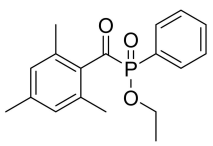

Irgacure TPO-L

Figure 116. Schematic representation of the structure of **Irgacure TPO–L**.

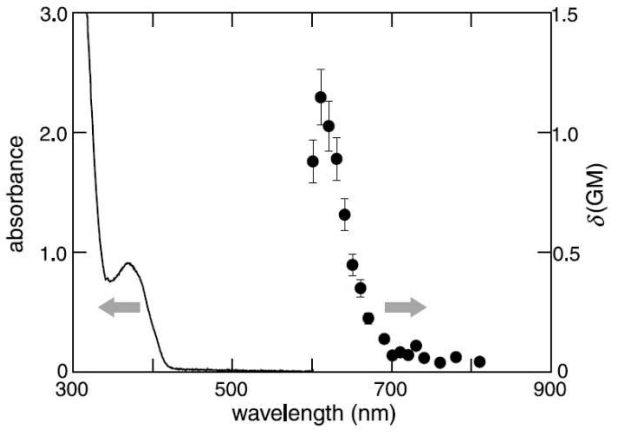

Figure 117. Linear absorption spectrum (left, curve, $c = 7 \times 10^{-3}$ mol/L) and two-photon absorption cross-section spectrum (right, circles, $c = 9 \times 10^{-1}$ mol/L) of **Irgacure TPO–L** in ethanol.[218] Reproduced with permission from Ref. [218]. Copyright 2008, Springer Nature.

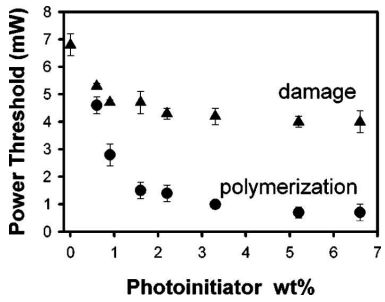

Figure 118. Determined polymerization (circle) and damage (triangle) thresholds in dependence on the 2PI concentration. Every sample was irradiated with 725 nm laser wavelength for 5 s.[218] Reproduced with permission from Ref. [218]. Copyright 2004, AIP Publishing.

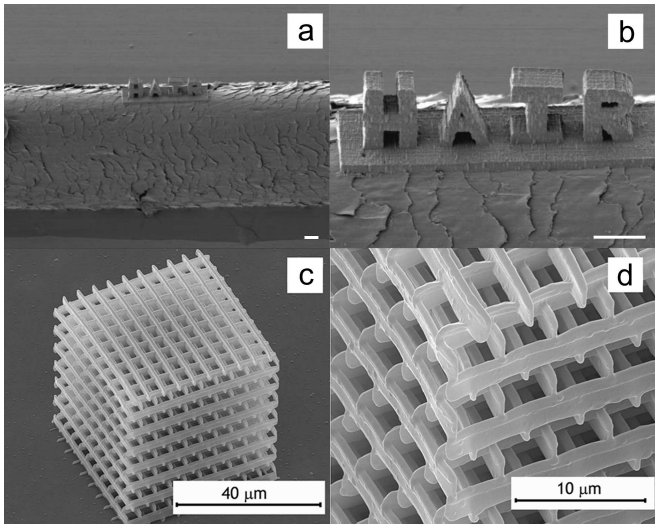

Figure 119. (a)/(b) SEM image of the fabricated 3D micro structure "HAIR" on top of a human hair. The scale bars are 10 μm each.[218] Reproduced with permission from Ref. [218]. Copyright 2004, AIP Publishing. (c)/(d) SEM images of a fabricated woodpile structure.[220] Reproduced with permission from Ref. [220]. Copyright 2013, American Chemical Society.

the 2PI concentration (Figure 118). For this purpose different monomer solutions containing ethoxylated(6) trimethylolpropane triacrylate and tris(2-hydroxyethyl)isocyanurate triacrylate were prepared and investigated.

The polymerization threshold decreased quickly with increasing 2PI concentration until it reaches 1.5 wt% from where it decreases only slowly. It can be assumed that an ideal dynamic range for 2PP fabrication is received starting at a 2PI concentration of 1.5 wt%. Based on this result 3D microstructures were fabricated using 3 wt% of **Irgacure TOP–L** with a laser power of 2.3 mW and a writing speed of 30 μm/s (Figure 119 a and b).

Irgacure TPO–L also was used in polymerization studies of a new a perfluoropolyether-based resin developed by De Marco et al., which should result in structures of high hydrophobicity and strong chemical resistance.[220] To evaluate the optimal polymerization parameters woodpile structures were fabricated with different laser intensities (*x* axis) and writing speeds (y axis) at a laser wavelength of 513 nm (Figure 119 c & d)

As expected the polymerization threshold increases with rising writing speed. This demonstrates that **Irgacure TPO–L** in combination with the perfluoronated monomer is capable of writing complex 3D structures via 2PP at high laser intensities as well as with fast writing speed up to 1000 μm/s (Figure 120). Figure 119 c and d displays a woodpile structure fabricated via the evaluated polymerization parameters. The structure shows high integrity and well-defined sub micrometer features. Several other groups have performed experiments, where the concentration of either the initiator or the monomer was varied to investigate the possibilities **Irgacure TPO–L** offers.[221–222] In a recent study **Irgacure TPO–L** was used for the fabrication of 3D scaffolds for the evaluation of *Komagataeibacter xylinus*, which produces bacterial celluloses, a polymer which occurs in nature with several properties important for biological applications.[223]

Ciprofloaxacin (**CPF**), a commercial available antibiotic drug, has drawn attention after it was discovered that it produces radicals under photo irradiation.[224] Because **CPF** itself possesses a low lipophilicity Bardakova et al. modified **CPF** with different substituents to increase the solubility for a successful use in 2PP experiments with methacryloyl modified poly(D,L-lactide).[225–226]

CPF–Allyl and **CPF–VBC** (Figure 121) reveal the same optical properties like **CPF** also the exhibition of the blue fluorescence at 420 to 450 nm, when irradiated at 365 nm. Unfortunately, the authors do not report further information regarding fluorescence quantum yields or two-photon cross-sections. Both initiators were able to initiate polymerization at a polymerization wavelength of 525 nm and a writing speed of 50 mm/s. Polymerization with **CPF–Allyl** was achieved at a laser power of 60 mW, where on the other hand **CPF–VBC** already initiated polymerization at 35 mW. No fabrication window was reported.[226] **CPF–Hex** also initiated polymerization at 525 nm but the fabrication window was determined at a faster writing speed of 25,000 μm/s. The FW of **CPF–Hex** was reported to be 45 to 60 mW. The initiation efficiency at such high writing speeds may be attributed to the low fluorescence quantum yield of 0.079, however no additional information photophysical properties were reported.[225]

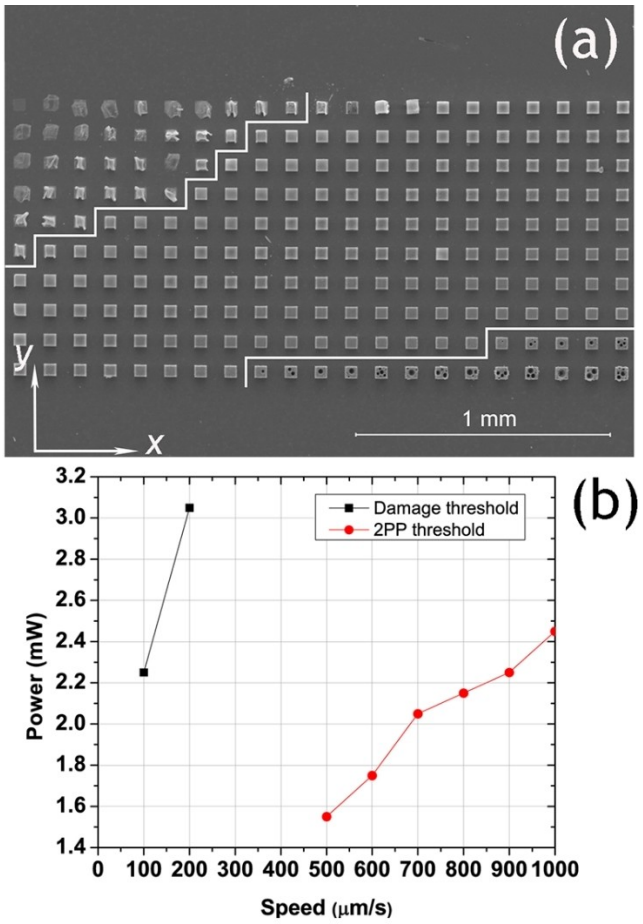

Figure 120. (a) SEM image of the fabricated woodpile structures fabricated with **Irgacure TPO**–**L**. The laser intensities varied from 1.55 mW (left) to 3.5 mW (right) and the writing speed from 100 μm/s (bottom row) to 1000 μm/s (top-left area) with 100 μm/s steps. (b) Plot of the processing parameters corresponding to the polymerization threshold (circles) and damage threshold (squares).[220] Reproduced with permission from Ref. [220]. Copyright 2013, American Chemical Society.

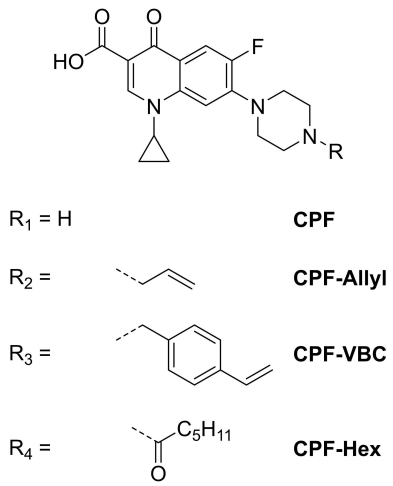

Figure 121. Schematic representation of the structures of modified **CPF** based photo initiators for 2PP.

7. Conclusion

Since its discovery in 1997, two-photon polymerization has proven to be a highly versatile polymerization method. Due to the high resolution of this polymerization technique, nanometer scale fabrication is possible, which enables its use in many different fields of research areas such as tissue engineering or functional micro devises.

The efficiency of a photo initiator for the use in the field of two-photon polymerization depends on many factors. The concentration of the 2PI, the laser intensity, solubility or monomer composition and its viscosity. One value which is always discussed, is the two-photon cross-section. It describes how well a molecule undergoes the two-photon absorption process. For a long time it was believed that a high two-photon cross-section results in a high efficiency for the 2PI in the polymerization process. However, many publications report 2PIs with comparable low σ_{TPA} values but with broad FW and/or low polymerization thresholds; which indicates that a high cross-section does not guarantees high efficiency. Additionally, for determination of the two-photon cross-section several techniques are used, like the Z-scan and two-photo excited fluorescence TPEF. Because the two techniques are based on different measurement principles, values are obtained which differ significantly as seen in the report of Nazir et al.[61] This makes a comparison of the available values difficult.

The fabrication window, the range in which the fabrication of stable structures is possible, describes quite well how efficient an initiator is, but these windows can differ depending on the laser setup, the used numerical aperture of the lenses and what monomer is used. Thus, while comparisons could be drawn between initiators within a review, there is a lack of some kind of standard, which would allow initiators from multiple reports to be compared to each other. Kiefer et al. met this challenge.[227] For that purpose over 70 photoresists from literature were compared in terms of writing speed, polymerization threshold, laser wavelength, laser pulse duration, pulse repetition rate, numerical aperture and 2PI concentration. These factors were combined into an equation, which represents the two-photon sensitivity of the photoresist. By comparing the sensitivity to a hypothetical reference, a figure of merit was established and the different photoresists could be compared.

The design and synthesis of new and efficient 2PI is a budding challenge, despite the extensive work done in the literature. Also, due to the ongoing development of the technical setups, more and more efficient devices are been developed for the use in two-photon polymerization. Despite the difficult comparison of the 2PIs, two-photon polymerization offers great potential to enter further research areas and to become an established technique not only in natural sciences, but also as a technique for the fabrication of electronic microelements or scaffolds in regenerative medicine.

Acknowledgements

The authors thank the Deutsche Forschungsgemeinschaft (DFG) for funding of this work (SCHU1229/25-1, LI 916/19-1 and GO1100/4-1). Open Access funding enabled and organized by Projekt DEAL.

Conflict of Interest

The authors declare no conflict of interest.

Data Availability Statement

The data that support the findings of this study are available from the corresponding author upon reasonable request.

Keywords: microfabrication · photo initiator · two-photon absorption · two-photon cross-section · two-photon polymerization

[1] M. Göppert-Mayer, *Ann. Phys.* **1931**, *401*, 273–294.
[2] W. Kaiser, C. G. B. Garrett, *Phys. Rev. Lett.* **1961**, *7*, 229–231.
[3] S. Maruo, O. Nakamura, S. Kawata, *Opt. Lett.* **1997**, *22*, 132–134.
[4] R. Wollhofen, B. Buchegger, C. Eder, J. Jacak, J. Kreutzer, T. A. Klar, *Opt. Mater. Express* **2017**, *7*, 2538–2559.
[5] T. K. Claus, B. Richter, V. Hahn, A. Welle, S. Kayser, M. Wegener, M. Bastmeyer, G. Delaittre, C. Barner-Kowollik, *Angew. Chem. Int. Ed.* **2016**, *55*, 3817–3822; *Angew. Chem.* **2016**, *128*, 3882–3887.
[6] Z. Xiong, C. Zheng, F. Jin, R. Wei, Y. Zhao, X. Gao, Y. Xia, X. Dong, M. Zheng, X. Duan, *Sens. Actuators B* **2018**, *274*, 541–550.
[7] X.-H. Qin, P. Gruber, M. Markovic, B. Plochberger, E. Klotzsch, J. Stampfl, A. Ovsianikov, R. Liska, *Polym. Chem.* **2014**, *5*, 6523–6533.
[8] T. Wloka, S. Czich, M. Kleinsteuber, E. Moek, C. Weber, M. Gottschaldt, K. Liefeith, U. S. Schubert, *Eur. Polym. J.* **2020**, *122*, 109295.
[9] B. H. Cumpston, S. P. Ananthavel, S. Barlow, D. L. Dyer, J. E. Ehrlich, L. L. Erskine, A. A. Heikal, S. M. Kuebler, I. Y. S. Lee, D. McCord-Maughon, J. Qin, H. Rockel, M. Rumi, X.-L. Wu, S. R. Marder, J. W. Perry, *Nature* **1999**, *398*, 51–54.
[10] J. H. Strickler, W. W. Webb, *Opt. Lett.* **1991**, *16*, 1780–1782.
[11] S. Basu, V. Rodionov, M. Terasaki, P. J. Campagnola, *Opt. Lett.* **2005**, *30*, 159–161.
[12] A. Koroleva, A. Deiwick, A. Nguyen, S. Schlie-Wolter, R. Narayan, P. Timashev, V. Popov, V. Bagratashvili, B. Chichkov, *PLoS One* **2015**, *10*, e0118164.
[13] M. T. Raimondi, S. M. Eaton, M. Laganà, V. Aprile, M. M. Nava, G. Cerullo, R. Osellame, *Acta Biomater.* **2013**, *9*, 4579–4584.
[14] M. Carlotti, V. Mattoli, *Small* **2019**, *15*, 1902687.
[15] M. T. Raimondi, S. M. Eaton, S. M. Eaton, M. M. Nava, M. M. Nava, M. Laganà, M. Laganà, G. Cerullo, G. Cerullo, R. Osellame, *J. Appl. Biomater. Funct. Mater.* **2012**, *10*, 55–65.
[16] S. C. Ligon, R. Liska, J. Stampfl, M. Gurr, R. Mülhaupt, *Chem. Rev.* **2017**, *117*, 10212–10290.
[17] A. I. Ciuciu, P. J. Cywinski, *RSC Adv.* **2014**, *4*, 45504–45516.
[18] C. Liao, A. Wuethrich, M. Trau, *Appl. Mater. Res.* **2020**, *19*, 100635.
[19] J. Song, C. Michas, C. S. Chen, A. E. White, M. W. Grinstaff, *Adv. Healthcare Mater.* **2020**, *9*, 1901217.
[20] Z. Faraji Rad, P. D. Prewett, G. J. Davies, *Microsyst. Nanoeng.* **2021**, *7*, 71.
[21] Z. Lao, N. Xia, S. Wang, T. Xu, X. Wu, L. Zhang, *Micromachines* **2021**, *12*, 465.
[22] A. J. G. Otuka, N. B. Tomazio, K. T. Paula, C. R. Mendonça, *Polymer* **2021**, *13*, 1994.
[23] Z. Huang, G. C.-P. Tsui, Y. Deng, C.-Y. Tang, *Nanotechnol. Rev.* **2020**, *9*, 1118–1136.
[24] N. A. Kuznetsova, G. V. Malkov, B. G. Gribov, *Russ. Chem. Rev.* **2020**, *89*, 173–190.
[25] M. Sheik-Bahae, A. A. Said, T. Wei, D. J. Hagan, E. W. V. Stryland, *IEEE J. Quantum Electron.* **1990**, *26*, 760–769.
[26] M. Pawlicki, H. A. Collins, R. G. Denning, H. L. Anderson, *Angew. Chem. Int. Ed.* **2009**, *48*, 3244–3266; *Angew. Chem.* **2009**, *121*, 3292–3316.
[27] K. Kamada, K. Matsunaga, A. Yoshino, K. Ohta, *J. Opt. Soc. Am. B* **2003**, *20*, 529–537.
[28] C. Xu, W. W. Webb, *J. Opt. Soc. Am. B* **1996**, *13*, 481–491.
[29] N. S. Makarov, M. Drobizhev, A. Rebane, *Opt. Express* **2008**, *16*, 4029–4047.
[30] R. Signorini, C. Ferrante, D. Pedron, M. Zerbetto, E. Cecchetto, M. Slaviero, I. Fortunati, E. Collini, R. Bozio, A. Abbotto, L. Beverina, G. A. Pagani, *J. Phys. Chem. A* **2008**, *112*, 4224–4234.
[31] L. A. Padilha, S. Webster, H. Hu, O. V. Przhonska, D. J. Hagan, E. W. Van Stryland, M. V. Bondar, I. G. Davydenko, Y. L. Slominsky, A. D. Kachkovski, *Chem. Phys.* **2008**, *352*, 97–105.
[32] R. Nazir, P. Danilevicius, A. I. Ciuciu, M. Chatzinikolaidou, D. Gray, L. Flamigni, M. Farsari, D. T. Gryko, *Chem. Mater.* **2014**, *26*, 3175–3184.
[33] R. Nazir, F. Bourquard, E. Balčiūnas, S. Smoleń, D. Gray, N. V. Tkachenko, M. Farsari, D. T. Gryko, *ChemPhysChem* **2015**, *16*, 682–690.
[34] B. S. Haq, H. U. Khan, K. Alam, S. Attaullah, I. Zari, M. Mateenullah, *Appl. Opt.* **2015**, *54*, 7020–7026.
[35] J. M. Song, T. Inoue, H. Kawazumi, T. Ogawa, *Anal. Sci.* **1999**, *15*, 601–603.
[36] B. S. Haq, H. U. Khan, K. Alam, S. Attaullah, M. Sultan, *Appl. Opt.* **2016**, *55*, 228–235.
[37] A. Ovsianikov, M. Malinauskas, S. Schlie, B. Chichkov, S. Gittard, R. Narayan, M. Löbler, K. Sternberg, K. P. Schmitz, A. Haverich, *Acta Biomater.* **2011**, *7*, 967–974.
[38] F. Claeyssens, E. A. Hasan, A. Gaidukeviciute, D. S. Achilleos, A. Ranella, C. Reinhardt, A. Ovsianikov, X. Shizhou, C. Fotakis, M. Vamvakaki, B. N. Chichkov, M. Farsari, *Langmuir* **2009**, *25*, 3219–3223.
[39] A. Ovsianikov, A. Gaidukeviciute, B. N. Chichkov, M. Oubaha, B. D. MacCraith, I. Sakellari, A. Giakoumaki, D. Gray, M. Vamvakaki, M. Farsari, C. Fotakis, *Laser Chem.* **2008**, *2008*, 1–7.
[40] A. Ovsianikov, J. Viertl, B. Chichkov, M. Oubaha, B. MacCraith, I. Sakellari, A. Giakoumaki, D. Gray, M. Vamvakaki, M. Farsari, C. Fotakis, *ACS Nano* **2008**, *2*, 2257–2262.
[41] S. A. Skoog, A. K. Nguyen, G. Kumar, J. Zheng, P. L. Goering, A. Koroleva, B. N. Chichkov, R. J. Narayan, *Biointerphases* **2014**, *9*, 029014.
[42] C. Xin, L. Yang, J. Li, Y. Hu, D. Qian, S. Fan, K. Hu, Z. Cai, H. Wu, D. Wang, D. Wu, J. Chu, *Adv. Mater.* **2019**, *31*, 1808226.
[43] Z. Li, M. Siklos, N. Pucher, K. Cicha, A. Ajami, W. Husinsky, A. Rosspeintner, E. Vauthey, G. Gescheidt, J. Stampfl, R. Liska, *J. Polym. Sci. Part A* **2011**, *49*, 3688–3699.
[44] S. Zhang, S. Li, X. Wan, J. Ma, N. Li, J. Li, Q. Yin, *Addit. Manuf.* **2021**, *47*, 102358.
[45] N. Pucher, A. Rosspeintner, V. Satzinger, V. Schmidt, G. Gescheidt, J. Stampfl, R. Liska, *Macromolecules* **2009**, *42*, 6519–6528.
[46] G. Lemercier, C. Martineau, J.-C. Mulatier, I. Wang, O. Stéphan, P. Baldeck, C. Andraud, *New J. Chem.* **2006**, *30*, 1606–1613.
[47] C. Martineau, G. Lemercier, C. Andraud, I. Wang, M. Bouriau, P. L. Baldeck, *Synth. Met.* **2003**, *138*, 353–356.
[48] Z. Li, N. Pucher, K. Cicha, J. Torgersen, S. C. Ligon, A. Ajami, W. Husinsky, A. Rosspeintner, E. Vauthey, S. Naumov, T. Scherzer, J. Stampfl, R. Liska, *Macromolecules* **2013**, *46*, 352–361.
[49] Q. Zou, Y. Zhao, N. S. Makarov, J. Campo, H. Yuan, D.-C. Fang, J. W. Perry, F. Wu, *Phys. Chem. Chem. Phys.* **2012**, *14*, 11743–11752.
[50] G. Weisgrab, O. Guillaume, Z. Guo, P. Heimel, P. Slezak, A. Poot, D. Grijpma, A. Ovsianikov, *Biofabrication* **2020**, *12*, 045036.
[51] A. Arslan, W. Steiger, P. Roose, H. Van den Bergen, P. Gruber, E. Zerobin, F. Gantner, O. Guillaume, A. Ovsianikov, S. Van Vlierberghe, P. Dubruel, *Mater. Today* **2021**, *44*, 25–39.
[52] H. Meier, *Angew. Chem. Int. Ed.* **2005**, *44*, 2482–2506; *Angew. Chem.* **2005**, *117*, 2536–2561.
[53] P. Hu, J. Zhu, R. Liu, Z. Li, *J. Photopolym. Sci. Technol.* **2019**, *32*, 257–264.
[54] D. P. Specht, P. A. Martic, S. Farid, *Tetrahedron* **1982**, *38*, 1203–1211.
[55] B. M. Monroe, G. C. Weed, *Chem. Rev.* **1993**, *93*, 435–448.
[56] J. P. Fouassier, F. Morlet-Savary, K. Yamashita, S. Imahashi, *Polymer* **1997**, *38*, 1415–1421.
[57] X. Allonas, J. P. Fouassier, M. Kaji, M. Miyasaka, T. Hidaka, *Polymer* **2001**, *42*, 7627–7634.
[58] T. Wang, Y. Zhao, M. Shi, F. Wu, *Dyes Pigm.* **2007**, *75*, 104–110.

[59] J. Xue, Y. Zhao, J. Wu, F. Wu, *J. Photochem. Photobiol. A* **2008**, *195*, 261–266.
[60] J. Xue, Y. Zhao, F. Wu, D.-C. Fang, *J. Phys. Chem. A* **2010**, *114*, 5171–5179.
[61] R. Nazir, B. Thorsted, E. Balciunas, L. Mazur, I. Deperasinska, M. Samoc, J. Brewer, M. Farsari, D. T. Gryko, *J. Mater. Chem. C* **2016**, *4*, 167–177.
[62] L. Poocza, M. Gottschaldt, E. Markweg, N. Hauptmann, G. Hildebrand, D. Pretzel, M. Hartlieb, C. Reichardt, J. Kuebel, U. S. Schubert, O. Mollenhauer, B. Dietzek, K. Liefeith, *Adv. Eng. Mater.* **2017**, *19*, 1600686.
[63] S. Czich, T. Wloka, H. Rothe, J. Rost, F. Penzold, M. Kleinsteuber, M. Gottschaldt, U. S. Schubert, K. Liefeith, *Molecules* **2020**, *25*, 5066.
[64] X. Huang, Y. Zhang, M. Shi, Y. Zhang, Y. Zhao, *Polym. Chem.* **2019**, *10*, 2273–2281.
[65] R. Liska, B. Seidl, *J. Polym. Sci. Part A* **2005**, *43*, 101–111.
[66] R. Infuehr, N. Pucher, C. Heller, H. Lichtenegger, R. Liska, V. Schmidt, L. Kuna, A. Haase, J. Stampfl, *Appl. Surf* **2007**, *254*, 836–840.
[67] C. Heller, N. Pucher, B. Seidl, K. Kalinyaprak-Icten, G. Ullrich, L. Kuna, V. Satzinger, V. Schmidt, H. C. Lichtenegger, J. Stampfl, R. Liska, *J. Polym. Sci. Part A* **2007**, *45*, 3280–3291.
[68] C. Li, X. Yang, R. Chen, J. Pan, H. Tian, H. Zhu, X. Wang, A. Hagfeldt, L. Sun, *Sol. Energy Mater. Sol. Cells* **2007**, *91*, 1863–1871.
[69] L.-F. Lai, C. Qin, C.-H. Chui, A. Islam, L. Han, C.-L. Ho, W.-Y. Wong, *Dyes Pigm.* **2013**, *98*, 428–436.
[70] S. C. Núñez Montoya, L. R. Comini, M. Sarmiento, C. Becerra, I. Albesa, G. A. Argüello, J. L. Cabrera, *J. Photochem. Photobiol. B* **2005**, *78*, 77–83.
[71] A. L. Capodilupo, V. Vergaro, E. Fabiano, M. De Giorgi, F. Baldassarre, A. Cardone, A. Maggiore, V. Maiorano, D. Sanvitto, G. Gigli, G. Ciccarella, *J. Mater. Chem. B* **2015**, *3*, 3315–3323.
[72] J. Dipold, R. J. M. B. Batista, R. D. Fonseca, D. L. Silva, G. L. C. Moura, J. V. dos Anjos, A. M. Simas, L. De Boni, C. R. Mendonca, *Chem. Phys. Lett.* **2016**, *661*, 143–150.
[73] C. J. Tiao, L. C. Hwang, T. C. Wen, *J. Chin. Chem. Soc.* **1998**, *45*, 659–665.
[74] L. Sun, Y. Chen, S. Kuang, G. Li, R. Guan, J. Liu, L. Ji, H. Chao, *Chem. Eur. J.* **2016**, *22*, 8955–8965.
[75] P. Brodard, A. Sarbach, J.-C. Gumy, T. Bally, E. Vauthey, *J. Phys. Chem. A* **2001**, *105*, 6594–6601.
[76] G. K. Pullen, N. S. Allen, M. Edge, I. Weddell, R. Swart, F. Catalina, S. Navaratnam, *Eur. Polym. J.* **1996**, *32*, 943–955.
[77] J.-F. Xing, W.-Q. Chen, X.-Z. Dong, T. Tanaka, X.-Y. Fang, X.-M. Duan, S. Kawata, *J. Photochem. Photobiol. A* **2007**, *189*, 398–404.
[78] S. Zhang, X. Y. Wan, Y. H. Peng, Q. Yin, *Iop. Conf. Ser. Mater. Sci. Eng.* **2019**, *479*, 012109.
[79] R. Guo, Y. Wang, Z. Huang, Q. Zhang, S. Xiang, S. Ye, W. Liu, L. Wang, *J. Mater. Chem. C* **2020**, *8*, 3705–3714.
[80] X. Tang, Y. Tao, H. Liu, F. Liu, X. He, Q. Peng, J. Li, P. Lu, *Front. Chem.* **2019**, *7*, 1–12.
[81] S. Lee, N. Park, J. Bang, *Phys. Rev. Mater.* **2020**, *4*, 044603.
[82] R. Yu, P. Wang, X. Meng, L. He, *Dalton Trans.* **2020**, *49*, 8967–8975.
[83] T. Hua, Z.-S. Huang, K. Cai, L. Wang, H. Tang, H. Meier, D. Cao, *Electrochim. Acta* **2019**, *302*, 225–233.
[84] C. Zhang, S. Wang, Y. Li, *Sol. Energy* **2017**, *157*, 94–102.
[85] S. Benhattab, R. Nakar, J. W. Rodriguez Acosta, N. Berton, J. Faure-Vincent, J. Bouclé, F. Tran Van, B. Schmaltz, *Dyes Pigm.* **2018**, *151*, 238–244.
[86] A. Venkateswararao, K. R. Justin Thomas, in *Sol. Energy Mater Sol. Cells*, John Wiley and Sons, **2013**, pp. 41–96.
[87] A. T. Gökçeören, *Fibers Polym.* **2015**, *16*, 86–94.
[88] D. K. Balta, N. Arsu, Y. Yagci, S. Jockusch, N. J. Turro, *Macromolecules* **2007**, *40*, 4138–4141.
[89] H. J. Timpe, K. P. Kronfeld, U. Lammel, J. P. Fouassier, D. J. Lougnot, *J. Photochem. Photobiol. A* **1990**, *52*, 111–122.
[90] R. Nazir, E. Balčiūnas, D. Buczyńska, F. Bourquard, D. Kowalska, D. Gray, S. Maćkowski, M. Farsari, D. T. Gryko, *Macromolecules* **2015**, *48*, 2466–2472.
[91] K. J. Schafer, J. M. Hales, M. Balu, K. D. Belfield, E. W. Van Stryland, D. J. Hagan, *J. Photochem. Photobiol. A* **2004**, *162*, 497–502.
[92] J. Fischer, G. von Freymann, M. Wegener, *Adv. Mater.* **2010**, *22*, 3578–3582.
[93] L. Li, R. R. Gattass, E. Gershgoren, H. Hwang, J. T. Fourkas, *Science* **2009**, *324*, 910–913.
[94] T. Chi, P. Somers, D. A. Wilcox, A. J. Schuman, V. Iyer, R. Le, J. Gengler, M. Ferdinandus, C. Liebig, L. Pan, X. Xu, B. W. Boudouris, *J. Polym. Sci. Part B* **2019**, *57*, 1462–1475.
[95] T. Chi, P. Somers, D. A. Wilcox, A. J. Schuman, J. E. Johnson, Z. Liang, L. Pan, X. Xu, B. W. Boudouris, *ACS Appl. Polym* **2021**, *3*, 1426–1435.
[96] B. Harke, W. Dallari, G. Grancini, D. Fazzi, F. Brandi, A. Petrozza, A. Diaspro, *Adv. Mater.* **2013**, *25*, 904–909.
[97] H. Zhang, T. Jia, K. Zhou, J. Liu, D. Feng, S. Zhang, Z. Sun, *J. Nonlinear Opt. Phys. Mater.* **2014**, *23*, 1450048.
[98] J. Ma, W. Cheng, S. Zhang, D. Feng, T. Jia, Z. Sun, J. Qiu, *Laser Phys. Lett.* **2013**, *10*, 085304.
[99] K. Kamada, K. Ohta, Y. Iwase, K. Kondo, *Chem. Phys. Lett.* **2003**, *372*, 386–393.
[100] Y. Iwase, K. Kamada, K. Ohta, K. Kondo, *J. Mater. Chem.* **2003**, *13*, 1575–1581.
[101] R. Kannan, G. S. He, L. Yuan, F. Xu, P. N. Prasad, A. G. Dombroskie, B. A. Reinhardt, J. W. Baur, R. A. Vaia, L.-S. Tan, *Chem. Mater.* **2001**, *13*, 1896–1904.
[102] M. Tromayer, P. Gruber, A. Rosspeintner, A. Ajami, W. Husinsky, F. Plasser, L. González, E. Vauthey, A. Ovsianikov, R. Liska, *Sci. Rep.* **2018**, *8*, 17273.
[103] H. Zhou, F. Zhou, S. Tang, P. Wu, Y. Chen, Y. Tu, J. Wu, Y. Tian, *Dyes Pigm.* **2012**, *92*, 633–641.
[104] C.-F. Chow, *RSC Adv.* **2013**, *3*, 18835–18843.
[105] B. Holzer, M. Lunzer, A. Rosspeintner, G. Licari, M. Tromayer, S. Naumov, D. Lumpi, E. Horkel, C. Hametner, A. Ovsianikov, R. Liska, E. Vauthey, J. Fröhlich, *Mol. Syst. Des. Eng.* **2019**, *4*, 437–448.
[106] D. W. Chang, H. J. Lee, J. H. Kim, S. Y. Park, S.-M. Park, L. Dai, J.-B. Baek, *Org. Lett.* **2011**, *13*, 3880–3883.
[107] Y. Du, X. Lin, T. Jia, J. Dong, *Opt. Commun.* **2015**, *338*, 257–260.
[108] T.-C. Lin, W. Chien, C.-Y. Liu, M.-Y. Tsai, Y.-J. Huang, *Eur. J. Org. Chem.* **2013**, *2013*, 4262–4269.
[109] X. Cao, F. Jin, Y.-F. Li, W.-Q. Chen, X.-M. Duan, L.-M. Yang, *New J. Chem.* **2009**, *33*, 1578–1582.
[110] J.-F. Xing, W.-Q. Chen, J. Gu, X.-Z. Dong, N. Takeyasu, T. Tanaka, X.-M. Duan, S. Kawata, *J. Mater. Chem.* **2007**, *17*, 1433–1438.
[111] Y. Lu, F. Hasegawa, T. Goto, S. Ohkuma, S. Fukuhara, Y. Kawazu, K. Totani, T. Yamashita, T. Watanabe, *J. Mater. Chem.* **2004**, *14*, 75–80.
[112] X. Wan, Y. Zhao, J. Xue, F. Wu, X. Fang, *J. Photochem. Photobiol. A* **2009**, *202*, 74–79.
[113] G. S. He, G. C. Xu, P. N. Prasad, B. A. Reinhardt, J. C. Bhatt, A. G. Dillard, *Opt. Lett.* **1995**, *20*, 435–437.
[114] X. Huang, X. Wang, Y. Zhao, *Dyes Pigm.* **2017**, *141*, 413–419.
[115] Z. Li, J. Torgersen, A. Ajami, S. Muhleder, X. Qin, W. Husinsky, W. Holnthoner, A. Ovsianikov, J. Stampfl, R. Liska, *RSC Adv.* **2013**, *3*, 15939–15946.
[116] K. Yamashita, S. Imahashi, S. Ito, *Dyes Pigm.* **2008**, *76*, 748–753.
[117] J. Lalevée, B. Graff, X. Allonas, J. P. Fouassier, *J. Phys. Chem. A* **2007**, *111*, 6991–6998.
[118] A. Ovsianikov, S. Mühleder, J. Torgersen, Z. Li, X.-H. Qin, S. Van Vlierberghe, P. Dubruel, W. Holnthoner, H. Redl, R. Liska, J. Stampfl, *Langmuir* **2014**, *30*, 3787–3794.
[119] P. Sanjuan-Alberte, J. Vaithilingam, J. C. Moore, R. D. Wildman, C. J. Tuck, M. R. Alexander, R. J. M. Hague, F. J. Rawson, *Polymer* **2021**, *13*, 1038.
[120] X. Huang, Y. Zhang, M. Shi, L.-P. Zhang, Y. Zhang, Y. Zhao, *Eur. Polym. J.* **2021**, *153*, 110505.
[121] J. Xing, J. Liu, T. Zhang, L. Zhang, M. Zheng, X. Duan, *J. Mater. Chem. B* **2014**, *2*, 4318–4323.
[122] O. K. Nag, R. R. Nayak, C. S. Lim, I. H. Kim, K. Kyhm, B. R. Cho, H. Y. Woo, *J. Phys. Chem. B* **2010**, *114*, 9684–9690.
[123] W. Saenger, T. Steiner, *Acta Crystallogr. Sect. A* **1998**, *54*, 798–805.
[124] J. Xing, L. Liu, X. Song, Y. Zhao, L. Zhang, X. Dong, F. Jin, M. Zheng, X. Duan, *J. Mater. Chem. B* **2015**, *3*, 8486–8491.
[125] S. D. Gittard, A. Ovsianikov, H. Akar, B. Chichkov, N. A. Monteiro-Riviere, S. Stafslien, B. Chisholm, C.-C. Shin, C.-M. Shih, S.-J. Lin, Y.-Y. Su, R. J. Narayan, *Adv. Eng. Mater.* **2010**, *12*, B77–B82.
[126] T. Weiß, G. Hildebrand, R. Schade, K. Liefeith, *Eng. Life Sci.* **2009**, *9*, 384–390.
[127] A. Koroleva, A. A. Gill, I. Ortega, J. W. Haycock, S. Schlie, S. D. Gittard, B. N. Chichkov, F. Claeyssens, *Biofabrication* **2012**, *4*, 025005.
[128] J. Serbin, A. Egbert, A. Ostendorf, B. N. Chichkov, R. Houbertz, G. Domann, J. Schulz, C. Cronauer, L. Fröhlich, M. Popall, *Opt. Lett.* **2003**, *28*, 301–303.
[129] C. Martineau, R. Anémian, C. Andraud, I. Wang, M. Bouriau, P. L. Baldeck, *Chem. Phys. Lett.* **2002**, *362*, 291–295.
[130] C. Martineau, G. Lemercier, C. Andraud, I. Wang, M. Bouriau, P. L. Baldeck, in *Optical Science and Technology, SPIE's 48th Annual Meeting, Vol. 5211*, SPIE, **2003**.

[131] F. Guo, R. Guo, Z. Jiang, Q. Zhang, W. Huang, B. Guo, *Biofabrication* **2005**, *202*, 2515–2520.
[132] J.-F. Xing, M.-L. Zheng, W.-Q. Chen, X.-Z. Dong, N. Takeyasu, T. Tanaka, Z.-S. Zhao, X.-M. Duan, S. Kawata, *Phys. Chem. Chem. Phys.* **2012**, *14*, 15785–15792.
[133] J.-F. Xing, X.-Z. Dong, W.-Q. Chen, X.-M. Duan, N. Takeyasu, T. Tanaka, S. Kawata, *Appl. Phys. Lett.* **2007**, *90*, 131106.
[134] X. Gan, H. Zhou, P. Shi, P. Wang, J. Wu, Y. Tian, J. Yang, G. Xu, Y. Zhou, M. Jiang, *Sci. China Ser. B* **2009**, *52*, 2180.
[135] X. Zhang, X. Q. Yu, B. Q. Zhang, Y. G. Feng, X. T. Tao, M. H. Jiang, *Chin. J. Chem.* **2006**, *24*, 701–704.
[136] X. Zhang, X. Yu, Y. Sun, H. Xu, Y. Feng, B. Huang, X. Tao, M. Jiang, *Chem. Phys.* **2006**, *328*, 103–110.
[137] C. Arnoux, T. Konishi, E. Van Elslande, E.-A. Poutougnigni, J.-C. Mulatier, L. Khrouz, C. Bucher, E. Dumont, K. Kamada, C. Andraud, P. Baldeck, A. Banyasz, C. Monnereau, *Macromolecules* **2020**, *53*, 9264–9278.
[138] G. Lemercier, J.-C. Mulatier, C. Martineau, R. Anémian, C. Andraud, I. Wang, O. Stéphan, N. Amari, P. Baldeck, *C. R. Chim.* **2005**, *8*, 1308–1316.
[139] K. D. Belfield, K. J. Schafer, Y. Liu, J. Liu, X. Ren, E. W. V. Stryland, *J. Phys. Org. Chem.* **2000**, *13*, 837–849.
[140] S. M. Kennedy, F. E. Lytle, *Anal. Chem.* **1986**, *58*, 2643–2647.
[141] W. G. Fisher, E. A. Wachter, F. E. Lytle, M. Armas, C. Seaton, *Appl. Spectrosc.* **1998**, *52*, 536–545.
[142] I. Fitilis, M. Fakis, I. Polyzos, V. Giannetas, P. Persephonis, *J. Photochem. Photobiol. A* **2010**, *215*, 25–30.
[143] I. Fitilis, M. Fakis, I. Polyzos, V. Giannetas, P. Persephonis, J. Mikroyannidis, *J. Phys. Chem. A* **2008**, *112*, 4742–4748.
[144] I. Fitilis, M. Fakis, I. Polyzos, V. Giannetas, P. Persephonis, P. Vellis, J. Mikroyannidis, *Chem. Phys. Lett.* **2007**, *447*, 300–304.
[145] S. H. Park, T.-W. Lim, D.-Y. Yang, H. J. Kong, R.-H. Kim, K.-S. Kim, K.-S. Lee, *Bull. Korean Chem. Soc.* **2004**, *25*, 1119–1120.
[146] I. Henning, A. W. Woodward, G. A. Rance, B. T. Paul, R. D. Wildman, D. J. Irvine, J. C. Moore, *Adv. Funct. Mater.* **2020**, *30*, 2006108.
[147] H. C. Kolb, K. B. Sharpless, *Drug Discovery Today* **2003**, *8*, 1128–1137.
[148] D. Brunel, F. Dumur, *New J. Chem.* **2020**, *44*, 3546–3561.
[149] A. J. Maroulis, C. P. Hadjiantoniou-Maroulis, B. Georgiou, G. Seretoudi, I. Sideridou-Karayannidou, *J. Macromol. Sci. A* **1994**, *31*, 487–494.
[150] M.-S. Yuan, D.-E. Wang, P. Xue, W. Wang, J.-C. Wang, Q. Tu, Z. Liu, Y. Liu, Y. Zhang, J. Wang, *Chem. Mater.* **2014**, *26*, 2467–2477.
[151] E. W. Nelson, T. P. Carter, A. B. Scranton, *Macromolecules* **1994**, *27*, 1013–1019.
[152] K. Tanaka, Y. Koizumi, T. Igarashi, T. Sakurai, *Macromolecules* **2006**, *39*, 8556–8558.
[153] W. J. Yang, C. H. Kim, M.-Y. Jeong, S. K. Lee, M. J. Piao, S.-J. Jeon, B. R. Cho, *Chem. Mater.* **2004**, *16*, 2783–2789.
[154] S. Kim, Q. Zheng, G. S. He, D. J. Bharali, H. E. Pudavar, A. Baev, P. N. Prasad, *Adv. Funct. Mater.* **2006**, *16*, 2317–2323.
[155] W. J. Yang, M. S. Seo, X. Q. Wang, S.-J. Jeon, B. R. Cho, *J. Fluoresc.* **2008**, *18*, 403–411.
[156] W. J. Yang, D. Y. Kim, M.-Y. Jeong, H. M. Kim, S.-J. Jeon, B. R. Cho, *Chem. Commun.* **2003**, 2618–2619.
[157] W. J. Yang, D. Y. Kim, M.-Y. Jeong, H. M. Kim, Y. K. Lee, X. Fang, S.-J. Jeon, B. R. Cho, *Chem. Eur. J.* **2005**, *11*, 4191–4198.
[158] H. Y. Woo, B. Liu, B. Kohler, D. Korystov, A. Mikhailovsky, G. C. Bazan, *J. Am. Chem. Soc.* **2005**, *127*, 14721–14729.
[159] J. Torgersen, A. Ovsianikov, V. Mironov, N. Pucher, X. Qin, Z. Li, K. Cicha, T. Machacek, R. Liska, V. Jantsch, J. Stampfl, *BIOMEDO* **2012**, *17*, 105008–105008.
[160] X. H. Qin, J. Torgersen, R. Saf, S. Mühleder, N. Pucher, S. C. Ligon, W. Holnthoner, H. Redl, A. Ovsianikov, J. Stampfl, R. Liska, *J. Polym. Sci. Part A* **2013**, *51*, 4799–4810.
[161] O. Nuyken, T. Knepper, B. Voit, *Makromol. Chem.* **1989**, *190*, 1015–1024.
[162] M. Tromayer, A. Dobos, P. Gruber, A. Ajami, R. Dedic, A. Ovsianikov, R. Liska, *Polym. Chem.* **2018**, *9*, 3108–3117.
[163] A. Ajami, W. Husinsky, M. Tromayer, P. Gruber, R. Liska, A. Ovsianikov, *Appl. Phys. Lett.* **2017**, *111*, 071901.
[164] W.-E. Lu, X.-Z. Dong, W.-Q. Chen, Z.-S. Zhao, X.-M. Duan, *J. Mater. Chem.* **2011**, *21*, 5650–5659.
[165] Z. Li, P. Hu, J. Zhu, Y. Gao, X. Xiong, R. Liu, *J. Polym. Sci. Part A* **2018**, *56*, 2692–2700.
[166] M. Albota, D. Beljonne, J.-L. Brédas, J. E. Ehrlich, J.-Y. Fu, A. A. Heikal, S. E. Hess, T. Kogej, M. D. Levin, S. R. Marder, D. McCord-Maughon, J. W. Perry, H. Röckel, M. Rumi, G. Subramaniam, W. W. Webb, X.-L. Wu, C. Xu, *Science* **1998**, *281*, 1653.
[167] G. Ramakrishna, T. Goodson, *J. Phys. Chem. A* **2007**, *111*, 993–1000.
[168] X. Wang, D. Wang, G. Zhou, W. Yu, Y. Zhou, Q. Fang, M. Jiang, *J. Mater. Chem.* **2001**, *11*, 1600–1605.
[169] A. Abbotto, L. Beverina, R. Bozio, A. Facchetti, C. Ferrante, G. A. Pagani, D. Pedron, R. Signorini, *Org. Lett.* **2002**, *4*, 1495–1498.
[170] Y.-F. Zhou, F.-Q. Meng, X. Zhao, S.-Y. Feng, M.-H. Jiang, *Chem. Phys.* **2001**, *269*, 441–445.
[171] C. F. Zhao, G. S. He, J. D. Bhawalkar, C. K. Park, P. N. Prasad, *Chem. Mater.* **1995**, *7*, 1979–1983.
[172] P. C. Ray, J. Leszczynski, *J. Phys. Chem. A* **2005**, *109*, 6689–6696.
[173] J. Gu, W. Yulan, W.-Q. Chen, X.-Z. Dong, X.-M. Duan, S. Kawata, *New J. Chem.* **2007**, *31*, 63–68.
[174] S. Li, C. Lu, X. Wan, S. Zhang, J. Li, Z. He, L. Zhang, *Mater. Today Commun.* **2020**, *24*, 101219.
[175] X. Ma, R. Gu, L. Yu, W. Han, J. Li, X. Li, T. Wang, *Polym. Chem.* **2017**, *8*, 6134–6142.
[176] J. Xu, G. Ma, K. Wang, J. Gu, S. Jiang, J. Nie, *J. Appl. Polym. Sci.* **2012**, *123*, 725–731.
[177] D. E. Fast, A. Lauer, J. P. Menzel, A.-M. Kelterer, G. Gescheidt, C. Barner-Kowollik, *Macromolecules* **2017**, *50*, 1815–1823.
[178] P. Hu, W. Qiu, S. Naumov, T. Scherzer, Z. Hu, Q. Chen, W. Knolle, Z. Li, *ChemPhotoChem* **2020**, *4*, 224–232.
[179] S.-J. Chung, K.-S. Kim, T.-C. Lin, G. S. He, J. Swiatkiewicz, P. N. Prasad, *J. Phys. Chem. B* **1999**, *103*, 10741–10745.
[180] A. Bhaskar, G. Ramakrishna, Z. Lu, R. Twieg, J. M. Hales, D. J. Hagan, E. Van Stryland, T. Goodson, *J. Am. Chem. Soc.* **2006**, *128*, 11840–11849.
[181] Y.-P. Tian, L. Li, J.-Z. Zhang, J.-X. Yang, H.-p. Zhou, J.-y. Wu, P.-p. Sun, L.-m. Tao, Y.-h. Guo, C.-K. Wang, H. Xing, W.-h. Huang, X.-T. Tao, M.-H. Jiang, *J. Mater. Chem.* **2007**, *17*, 3646–3654.
[182] R. Whitby, Y. Ben-Tal, R. MacMillan, S. Janssens, S. Raymond, D. Clarke, J. Jin, A. Kay, M. C. Simpson, *RSC Adv.* **2017**, *7*, 13232–13239.
[183] J.-P. Malval, M. Jin, F. Morlet-Savary, H. Chaumeil, A. Defoin, O. Soppera, T. Scheul, M. Bouriau, P. L. Baldeck, *Chem. Mater.* **2011**, *23*, 3411–3420.
[184] J. Wu, M. Shi, Y. Zhao, F. Wu, *Dyes Pigm.* **2008**, *76*, 690–695.
[185] S. J. Strickler, R. A. Berg, *J. Chem. Phys.* **1962**, *37*, 814–822.
[186] F. Terenziani, C. Katan, E. Badaeva, S. Tretiak, M. Blanchard-Desce, *Adv. Mater.* **2008**, *20*, 4641–4678.
[187] Y.-C. Zheng, Y.-Y. Zhao, M.-L. Zheng, S.-L. Chen, J. Liu, F. Jin, X.-Z. Dong, Z.-S. Zhao, X.-M. Duan, *ACS Appl. Mater. Interfaces* **2019**, *11*, 1782–1789.
[188] J. Lagona, P. Mukhopadhyay, S. Chakrabarti, L. Isaacs, *Angew. Chem. Int. Ed.* **2005**, *44*, 4844–4870; *Angew. Chem.* **2005**, *117*, 4922–4949.
[189] N. K. Petrov, D. A. Ivanov, D. V. Golubkov, S. P. Gromov, M. V. Alfimov, *Chem. Phys. Lett.* **2009**, *480*, 96–99.
[190] P. Xiao, F. Dumur, B. Graff, F. Morlet-Savary, L. Vidal, D. Gigmes, J. P. Fouassier, J. Lalevée, *Macromolecules* **2014**, *47*, 26–34.
[191] M.-A. Tehfe, F. Dumur, B. Graff, F. Morlet-Savary, J.-P. Fouassier, D. Gigmes, J. Lalevée, *Macromolecules* **2013**, *46*, 3761–3770.
[192] M.-A. Tehfe, F. Dumur, B. Graff, D. Gigmes, J.-P. Fouassier, J. Lalevée, *Macromolecules* **2013**, *46*, 3332–3341.
[193] Z. Li, A. Rosspeintner, P. Hu, G. Zhu, Y. Hu, X. Xiong, R. Peng, M. Wang, X. Liu, R. Liu, *Polym. Chem.* **2017**, *8*, 6644–6653.
[194] M. Drobizhev, F. Meng, A. Rebane, Y. Stepanenko, E. Nickel, C. W. Spangler, *J. Phys. Chem. B* **2006**, *110*, 9802–9814.
[195] A. Rebane, M. Drobizhev, N. S. Makarov, E. Beuerman, J. E. Haley, D. M. Krein, A. R. Burke, J. L. Flikkema, T. M. Cooper, *J. Phys. Chem. A* **2011**, *115*, 4255–4262.
[196] J. Lalevée, N. Blanchard, M. El-Roz, B. Graff, X. Allonas, J. P. Fouassier, *Macromolecules* **2008**, *41*, 4180–4186.
[197] J. Lalevée, N. Blanchard, M. A. Tehfe, C. Fries, F. Morlet-Savary, D. Gigmes, J. P. Fouassier, *Polym. Chem.* **2011**, *2*, 1077–1084.
[198] S. Chen, C. Cao, X. Shen, Y. Qiu, C. Kuang, D. Wan, M. Jin, *Eur. Polym. J.* **2021**, *153*, 110525.
[199] T. Mori, H. Saomoto, K. Machitani, K. Inoue, Y. Aoki, T. Koshitani, N. Koumura, T. N. Murakami, *RSC Adv.* **2016**, *6*, 13964–13970.
[200] W. Qiu, P. Hu, J. Zhu, R. Liu, Z. Li, Z. Hu, Q. Chen, K. Dietliker, R. Liska, *ChemPhotoChem* **2019**, *3*, 1090–1094.
[201] R. Zhou, J.-P. Malval, M. Jin, A. Spangenberg, H. Pan, D. Wan, F. Morlet-Savary, S. Knopf, *Chem. Commun.* **2019**, *55*, 6233–6236.
[202] A. Ovsianikov, A. Deiwick, S. Van Vlierberghe, M. Pflaum, M. Wilhelmi, P. Dubruel, B. Chichkov, *Materials* **2011**, *4*, 288.
[203] A. Ovsianikov, A. Deiwick, S. Van Vlierberghe, P. Dubruel, L. Möller, G. Dräger, B. Chichkov, *Biomacromolecules* **2011**, *12*, 851–858.

[204] O. Kufelt, A. El-Tamer, C. Sehring, S. Schlie-Wolter, B. N. Chichkov, *Biomacromolecules* **2014**, *15*, 650–659.
[205] G. D. Giustina, S. Giulitti, L. Brigo, M. Zanatta, M. Tromayer, R. Liska, N. Elvassore, G. Brusatin, *Macromol. Rapid Commun.* **2017**, *38, 1600570*.
[206] A. L. Chibac, T. Buruiana, V. Melinte, I. Mangalagiu, G. Epurescu, E. C. Buruiana, *Des. Monomers Polym.* **2016**, *19*, 12–23.
[207] E. Käpylä, T. Sedlačík, D. B. Aydogan, J. Viitanen, F. Rypáček, M. Kellomäki, *Mater. Sci. Eng. C* **2014**, *43*, 280–289.
[208] A. Ovsianikov, M. Gruene, M. Pflaum, L. Koch, F. Maiorana, M. Wilhelmi, A. Haverich, B. Chichkov, *Biofabrication* **2010**, *2*, 014104.
[209] A. Ovsianikov, B. Chichkov, P. Mente, N. A. Monteiro-Riviere, A. Doraiswamy, R. J. Narayan, *Int. J. Appl. Ceram. Technol.* **2007**, *4*, 22–29.
[210] S. Schlie, A. Ngezahayo, A. Ovsianikov, T. Fabian, H.-A. Kolb, H. Haferkamp, B. N. Chichkov, *J. Biomater. Appl.* **2007**, *22*, 275–287.
[211] M. M. Nava, N. D. Maggio, T. Zandrini, G. Cerullo, R. Osellame, I. Martin, M. T. Raimondi, *J. Tissue Eng. Regener. Med.* **2017**, *11*, 2836–2845.
[212] J. Giltinan, V. Sridhar, U. Bozuyuk, D. Sheehan, M. Sitti, *Adv. Intell. Syst* **2021**, *3*, 2000204.
[213] K.-W. Yeung, Y. Dong, L. Chen, C.-Y. Tang, W.-C. Law, G. C.-P. Tsui, D. S. Engstrøm, *Nanotechnol. Rev.* **2020**, *9*, 418–426.
[214] J. Heitz, C. Plamadeala, M. Wiesbauer, P. Freudenthaler, R. Wollhofen, J. Jacak, T. A. Klar, B. Magnus, D. Köstner, A. Weth, W. Baumgartner, R. Marksteiner, *J. Biomed. Mater. Res. Part A* **2017**, *105*, 891–899.
[215] E. Scarpa, E. D. Lemma, R. Fiammengo, M. P. Cipolla, F. Pisanello, F. Rizzi, M. De Vittorio, *Sens. Actuators B* **2019**, *279*, 418–426.
[216] E. Harnisch, M. Russew, J. Klein, N. König, H. Crailsheim, R. Schmitt, *Opt. Mater. Express* **2015**, *5*, 456–461.
[217] T. Zandrini, N. Liaros, L. J. Jiang, Y. F. Lu, J. T. Fourkas, R. Osellame, T. Baldacchini, *Opt. Mater. Express* **2019**, *9*, 2601–2616.
[218] C. R. Mendonca, D. S. Correa, T. Baldacchini, P. Tayalia, E. Mazur, *Appl. Phys. A* **2008**, *90*, 633–636.
[219] T. Baldacchini, C. N. LaFratta, R. A. Farrer, M. C. Teich, B. E. A. Saleh, M. J. Naughton, J. T. Fourkas, *J. Appl. Phys.* **2004**, *95*, 6072–6076.
[220] C. De Marco, A. Gaidukeviciute, R. Kiyan, S. M. Eaton, M. Levi, R. Osellame, B. N. Chichkov, S. Turri, *Langmuir* **2013**, *29*, 426–431.
[221] P. M. Cônsoli, A. J. G. Otuka, D. T. Balogh, C. R. Mendonça, *J. Polym. Sci. Part B* **2018**, *56*, 1158–1163.
[222] G. Ummethala, A. Jaiswal, R. P. Chaudhary, S. Hawal, S. Saxena, S. Shukla, *Polymer* **2017**, *117*, 364–369.
[223] A. J. G. Otuka, R. R. Domeneguetti, J. Q. R. Moraes, D. T. Balogh, S. J. L. Ribeiro, C. R. Mendonça, *J. Phys. Photon.* **2021**, *3*, 024003.
[224] S. Soldevila, M. Consuelo Cuquerella, V. Lhiaubet-Vallet, R. Edge, F. Bosca, *Free Radical Biol. Med.* **2014**, *67*, 417–425.
[225] K. N. Bardakova, Y. V. Faletrov, E. O. Epifanov, N. V. Minaev, V. S. Kaplin, Y. A. Piskun, P. I. Koteneva, V. M. Shkumatov, N. A. Aksenova, A. I. Shpichka, A. B. Solovieva, S. V. Kostjuk, P. S. Timashev, *Polymer* **2021**, *13*, 3385.
[226] E. O. Epifanov, P. S. Timashev, Y. V. Faletrov, Y. A. Piskun, S. V. Kostjuk, N. V. Minaev, K. N. Bardakova, *Bull. Russ. Acad. Sci.: Phys.* **2020**, *84*, 1406–1410.
[227] P. Kiefer, V. Hahn, M. Nardi, L. Yang, E. Blasco, C. Barner-Kowollik, M. Wegener, *Adv. Opt. Mater.* **2020**, *8*, 2000895.

Manuscript received: November 22, 2021
Accepted manuscript online: February 24, 2022
Version of record online: April 12, 2022